THEORETICAL STUDY OF PHOTOEMISSION FROM METALS AND SEMICONDUCTORS

ABSTRACT

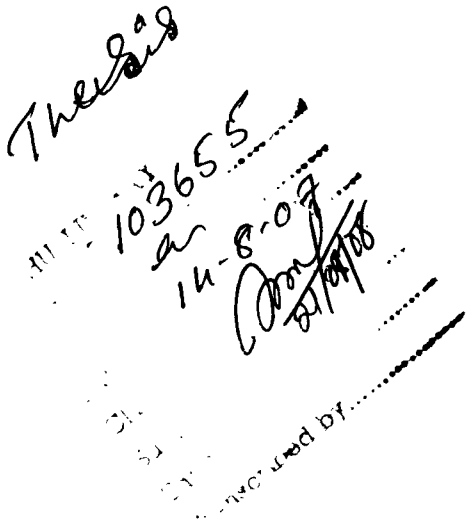
Thesis
103655
14-6-07

CHAPTER 1

INTRODUCTION

Photoemission is basically concerned with the emission of electrons from the surface/bulk of metals by the incident electromagnetic radiation in the ultra-violet (UV) region. Photoemission spectroscopy has now been widely used as a method for studying the electronic properties of solids. But the detailed interpretation of the photoemission data requires the use of a theory of photoemission which should in its simplest form be able to calculate the initial and final state electronic wave functions, as well as the spatial form of the vector potential which is involved in photoemission matrix element i.e. $< \psi_f |H'| \psi_i >$. Except Feibelman, very few authors have taken care to evaluate the initial state wave function ψ_i involved in the formula for photocurrent in photoemission. However, the method of Feibelman could be extended only to free electron metals. In this thesis, we will be interested mainly in the formulation of initial state wavefunction by suitably choosing a model potential which would be equally applicable to free electron metals, d-band metals as well as semiconductors. This would enable one to interpret the measured photocurrent data in a more realistic approach.

Electronic properties of solids are found to be different in the surface region than in the bulk region. The reason for this being that the presence of surface modifies the electronic properties due to loss of the periodicity in the direction normal to the surface. The electronic distribution may differ quite significantly from that in the

bulk, although the region important for this departure from bulk value is only a few lattice parameters. There may be new types of states, surface states or resonances which are spatially located in the surface region, and the case of pure surface states are forbidden in the bulk. Experimental techniques like angle-resolved photoemission, field-emissions, photo-field emissions, inverse photoemissions etc. can well be used to probe these states in the surface region. However, while angle-resolved photoemissions can also be used to study these states, the variations of the electromagnetic fields associated with photon in the surface presents an additional problem. Due to complex problem created by the presence of the surface in photoemission studies, many authors have neglected the effect of the variation of the electromagnetic fields with photon energy.

As *ab initio* treatment of the variation of fields near surfaces is extremely a complex situation involving tremendously a large computational effort, we will be using simple dielectric model to compute these fields. The dielectric model in which the dielectric function is assumed to vary linearly as a function of the distance from the surface region, can be solved to get the electromagnetic fields in the region of interest. The important thing with this model being that the dielectric function is a function of both frequency and spatial co-ordinate. The dielectric function interpolates linearly between the bulk value inside the metal and the vacuum value (unity) outside. In this model, the complex dielectric constant of metals is evaluated by using the experimentally determined frequency-dependent dielectric functions. We have used this model or its modified form for calculations of electromagnetic fields in the

metals and semiconductors. The fields so determined will be used for calculating the photoemission cross-sections for determining the photocurrent as a function of photon energy by evaluating the matrix element $< \psi_f |H'| \psi_i >$. The behaviour of photocurrent especially near the plasmon energy of metals under study would be of particular interest.

The exact formulation of the initial state wavefunction by choosing the appropriate potential model for the surface and the bulk regions of the solid is very important and complex too in photoemission study. There are various approaches to surface and bulk photoemission calculations which had been applied to real cases. In this proposal, we are considering as a first step, the applications of Kronig-Penney(KP) model potential as applied by Thapa and others to metals and semiconductors. We have formulated the initial state wavefunction ψ_i in such a way that it takes into account both the surface and the bulk potential using the Mathieu potential model. A realistic type of calculations for the surface state in photoemission has been done by Levine using this model which was proposed at first by Statz. In this type of potential given by $V = V_o \cos(\frac{2\pi x}{a})$, the amplitude V_o is a measure of the crystal potential strength in a mono-atomic crystal, and the ionicity in a di- atomic one. When V_o is small (large), the Mathieu potential model approaches the Nearly Free Electron(Tight Binding Approximation) limit, and thus acts as a bridge between these two extreme conditions. Davison and Levine, Slater and Carver have used the Mathieu potential to describe the energy bands in a realistic crystal. We, therefore, find that no such calculations have been done in photoemission which incorporates both the

photon field variation and the initial state derived by using the Mathieu potential model. This potential would be used to solve Schroedinger's equation, the wavefunction and its derivative being evaluated at z = 0 plane. The formulated ψ_i would be then used to calculate the photocurrent from metals and semiconductors. The final state wavefunction ψ_f will be the scattering final state of the step like potential existing at the surface defined by $V(z) = -V_o\theta(z)$, which an electron encounters when it is being transmitted through the surface. The Golden Rule formula for calculating the photocurrent density is given by

$$\frac{dj}{d\omega} = \frac{2\pi}{\hbar} \Sigma | < \psi_f|H'|\psi_i > |^2 \delta(E - E_f)\delta(E_f - E_i - \hbar\omega)\, f_o(E - \hbar\omega)\, [1 - f_o(E)] \qquad (1.1)$$

where H' is the perturbation responsible for photoemission by radiation of frequency, $|\psi_i>$ and $|\psi_f>$ refers to the initial(final) state wavefunction, $E_i(E_f)$ refers to the initial(final) state energy, $f_o(E)$ denotes the Fermi occupation function. We are considering the photoemission to take place along z-axis which is normal to the surface. We may therefore write H' as

$$H' = \frac{e}{mc}[\tilde{A}_\omega(z)\frac{d}{dz} + \frac{1}{2}\frac{d}{dz}\tilde{A}_\omega(z)] \qquad (1.2)$$

where $\tilde{A}_\omega(z) = \frac{A^z_\omega(z)}{A_o}$ with $A^z_\omega(z)$ as the component of vector potential along z-axis, A_o is the amplitude of the incident beam. The formula for photoemision cross-section can be written as

$$\frac{d\sigma}{d\Omega} \approx \frac{k^2}{\omega} | < \psi_f|\tilde{A}_\omega(z)\frac{d}{dz} + \frac{1}{2}\frac{d}{dz}\tilde{A}_\omega(z)|\psi_i > |^2 \qquad (1.3)$$

In this thesis, we have developed a simple formalism for photoemission calculation in which the free electron states are derived by using the Mathieu potential. The Mathieu potential has been at first used by Statz for surface state calculation. Levine had also used Mathieu potential for calculating the condition for arbitrary surface termination. We have used in this formalism the model as described by Davison and Steslicka for describing the crystal potential which was then used for deriving the initial state wavefunction for photocurrent calculations.

To compute the photon field, we have used the simple model of Bagchi and Kar which has been used earlier also. To determine the inital state wavefunction ψ_i , we have considered, at first an empty lattice with a finite step potential. The photocurrent was calculated as a function of photon energy ($\hbar\omega$). The formalism was then applied to the case of free electron metals like aluminium and berylium. For these metals, we have used the experimentally determined dielectric function for calculating the photocurrent through the subroutine of the main FORTRAN program. We find that in the case of Al and Be, there is a qualitative agreement between the theoretical and experimental data. We then extend this model for a finite surface potential with strong periodic lattice and apply it to solids like tungsten, molybdenum and semiconductor silicon. Using the initial state wavefunction derived with this model, we used the field obtained from the experimental data of dielectric functions and discuss the photocurrent calculations.

The topics in this thesis are arranged as follows : In Chapter 2, we shall discuss the model of dielectric response function used for the calculation of the electromagnetic field (photon field vector) for the vacuum, surface and bulk region of the solids. This photon field vector was then used to calculate the field for solids like

beryllium, molybdenum, tungsten and silicon. In Chapter 3, photoemission calculations using the Kronig-Penney model will be discussed. The dielectric model of Bagchi and Kar and also Lorentz-Drude dielectric model will be used to calculate the field which were then applied to calculate the photocurrent in the case of metals like molybdenum, copper, tungsten and semiconductors silicon and gallium arsenide. The relativistic effect in the band state calculation of photoemission is also briefly discussed in Chapter 3. In Chapter 4, we shall discuss the formulation of the initial state wavefunction by using the Mathieu potential model and discuss a number of applications.

CHAPTER 2

DIELECTRIC MODEL AND ELECTROMAGNETIC FIELD

In this chapter, we shall discuss the dielectric model used and the calculation of electromagnetic field in a solid when electromagnetic radiation is incident on it. The calculation of the fields near a surface is a complex problem and *ab initio* calculations have been done only for jellium. However, these calculations have not been exentended to other metals where the jellium model is not applicable. Further, if one wants to consider the field variation in the presence of surface for metals, e.g. d-band metals like tungsten, molybdenum, palladium,etc., one has to use simpler models. The dielectric model used by Bagchi and Kar for the case of tungsten has been used for the calculation of the electromagnetic field in the surface region. This model involves the linear interpolation in the surface region between the bulk dielectric function and the vacuum value. Though it has some deficiencies, it is important to note that it is a local response function and can be traced as shown by the application to tungsten and aluminium. It also gives good results in agreement with the experimentally determined value. Since the bulk dielectric value required for this model is obtained experimentally, the field calculation can be extended to the case of semiconductors. We will briefly describe the dielectric model used and the calculation of the electromagnetic fields from it.

2.1 **Calculation of Dielectric Model and Electromagnetic Field** :

The dielectric model used is the one given by Bagchi and Kar which is shown in Fig. (2.1). The metal is assumed to occupy the space to the left of the z-plane. In the region $-a \leq z \leq 0$, the dielectric constant is chosen to be a local function which

interpolates linearly between the bulk value inside the metal and the vacuum value(unity) outside. The model frequency-dependent dielectric function is, therefore, given by

$$\varepsilon(\omega,z) = \begin{cases} \varepsilon_1(\omega)+i\varepsilon_2(\omega), & \text{for} \quad z<-a \\ 1+[1-\varepsilon(\omega)]\frac{z}{a} & \text{for} \quad -a\le z\le 0 \\ 1, & \text{for} \quad z>0. \end{cases} \tag{2.1}$$

The incident radiation is taken to be p-polarised of frequency ω and incident on the surface at an angle of incidence θ_i . A gauge was chosen in which the scalar potential A is set equal to zero and the electromagnetic field $E(\boldsymbol{Q},\omega,z)$ is expressed in terms of the vector potential as

$$E(\boldsymbol{Q},\omega,z) = \frac{i\omega}{c} A(\boldsymbol{Q},\omega,z) \tag{2.2}$$

where $Q=\frac{\omega}{c}\sin\theta_i$. The magnetic field B(z)= $A(\boldsymbol{Q},\omega,z)$ points in the y-direction and it follows that :

$$\frac{d}{dz}\left(\frac{1}{\varepsilon}\frac{dB}{dz}\right) + \left(\frac{\omega^2}{c^2} - \frac{Q^2}{\varepsilon}\right) B = 0, \tag{2.3}$$

where $\varepsilon = \varepsilon(\omega,z)$. The electric field component can be obtained from the magnetic field as

$$\begin{aligned} E^x(\boldsymbol{Q},\omega,z) &= \frac{c}{i\omega\varepsilon}\frac{dB}{dz} \\ E^z(\boldsymbol{Q},\omega,z) &= -\frac{\sin\theta_i}{\varepsilon} B \end{aligned} \tag{2.4}$$

To solve Eq. (2.3), a new variable u(z) was introduced according to the discussion of Landau and Lifshitz which is given by $B(z) = u(z)\sqrt{\varepsilon}$. Then u(z) satisfies the equation :

$$\frac{d^2u}{dz^2} + \frac{\omega^2}{c^2}(\varepsilon - \sin^2\theta_i)\,u + [\frac{1}{2\varepsilon}\frac{d^2\varepsilon}{dz^2} - \frac{3}{4}\frac{1}{\varepsilon^2}(\frac{d\varepsilon}{dz})^2]\,u = 0 \qquad (2.5)$$

For the dielectric model used, $\frac{d\varepsilon}{dz}$ is finite only in the region $-a \le z \le 0$ and $\frac{d^2\varepsilon}{dz^2}$ vanishes everywhere except for singularities at $z = \pm a$. The vector potential $\tilde{A}_\omega(z) = \frac{E^z_\omega(z)}{E_o}$ in the long wavelength limit $(\omega\frac{a}{c}) \to 0$ is then given by :

$$\tilde{A}_\omega(z) = \begin{cases} -\dfrac{\sin 2\theta_i}{[\varepsilon(\omega)-\sin^2\theta_i]^{\frac{1}{2}}+\varepsilon(\omega)\cos\theta_i} & z < -a \\ -\dfrac{\sin 2\theta_i}{[\varepsilon(\omega)-\sin^2\theta_i]^{\frac{1}{2}}+\varepsilon(\omega)\cos\theta_i}\cdot\dfrac{ac(\omega)}{[1-\varepsilon(\omega)]z+a} & -a \le z \le 0 \\ -\dfrac{\varepsilon(\omega)\sin 2\theta_i}{[\varepsilon(\omega)-\sin^2\theta_i]^{\frac{1}{2}}+\varepsilon(\omega)\cos\theta_i} & z > 0. \end{cases} \qquad (2.6)$$

The electromagnetic fields have been calculated for photon energy below and above the plasmon energy of the metals and semiconductors. The electromagnetic fields have been for beryllium, molybdenum, tungsten and silicon. We have plotted $|\tilde{A}_\omega(z)|$ as a function of photon energy ($\hbar\omega$) and the distance (z) from the surface of the solids and the results are discussed.

CHAPTER 3

PHOTOCURRENT CALCULATIONS USING KRONIG-PENNEY MODEL

We have used the Kronig-Penney model potential to find the initial state wavefunction. The initial state wavefunction ψ_i was formulated by the method of normal matching of the wavefunctions at the boundary surface of the solid. The photocurrent was then calculated by using the electromagnetic fields developed by Bagchi and Kar. The free electron(FE) model has been successful in explaining the photoemission phenomena from free electron metals. But it has drawback in explaining the band structure effects of solid. Kronig-Penney(K-P) model has then been used for the calculations of surface electronic states by several authors. Schaich and Ashcroft have calculated numerically the photoyield by using the modified form of the Kronig-Penney model. Steslicka had done a detailed calculations of the surface states using the Kronig-Penney model both for the semi-infinite and infinite crystals. Eldib *et. al.* has also applied the Kronig-Penney model to one dimensional crystal.

3.1 **Kronig-Penney potential model** :

In this section, we shall discuss the Kronig-Penney(K-P) model as developed by Thapa *et. al.* for the calculation of photocurrent from metals and semiconductors. The Kronig-Penney model was used to represent the crystal potential field by a linear array of rectangular well (Fig. 3.1), which was later transformed into a chain of δ-function potential well such that the area of each well remains constant. The initial state wavefunction was obtained by matching at the surface.

To evaluate the initial state wavefunction $\psi_i(z)$, one can solve the one-dimensional Schroedinger's equation given by :

$$\frac{d^2\psi(z)}{dz^2} + k_i^2(z) = -2V(z)\psi(z), \tag{3.1}$$

where $k_i^2 = 2E_i$ and $V(z)$ is the δ-function potential of the K-P model.

Let $\phi(z)$ denote the Bloch wavefunction deep inside the metal and $\phi^*(z)$ the time reversal of $\phi(z)$. The eigenfuction in the semi-infinite solid $(z < 0)$ was chosen to have the form as :

$$\psi_i(z) = \phi(z) - P\phi^*(z) \tag{3.2}$$

where P is the reflection coefficient obtained by matching the wavefunction and its derivative at $z = 0$. The potential $V(z)$ was considered to be one-dimensional Kronig-Penney type given by :

$$V(z) = = \Sigma\, g\ \delta[z - (2n+1)\tfrac{d}{2}] \tag{3.3}$$

One can then show that the initial state wavefunction for the bulk, surface and vacuum regions may be written as

$$\psi_i = \begin{cases} (1 - iPe^{-i\delta}\sin\delta)e^{ik_i z} - (P - ie^{i\delta}\sin\delta)e^{-ik_i z}, & z \le 0 \\ & \text{(bulk \& surface)} \\ Te^{-\kappa z}, & z < 0 \text{ (vacuum)} \end{cases} \tag{3.4}$$

where $\cot\delta = -\frac{k_i}{g}$, δ is the phase shift introduced in the transmitted wave, g is the strength of the δ - potential which describes the bulk potential, T being the transmission coefficient across the boundary plane and $\kappa^2 = 2(V_o - E_i)$, where V_o is the potential at the surface which an electron encounters while transmitting through the boundary surface. From the matching conditions at z = 0, one can easily deduce the values of P and T in Eq. (3.4) which is given by :

$$P = \frac{(\kappa - ik_i) - (k_i - i\kappa)e^{i\delta}\sin\delta}{(\kappa - ik_i) - (k_i - i\kappa)e^{-i\delta}\sin\delta} \tag{3.5}$$

and

$$T = \frac{2k_i \sin 2\delta}{(\kappa - ik_i) + (k_i - i\kappa)e^{-i\delta}\sin\delta} \tag{3.6}$$

The proper evaluation of P and T with the correct numerical values for other factors enables one to write the most explicit form of initial state wavefunction $|\psi_i>$. The photo emission cross-section was obtained by using the formula

$$\frac{d\sigma}{d\Omega} = \frac{k^2}{\omega}\Sigma |<\psi_f|H'|\psi_i>|^2 \tag{3.7}$$

The matrix element given in Eq. (3.7) can be written as

$$I = \int_{-\infty}^{-d} \psi_f^* \tilde{A}_\omega(z)\frac{d\psi_i}{dz}dz + \int_{-d}^{0} \psi_f^* \tilde{A}_\omega \frac{d\psi_i}{dz}dz$$

$$+\frac{1}{2}\int_{-d}^{0} \psi_f^* \frac{d\tilde{A}_\omega}{dz}\psi_i dz + \int_0^\infty \psi_f^* \tilde{A}_\omega(z)\frac{d\psi_i}{dz}dz. \tag{3.8}$$

In Eq. (3.8), the final state wavefunction $\psi_f(z)$ is the scattering state of the step potential V(z) given by $V(z) = -V_o\theta(z)$. Here $V_o = E_F + \phi$, where E_F is the Fermi level and ϕ is the work function. The final state wavefunction can be written as (in atomic units) :

$$\psi_f(z) = \begin{cases} \left(\frac{1}{2\pi q_f}\right)^{\frac{1}{2}} \frac{2q_f}{q_f+k_f} e^{ik_f z} e^{-\alpha|z|}, & z \le 0 \text{ (bulk \& surface)} \\ \left(\frac{1}{2\pi q_f}\right)^{\frac{1}{2}} \left[e^{iq_f z} + \left(\frac{q_f-k_f}{q_f+k_f}\right) e^{-iq_f z}\right], & z > 0 \text{ (vacuum)} \end{cases} \quad (3.9)$$

where $k_f^2 = 2E_f$, $q_f^2 = 2(E_f - V_o)$ and $E_f = E_i + \hbar\omega$. In Eq. (3.9), the factor $e^{-\alpha|z|}$ (α is the scattering factor) is included on the surface and bulk side to take into account the inelastic scattering of the electrons. The photocurrent was calculated numerically by evaluating (3.8). The FORTRAN program used is given in Appendix- E. In our calculations, we have used the respective dielectric functions corresponding to different solids as given by Weaver and Edwards. The solids which we have used are molybdenum, copper, tungsten and silicon.

3.2 **Kronig-Penney model calculations using Lorentz-Drude dielectric model** :

In this section, we show the behaviour of photocurrent calculated by using the Lorentz-Drude model for the dielectric constant in the case of semiconductors. As discussed in the previous chapter, the existence of surface states on semiconductor surfaces was experimentally verified by using the angle integrated photoemission. The semiconductor surfaces are more complex than metal surfaces for the reason that semiconductor surfaces reconstruct. The presence of these reconstructed ions and atomic displacements on semiconductor surfaces makes the studies of electronic structure a

very interesting topic. Of the various tools and techniques, angle resolved photoemission studies has also been widely used in understanding the surface states of semiconductors. But in this section, we will be mainly concerned with the photoemission studies by adopting a simple procedure which will be applied to the case of silicon and gallium arsenide.

The Drude-Lorentz model for calculating the frequency dependent dielectric constants which is given by :

$$\varepsilon(\omega) = \varepsilon_\infty[1 - \frac{\omega_p^2}{\omega(\omega+i\gamma_1)}] + \frac{(\varepsilon_o-\varepsilon_\infty)\omega_0^2}{(\omega_0^2-\omega^2-i\gamma_2\omega)} \qquad (3.10)$$

In Eq. (3.10) above, ε_o and ε_∞ are the static and high frequency dielectric constants. By using the appropriate values of constants ε_o , ε_∞ , γ_1, γ_2 etc. respectively for silicon and gallium arsenide, the real and imaginary parts of $\varepsilon(\omega)$ were calculated. Using the electromagnetic fields for p-polarized radiation, we calculate the photoemission cross-section by evaluating the matrix element in Eq. (3.9). and applied to the case of silicon and gallium arsenide. In our calculations though we have not taken into consideration the effect of type of semiconductor, density, etc., we find that the spatial dependence of vector potential is an essential ingredient in photoemission calculations. It would be more realistic if one can employ the method as developed by Cappellini *et. al.* which is specifically defined only for the semiconductors. Further, the inclusion of crystal structure into this type of calculations will enable one to compare the data with experiment in a more realistic way. For example, a detailed study of photoemission from gallium arsenide by using the one-step model of photoemission had been done by Schattke. The photoemission data for the ideal gallium arsenide surface agreed well with the experimental data.

3.3 Relativistic Kronig-Penney potential model calculation of photoemission :

In the above treatments of photoemission calculations both in the case of metals and seminconductors, the spin of the electrons in the formulations of the initial state wavefunctions were not taken into considerations. This implied that the relativistic effects were omitted and it was purely a non-relativistic type of calculations. We have considered in the same way the variations of the dielectric functions for the calculations of the photon fields but adopted the wavefunctions for the initial state of the electrons as developed by Davison and Steslicka. We have introduced the surface of width '*d*' into the potential model and used the wavefunctions for the evaluation of the matrix elements for photocurrent calculations. The model was applied to the case of heavy atomic solids like tungsten and silicon.

The crystal potential model as used by DS for deriving ψ_i has a surface width d. The crystal potential is given by $LtV_3 b = a_o$ with b as the width of

$$V_3 \to 0$$

$$b \to 0$$

the potential barrier and (a+b) the period of the potential, a_o being a positive quantity. On solving the one-dimensional time-independent Dirac equation, we get :

$$i\hbar c\frac{d\phi_k^{(1)}}{dx} = (\varepsilon_o - V_k)\phi_k^{(2)} \qquad (3.11)$$

and

$$i\hbar c\frac{d\phi_k^{(2)}}{dx} = \{(\varepsilon_o - V_k) + 2m_o c^2\}\phi_k^{(1)} \qquad (3.12)$$

Decoupling Eqs. (3.11) and (3.12) leads to

$$i\hbar c\frac{d\phi_k^{(j)}}{dx} = -\rho_k^2\phi_k^{(j)}, \qquad j = 1,2 \qquad (3.13)$$

where wave vector $\rho_k^2 = (\varepsilon_o - V_k)[(\varepsilon_o - V_k) + 2m_oc^2]/\hbar^2c^2$.

The plane wave solution of Eq. (3.13) for bulk (x>0) and vacuum (x<0) regions can be written as :

$$\psi_i(x) = \begin{cases} \phi_2(x) = a_2^{(2)}\left\{\begin{pmatrix} -\gamma_2 \\ 1 \end{pmatrix}e^{i\rho_2 x} + \lambda\begin{pmatrix} \gamma_2 \\ 1 \end{pmatrix}e^{-i\rho_2 x}\right\}, & x > 0 \\ \phi_1(x) = \begin{pmatrix} \gamma_1 \\ 1 \end{pmatrix}\beta_1^{(2)}e^{l_1 x}, & x < 0 \end{cases} \qquad (3.14)$$

where $l_1 = -i\rho_1 > 0$ and is real. The constants in Eq. (3.14) are defined as

$$\varepsilon_o = \varepsilon - m_oc^2, \qquad a_k^{(1)} = -\gamma_k a_k^{(2)},$$

$$\beta_k^{(1)} = \gamma_k\beta_k^{(2)}, \qquad \gamma_k = \frac{\varepsilon_o - V_k}{\hbar c\rho_k}, \quad \text{and} \quad \lambda = \frac{\beta_2^{(2)}}{a_2^{(2)}} = \frac{1-e^{i(\rho_2-\mu)a}}{e^{-i(\rho_2+\mu)a}-1}.$$

μ is the wave number and is given by $\mu = \frac{n\pi}{a} + i\zeta$ where ζ is real and $\zeta > 0$.

The final state wavefunction ψ_f which is correctly normalized in energy will be the scattering state of the step potential $V_1 = -V_o\theta(x)$, where $\theta(x)$ is a unit function. The vector potential A is assumed to be a constant in the bulk and vacuum

regions but in the surface region, it is a function of x as the solution of Maxwell's equation for dielectric function $\in(x)$. The formula for the vector potential in one-dimension following Bagchi and Kar is given by

$$A_\omega(x) = \begin{cases} A_1, & x < 0 \text{ (bulk)} \\ \frac{A_1 \in(\omega) d}{[\in(\omega)-1]x+d}, & -d \leq x \leq 0 \text{ (surface)} \\ A_1 \in(\omega), & x > 0 \text{ (vacuum)} \end{cases} \qquad (3.15)$$

where A_1 is a constant depending on dielectric function $\in(\omega)$, photon energy $\hbar\omega$ and angle of incidence θ_i.

We have calculated photocurrent against the incident photon energy ($\hbar\omega$) as a function of the band number (n) in the case of W and Si for n = 2,4,6,8,10. The photoemission calculations in the case of W and Si using the non-relativistic Kronig-Penney(NR-KP) model have been done earlier. However, the behaviour of photocurent data in RKP case is completely different from that of NR-KP model.

The interesting feature which is seen in both the case of W and Si is that for the increase in band numbers the peak in photocurrent also goes on increasing. The only difference is that in the case of W, the highest peak on photocurrent is observed at $\hbar\omega - \hbar\omega_p$ (plasmon energy of tungsten which is 26 eV), whereas for Si it is obtained at photon energy 20 eV which is greater than its plasmon energy. This can be attributed to the fact that the band width ΔE_b goes on decreasing for the increase in band number. In other words, the relativistic correction reduces ΔE_b which causes the electrons to gain sufficient momenta due to rapid spatial variation of the incident radiation to be photoexcited. This causes the enhancement of photocurrent with the increase in n in

both the cases of W and Si. In both the NR-KP and RKP treatment of photoemission, we find that only in the low frequency region photoemission is dominant due to spatial variation of the photon field vector. But the occurrence of peaks in photoemission by using the RKP model may be described as the manifestation of band structure effects in photoemission which has not been observed in the NR-KP cases. However, the occurrence of peaks in photocurrent data in the case of the relativistic treatment is attributed mainly due to inclusion of relativistic effects in photoemission.

The main drawback of including the initial state wavefunction ψ_i as derived by DS is that it does not take into account the surface width. It has been well defined for both the vacuum and bulk regions. Further, we have not done any detailed calculations to derive the initial state wavefunction ψ_i. We also conclude from this study that the incorporation of the spatially variant vector potential is not sufficient. Further, the measured ultraviolet photoemission spectra(UPS) data have shown that effects due to spin-orbit coupling cannot be omitted in photoemissin spectra. Also the solution of Schrodinger's equation without the inclusion of spin-orbit interaction will become more and more inadequatein photoemission spectral measurements. One has to also modify the calculation for vector potential keeping in view the relativistic effects. There is, therefore, a need for relativistic theory of photoemission for accurate presentation of the UPS data.

CHAPTER 4

PHOTOCURRENT CALCULATIONS USING MATHIEU POTENTIAL MODEL

In the previous chapters, we have seen that photocurrent calculations was done by using various potential models in the case of metals and semiconductors. For example, free electron and Kronig-Penney potential models were used in the case of beryllium, tungsten, copper, silicon, etc. Photoemission studies were also carried out in the case of tungsten and silicon by using the relativistic Kronig-Penney model. We found that in the case of copper, Kronig-Penney model did not fit well since the plot did not show peak in photocurrent below the plasmon energy. With the increase of photon energy, the photocurrent also did not show a minimum at the plasmon energy. In the case of copper, maxima in photocurrent was measured at $\hbar\omega = 20$ eV with a minimum at $\hbar\omega = 26$ eV. Also, the application of relativistic Kronig-Penney model to W and Si showed too many peaks in photocurrent with the increase of photon energy. This is quite a different trend in the behaviour of photocurrent. These results do not conform to the calculated and measured data in photoemission when one is usually concerned with the variation of photocurrent against photon energy especially from the surface of metals. For this reason, we have applied Mathieu potential model to evaluate the initial state wavefunction to calculate the matrix element in photocurrent by using the same dielectric model as used in the earlier chapters. The photocurrent data obtained in this formalism could explain the behaviour of photocurrent also in the case of copper.

In this chapter, we shall use the Mathieu Potential model to represent the crystal potential. In this model, the potential is represented by a periodic sinusoidal wave in one-dimensional crystal. For such a potential, the Schrodinger equation reduces to the *Mathieu equation* whose solutions have been discussed in detail by McLachlan. The Mathieu potential had been used early by Brillouin and Morse. Brillouin had used this model as an appropriate model for developing the energy band theory of solids, while Morse used it in his study of electron diffraction. Slater used the Mathieu potential problem in one, two and three dimensions to describe the energy bands in a realistic crystal. Then Carver has discusssed the symmetries of Mathieu functions, and the relations between the functions and the electron wave functions at the centres and edges of the crystal bands. The Mathieu potential has been at first used by Statz for surface state calculation. Levine has used Mathieu potential for calculating the condition for arbitrary surface termination. In this chapter, we will discuss a formalism developed for photoemission calculations in which the electron states are derived by using the Mathieu potential. Two cases will be discussed namely, the effects of the empty lattice and strong periodic lattice potential on the electronic states for deriving the initial state wavefunctions as described by Davison and Steslicka.

4.1 **Empty Potential with Finite Surface :**

Let us consider a one-dimensional crystal whose potential is represented by a sinusoidal potential given by

$$V(x) = V_o \cos(\frac{2\pi x}{a}) \qquad (4.1)$$

where 'a' is the period of the potential having a maximum value V_o at x = 0.

The one-dimensional Schrodinger equation can be written as

$$\psi''(z) + (a - 2q\cos 2z)\psi(z) = 0 \qquad (4.2)$$

where $z = \frac{\pi x}{a}, T = \frac{\pi^2}{a^2}, a \approx \frac{E}{T}$ and $2q = \frac{V_o}{T}$

Eq. (4.2) is the Mathieu equation and its solution is derived for free electron or empty potential (q ~ 0) when the crystal potential is flat as shown in Fig. (4.1). To determine the initial state wavefunction $\psi_i(x)$ in Eq. (4.2), we have included a surface of width (d) in the crystal potential. The initial state wavefunction for the bulk and surface and for the vacuum regions is given by

$$\psi_i(x,q) = \begin{cases} (\frac{1}{4\pi k_i})^{\frac{1}{2}} \phi(x_0,q) e^{-\mu(x_o - x)} & x \leqslant 0 \\ (2\xi)^{\frac{1}{2}} e^{-\xi(x - x_o)} & x > 0 \end{cases} \qquad (4.3)$$

where x_0 = location of the crystal surface. In Eq. (4.3) above, we have $k_i = \sqrt{2E_i}$ and

$$\phi(x_0,q) = \lambda\cos m'x - \sin m'x,$$
$$\lambda = \tan m'(x_0 - \xi^{-1}). \qquad (4.4)$$

such that $m' = \frac{m\pi}{a}$, m being the band gap index, ξ is the height of step potential and λ is the hybridization parameter.

Using the final state wavefunction ψ_f as the scattering state of the step potential at x = 0, the photocurrent density is calculated by using the Fermi golden rule formula as

$$\frac{dj(E)}{d\Omega} = \frac{2\pi}{\hbar}\Sigma |<\psi_f|H'|\psi_i>|^2 \delta(E-E_f)\delta(E_f-E_i-\hbar\omega) f_o(E-\hbar\omega)[1-f_o(E)] \tag{4.5}$$

Here the perturbation is given by

$$H' = \frac{e}{2m_e c}(\boldsymbol{p}.\boldsymbol{A}+\boldsymbol{A}.\boldsymbol{p}) \tag{4.6}$$

and in one dimension, H' can be written as

$$H' = \frac{e}{mc}[\tilde{A}_\omega(x)\frac{d}{dx} + \frac{1}{2}\frac{d}{dx}\tilde{A}_\omega(x)]$$

To compute the photon field, we have used the simple model of Bagchi and Kar which has been used earlier also. With simple modification the photon field used in our calculation can be written as

$$\tilde{A}_\omega(\omega,x) = \begin{cases} A_1, & x<-d \\ \dfrac{A_1.\varepsilon(\omega).d}{[1-\varepsilon(\omega)]x+d}, & -d \leqslant x \leqslant 0 \\ A_1.\varepsilon(\omega), & x>0 \end{cases} \tag{4.7}$$

where A_1 is a constant depending on the dielectric function $\varepsilon(\omega)$, photon energy $\hbar\omega$ and angle of incidence θ_i. We have chosen $x_0 = \frac{a}{2}, \xi = \frac{12}{a}$ and $m = 1$. The reason

for the choice of m = 1 is that the surface state exists in the band gap for finite potential case. The matrix element in Eq. (4.5) can be written as the following for calculating the photocurrent :

$$I = \int_{-\infty}^{-d} \psi_f^* \tilde{A}_\omega(x) \frac{d\psi_i}{dx} dx + \int_{-d}^{0} \psi_f^* \tilde{A}_\omega \frac{d\psi_i}{dx} dx$$

$$+\frac{1}{2} \int_{-d}^{0} \psi_f^* \frac{d\tilde{A}_\omega(x)}{dx} \psi_i dx + \int_{0}^{\infty} \psi_f^* \tilde{A}_\omega(z) \frac{d\psi_i}{dx} dx. \qquad (4.8)$$

Photocurrent was calculated as a function of photon energy ($\hbar\omega$) by evaluating the integrals in Eq. (4.8). The formalism was then applied to the case of metals aluminium and beryllium as they are free electron type of metals. We see from the variation of photocurrent data that even in the case of Al and Be, it showed the qualitative behaviour as seen earlier in the theoretical and experimental data. The features seen in the behaviour of photocurrent in Al and Be can be attributed to the fact that in the free electron metals the change in bulk potential is too weak to impart sufficient momentum for photoexcitation. The surface photo-effect is due to the rapid variation of photon field in the surface region. This is evident from the matrix element in Eq. (4.5) where $d\tilde{A}_\omega/dx$ is directly dependent on photocurrent as the photon energy passes through the threshold for plasmon excitation. Moreover, we have considered a low photon energy photoemission, hence the incident radiation is too weak to photoexcite electrons from the bulk bands. The origin of peak in photocurrent data in the case of Be for $\hbar\omega < \hbar\omega_p$ has been explained by Karlsson *et. al.* from band picture. He attributed this to the existence of surface state at $\bar{\Gamma}$ with energy 2.8 eV in the bulk energy band gap $\Gamma_3^+ - \Gamma_4^-$.

4.2 **Strong Periodic Potential with Finite Surface** :

The case of empty lattice potential is not applicable to the strongly bonded metals like d-band metals or semiconductors. Hence one needs to develop the intial statre wavefunctions by solving the Mathieu equation in Eq. (4.2) by incorporating the sine and cosine elliptic functions. We have considered the same model as in the case of empty lattice potential model , but used for strong periodic lattice (i.e. q > 0).

It is therefore, necessary to find an explicit form for $\phi(x'_{0,}q)$ in Eq. (4.3) to derive the intial state wavefunction $\psi_i(x)$. The most general form is a linear combination of all the bulk standing states $se_m(x'_{0,}q)$ and $ce_m(x'_{0,}q)$ for all the Fermi energy gap m . Thus the surface states will be largely a hybrid of sine and cosine elliptic functions which is given by

$$\phi(x'_{0,}q) = \lambda_m ce_m(x'_{0,}q) - se_m(x'_{0,}q) \tag{4.9}$$

where λ_m is the hybridization parameter which can be written as

$$\lambda_m = \frac{se_m(x'_{0,}q) - (\xi+\mu)^{-1} se'_m(x'_{0,}q)}{ce_m(x'_{0,}q) - (\xi+\mu)^{-1} ce_m(x'_{0,}q)} \tag{4.10}$$

Here $se_m(x'_{0,}q)$ and $ce_m(x'_{0,}q)$ are the sine and cosine elliptic functions in Eq. (4.9). These functions in expanded form can be written as

$$se_m(x'_{0,}q) = \sin mx'_0 - \frac{q}{4}\left[\frac{\sin(m+2)x'_0}{m+1} - \frac{\sin(m-2)x'_o}{m-1}\right] + \frac{q2}{32}\left[\frac{\sin(m+4)x'_o}{(m+1)(m+2)} + \frac{\sin(m-4)x'_o}{(m-1)(m-2)}\right] + ... \tag{4.11}$$

and $$ce_m(x'_{0,}q) = \cos mx'_0 - \frac{q}{4}\left[\frac{\cos(m+2)x'_0}{m+1} - \frac{\cos(m-2)x'_o}{m-1}\right]$$

$$+\frac{q2}{32}\left[\frac{\cos(m+4)x'_o}{(m+1)(m+2)} + \frac{\cos(m-4)x'_o}{(m-1)(m-2)}\right] + ... \qquad (4.12)$$

For finite surface potential, surface state existence condition implies that

$$x'_0 = x_0\tfrac{a}{2},\ \xi = \tfrac{12}{a},\ \lambda > 0 \ \text{ and } \ m = 3, 5, .. \qquad (4.13)$$

We are considering surface state occuring for m = 3 and hence from Eqs. (4.11), (4.12) and (4.13), we can write,

$$ce_3(x'_o, q) = 0 \ , \qquad ce'_3(x'_o, q) = 3(1 + \frac{q}{16} - \frac{q^2}{640})$$
$$se_3(x'_o, q) = -1 + \frac{q}{16} - \frac{11}{640}q^2 \ , \qquad se_3(x'_o, q) = 0 \qquad (4.14)$$

Hence, we may obtain the value of λ_3 as :

$$\lambda_3 = \frac{(\xi+\mu)\left[1 - \frac{q}{16} + \frac{11}{640}q^2\right]}{3(1 + \frac{q}{16} - \frac{q^2}{640})} \qquad (4.15)$$

Using Eqs. (4.13) and (4.14) into Eq. (4.9), the intial state wavefuntion in the case of strong periodic potential becomes

$$\psi_i(x_{\beta}q) = \begin{cases} (\frac{1}{4\pi k_i})^{\frac{1}{2}}(-1 + \frac{q}{16} - \frac{11}{640}q^2)e^{-\mu(x'_o - x)} & x \leqslant 0 \\ (\frac{1}{4\pi k_i})^{\frac{1}{2}} e^{-\xi(x - x'_o)} & x > 0 \end{cases} \qquad (4.16)$$

The final state wavefunction ψ_f as the scattering state of the step potential and photon field vector of Eq. (4.7) is used for computing the photocurrent by evaluating the matrix element in Eq. (4.8). Photocurrent was calculated as a function of photon energy ($\hbar\omega$) in the case of d-band metals like molydenum, tungsten, copper and semiconductor silicon. For each of these metals, the experimentally determined dielectric function were used for calculating the photon fields but the same surface parameters were used for all of these solids as it is a model calculation. The photocurrent data showed the experimental behaviour in photocurrent as measureed by Weng *et. al.* But the only difference in their case was that the photocurrent decreased to minimum at the plasmon energy. The plasmon energies for W and Mo are 25.3 eV and 24.4 eV respectively. For a narrow surface width(d = 0), the behaviour of photocurrent is completely different. We did not find any prominent peak for the values of photon energy below and above 15 eV photon energy.

It has been reported by Himpsel and Ortega that for Cu(100), Fermi level photoemission intensity when plotted as a function of photon energy, the data showed maxima at $\hbar\omega$ = 10.5 eV. Similar reports were also given by Eastman *et. al.* but with maximum intensity occuring at $\hbar\omega$ = 10.6 eV. In our case, our model calculations has shown peak in photocurrent at $\hbar\omega$ = 10 eV. The occurence of such peak in photocurrent in the band structure had been attributed to transition energy between the lower and upper s-p branch either at Fermi level or near it and has Δ_5 symmetry. The case of photocurent for narrow surface width just produced a linear line of very negligible magnitude in photocurrent. We find that Cu has shown atleast the qualitative feature with the behaviour of photocurrent as indicated also by other metals like Pd, W, Si, etc. which were calculated earlier.

We also have calculated the wavefunction given in Eq. (4.16) to see whether this can reproduce the results calculated in the case of empty potential ($q \sim 0$) and for surface state condition $m = 1$. This was then applied to the case of Al and Be. It was seen that the photocurrent data was exactly the same as reported earlier both for Al and Be respectivley, which was shown in Fig. (4.2). In our calculations, we have included the case of narrow surface width. The reason for inclusion of narrow surface width is that it considers the Fresnel type of electromagnetic field. In Fresnel optics, the spatial variation of the photon field is not taken into consideration.

A study of these cases show that one can also make use of Mathieu type of potential in photoemission calculations. Though the model used is very simple, however, the inclusion of initial state wavefunction into the matrix element appears to produce the qualitative features as observed earlier in the experimentally measured data of photocurrent. The main drawback of the model used is that the same initial state wavefunction ψ_i is used to describe both the surface and bulk regions of the solids under study. Also, we have used the same initial state energy for all the cases and also keeping constant the other parameters as it is a model calculation. However, it is interesting to note that the wavefunctions formulated for strong periodic potential easily reproduces the wavefunctions for empty potential(free electron) cases. It would be further interesting to extend such type of model to include the band structure effects in the electronic structure calculations.

THEORETICAL STUDY OF PHOTOEMISSION FROM METALS AND SEMICONDUCTORS

By
Zaithanzauva Pachuau
Department of Physics

Submitted
in partial fulfillment of the requirement of the
Degree of Doctor of Philosophy in Physics of
North Eastern Hill University, Shillong

Dedicated to my mother Sawmi who cares and loves me

TABLE OF CONTENTS

The North Eastern Hill University
Department of Physics
September **2001**

I, Zaithanzauva Pachuau, hereby declare that the subject matter of this Thesis is the record of work done by me, that the contents of this Thesis did not form basis of the award of any previous degree to me or to the best of my knowledge to anybody else, and that the Thesis has not been submitted by me for any research degree in any other University/Institute.

This is being submitted to the North Eastern Hill University for the degree of Doctor of Philosophy in Physics

(ZAITHANZAUVA PACHUAU)
Candidate

6.9.01

(DR. M.K. PARIDA)
Professor & Head
Department of Physics
North-Eastern Hill University

Professor & Head
Department of Physics
North Eastern Hill University
Shillong-793022

पूर्वोत्तर पर्वतीय विश्वविद्यालय
पू० प० विवि० परिसर, शिलांग-७९३०२२ (मेघालय)
North-Eastern Hill University
NEHU Campus, Shillong - 793 022 (Meghalaya)

Phone :
Grams : NEHU

CERTIFICATE

This is to certifiy that the thesis entitled" Theoretical Study of Photoemission from Metals and Semiconductors " submitted by Mr. Zaithanzauva Pachuau for the degree of Doctor of Philosophy in Physics of North-Eastern Hill University, Shillong, embodies the record of original research investigations carried out by him under our supervision. He has been duly registered and the thesis presented is worthy of being considered for the award of the Ph.D. degree. This work has not been submittted elsewhere for the ward of a degree.

(DR. D.T. KHATHING)
Professor of Physics
North-Eastern Hill University
Shillong-793022
Supervisor

1/9/01

(DR. R.K.THAPA)
Reader
Department of Physics
Pachhunga University College
Aizawl, Mizoram
Joint Supervisor

ACKNOWLEDGEMENT

I would like to thank first of all, my Research Supervisor Prof. D.T. Khathing, Department of Physics, North-Eastern Hill University, Shillong-793022 (India) for his encouraging guidance and help during my works related to this thesis. I would like to thank especially my Joint Supervisor Dr. R.K. Thapa, Reader, Department of Physics, Pachhunga University College, Aizawl, Mizoram for his constant guidance, help, support and so much encouragements without which I could not have completed my research works. It was him who got me introduced into this area of Solid State Physics. He further developed inside me the scientific temperament and suggested the topic of research investigation which is reported in this thesis.

I would take this opportunity to thank Dr. P.K. Patra, Department of Physics, Pachhunga University College, Aizawl and Mr. B. Zoliana, Department of Physics, Govt. Zirtiri Residential Science College, Aizawl for all their great help and cooperations.

I would also like to thank the Faculty Members of the Department of Physics, North-Eastern Hill University, Shillong for their kind help and encouragements during my stay at the Department.

Prof. S.G. Davison and Mrs. Prue Davison, University of Waterloo, Ontario, Canada have been helpful to me by providing several literatures and also the journal Progress in Surface Science regularly.

Dr. N. Kar, Department of Physics, North Bengal University, Darjeeling, West Bengal has also helped me with several relevent literatures. Mrs. K. Thapa has always been very kind to me and thanks for her hospitability.

Lastly, this work would not have been completed without the physical and moral support of my family.

Dated : 5th Sept. , 2001

Department of Physics
North-Eastern Hill University
Shillong-793 022

(Zaithanzauva Pachuau)

CHAPTER 1

INTRODUCTION

Photoelectron spectroscopy has been used as a method for studying the electronic properties of solids which was mainly determined by two considerations viz. the experimental and the theoretical approach. As a first step, the preparation of a clean emitter surface was important which was much dependent on ultrahigh vacuum techniques. For the detailed study of experimental data, the demand for high quality instruments, the design of electron energy analyser of high resolving power and angular selectivity, etc. were increasingly high. With the production of synchrotron radiation facilities, it has provided great advantage for the calculations of the energy levels of electronic states. Now, the use of high technology computers has made the possibility of accurate calculations of band structure. However, to know the details of photoemission and to formulate a theoretical framework, the knowledge of the electronic properties of surfaces was quite necessary.

The early theoretical study of photoelectric emission from solids was based on Sommerfeld's free electron model of a metal. With this model, the experimentally observed frequency dependence of the total photoelectric yield near the work function[1] can be explained. But this model could not explain the momentum associated with the excited photoelectrons. However, Tamm and Schubin[2] has proposed two possible solutions arising from the conservation of momentum viz. the potential step at the surface and the periodic potential variation arising from the ion cores of the lattice, and these two potentials give rise to surface photoeffect and volume photoeffect

respectively. The surface photoeffect was considered to be the dominant source of photoemission[3-5] in free electron metals. The results on alkali metals have supported this so that photoemission was regarded as a surface effect rather than a bulk effect.

However, during this period of development in the theory of a surface photoeffect, the band theory of solid was being improved considerably. The photoemission experiments were performed over wider range of wavelength on many solids, including semiconductors. It became evident that the surface photoeffect could not explain all these results. Fan[6] showed that a volume photoeffect might be comparable to the surface photoeffect. This idea was later developed by Mayer and Thomas[7], and by Puff [8]. Kane[9] has pointed out that the bulk band structure of a single-oriented crystal could be explained from the measurements of energy distribution and momenta of the emitted photoelectrons. The experimental result by Gobeli, Allen and Kane[10] has shown that such assumptions were valid and also could explain the angular distribution of the photoemitted electrons.

The experimental work on semiconductors by Gobeli and Allen[11], and on metals by Berglund and Spicer[12] has further supported the theoretical works. The volume photoeffect was then used to explain the photoemission spectra and the band structure calculations of solids. This photoeffect was expressed in terms of the *three-step model* as explained in detail by Berglund and others[13,14]. As the energy and angular resolution of the experimental system became increased and single crystal faces were studied with the synchrotron radiation, it was clear that several drawbacks existed. Some were explained in terms of a possible lack of conservation of momentum in the bulk photo-excitation process[15], but the problem of interpretation was not solved. When photoemission from the surface states on metals[16] were studied, it was found

that the surface was indeed contributing to the photocurrent. It was also observed that photoemission has occurred corresponding to the regions of energy-wave vector space that constituted a forbidden band gap on the allowed states of the bulk solid[17]. This was eventually regarded as the surface photoemission.

These results clearly indicated the need to incorporate both the surface and volume effects in order to explain photoemission. Schaich and Ashcroft[18] have used a quadratic response formalism to describe the photoemission process, but the dielectric response function was not defined for the surface. They used a computationally simple model to study the electronic structure in solids and surfaces in order to explain photoemission. In this model, the spatial dependence of the vector potential was neglected and it was assumed to be constant. A more realistic approach was considered by Mahan[19] who extended a wave mechanical scattering theory, that was originally proposed by Adawi[20]. This approach regarded the wavefunction of the emitted electron as equivalent to that used in *Low Energy Electron Diffraction* (LEED) calculation by Pendry[21], but in a time-reversed state. It was noted that by treating the emitted electron in terms of its final state wavefunction, such a formulation could avoid many difficulties inherent in the *three-step model* of Berglund and others[13,14]. Mahan[19] has shown that such approach could provide a theoretical formulation for determining the observed angular dependence of photoemission from solids. These developments were generally concerning with ultraviolet photoemission spectroscopy (UPS). However, instrumental innovation in X-ray photoelectron spectroscopy (XPS) has developed the process of calculations of the inner core levels of solids. In fact, both UPS and XPS can provide the information with regard to surface state as well as the bulk band structure. The UPS is widely used as a method for determining the electronic states of the surface and the

bulk of a solid. Moreover, UPS has a great advantage over the other methods of investigation due to the high absorption coefficient of UV radiation and the small escape depth of the electrons from the solid. Now, angle-resolved ultraviolet photoemission spectroscopy (ARUPS) allows the measurement of the energy and momentum of the photoemitted electrons, and it can be used to explain the electronic structure of the surface and the bulk of solid. In the UPS experiments, UV radiation in the range of 10-300 A^{o} excites electrons which are within the escape depth and can get out of the solid. The small value of the escape depth in the range of 10-100 A^{o} makes photoemission a useful method for surface studies. The variation of photon energy leads to a variation in escape depth so that the relative importance of the surface and the bulk effects can be varied.

In the measurement of the energy distribution of the emitted electrons, two types of energy analyser are usually used. In the first method, electrons emitted in all angles are collected in a hemi-spherical analyser which is known as angle-integrated ultraviolet photoemission spectroscopy. The second method which is known as angle-resolved ultraviolet photoemission spectroscopy (ARUPS), can analyse the energy of the electrons emitted at a fixed angle which gives rise to the energy distribution curve. By determining the momentum of electrons which shows maximum on the curve and by measuring the change in energy positions of the maxima on the curve with the change of momentum, one can determine the energy-wave vector relationship. The absolute value of the momentum (k) of the electron can be determined from the relation $E = \frac{h^2k^2}{2m}$.

Figure (1.1) illustrates the method of ARUPS. The UV radiation is incident on the crystal at an angle $\theta_i = 45^\circ$ with respect to the normal. The angle of the electron energy analyser can be varied between 0° and 90°. One can determine the energy and angular distribution of the emitted electrons as a function of the energy, polarisation and angle of incidence (θ_i) of the applied radiation. The theoretical explanation of such data clearly requires a detailed knowledge of both the electronic structure of the photoemitting solid and its interaction with radiation.

The probing of bonding of atoms which lie in the outermost layer of a solid has been studied by photoemission spectroscopy. But the detailed interpretation of photoemission data requires the use of photoemission theory which should be able to calculate the initial and final state wavefunctions of the electron, and also the spatial form of the vector potential which is involved on the photoemission matrix element. The calculation of self-consistent wavefunctions corresponding to electron states below the vacuum level for semi-infinite solids[22,23] had been done earlier. The techniques for the calculation of electron energies in the range 30 - 300 eV and above the vacuum level had been then developed. But these techniques have drawbacks for calculation of the electromagnetic fields which excites photoelectrons especially from the surface of solid. One should incorporate the variation of the electromagnetic field in the presence of the surface. The calculation of the vector potential has made a difficult problem in general case. In most of the calculations, therefore, one usually proceeds with the assumption of spatially constant vector potential. However, in certain conditions one has to include photon field variation to obtain a good agreement with the experimental data.

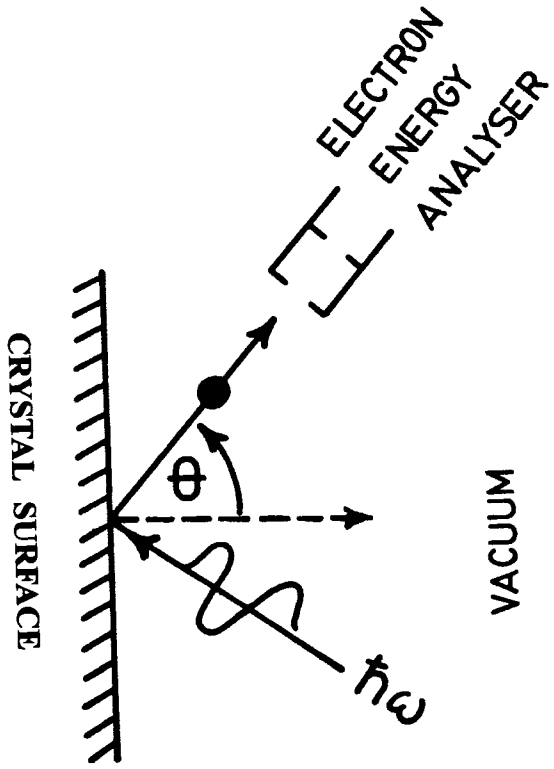

Figure 1.1

A simple calculation of photocurrent involves the evaluation of the matrix element $< \psi_f|H'|\psi_i >$ where ψ_i and ψ_f are the initial and final one-electron states whose energies are related by $E_f = E_i - \hbar\omega$. The perturbation in the Hamiltonian responsible for the photoexcitation of electron is given by

$$H' = \frac{e}{2mc}(\boldsymbol{p}\cdot\boldsymbol{A} + \boldsymbol{A}\cdot\boldsymbol{p}) \qquad (1.1)$$

where $\boldsymbol{p}$ is the one-electron momentum operator and $\boldsymbol{A}$ is the vector potential. We are considering the photoemission to take place along z - axis which is normal to the surface. We may, therefore write the perturbation H' in one-dimension as

$$H' = \frac{e}{mc}[\tilde{A}_\omega(z)\frac{d}{dz} + \tfrac{1}{2}\frac{d}{dz}\tilde{A}_\omega(z)] \qquad (1.2)$$

where $\tilde{A}_\omega(z) = \frac{A^z_\omega(z)}{A_o}$ with $A^z_\omega(z)$ as the component of vector potential along z-axis, A_o is the amplitude of the incident beam. In the standard calculation of photoemission, the one-electron states are calculated with a high degree of accuracy but the variation of photon field is generally neglected. When one considers the photocurrent as a function of the photon energy with constant initial state, the photon field variation in the surface needs to be taken more carefully. This is evident from the second term in Eq. (1.2). A first principle calculation of the electromagnetic field in the presence of surface is an extremely complex problem. The calculation of the vector potential in the surface region, therefore needs a detailed microscopic analysis of the surface in terms of the dielectric response function.

Several authors[4,18,19,24] have derived the photocurrent due to the interaction of the electromagnetic field with the solid. The photocurrent density formula may be written with the help of Fermi golden rule[25] as

$$\frac{dj(E)}{d\Omega} = \frac{2\pi}{\hbar}\Sigma |< \psi_f|H'|\psi_i >|^2 \delta(E - E_f)\delta(E_f - E_i - \hbar\omega) f_0(E - \hbar\omega)[1 - f_0(E)] \quad (1.3)$$

In Eq. (1.3), E_i and E_f are the initial and final state energy, f_0 is the Fermi occupation function, δ - function describes the conservation of energy. The formula for photoemision cross-section can be written as

$$\frac{d\sigma}{d\Omega} \approx \frac{k^2}{\omega} |< \psi_f|\tilde{A}_\omega(z)\frac{d}{dz} + \frac{1}{2}\frac{d}{dz}\tilde{A}_\omega(z)|\psi_i >|^2 \quad (1.4)$$

Thus, we see that the calculation photocurrent density is based on the evaluation of matrix element $< \psi_f|H'|\psi_i >$.

Several authors have done photocurrent calculations by using various methods. Endriz[26] has used the modified form of the Mitchell-Makinson time-dependent perturbation calculation of the surface photoeffect. He calculated the photocurrent by using the hydrodynamic approximation and applied it to the case of aluminium and other alkali metals. The photocurrent data for photon energy at plasmon energy agreed with the experimental data. However, the model of Endriz did not reproduce the experimental data of Petersen and Hagstrom[27] which showed a maximum at 12 eV in the photoemission cross-section. Schaich and Ashcroft[18] had also used the Kronig-Penney (KP) model to incorporate the band structure effects of photoemission.

The calculation of the matrix element in Eq. (1.3) involves the knowledge of ψ_i and ψ_f. Liebsch[28], Pendry[29] and others have recognised that the calculation of ψ_i and ψ_f was in principle, similar to LEED calculation. They considered the solid to be a stack of identical layers terminated at the surface. The final state was shown to be a time-reversed LEED state. As for example, Pendry has given a detailed method of calculation using this method and developed a detailed program for application to real system with success. In his calculations, the initial and final states were computed quite accurately but however, the vector potential was taken to be a constant. Pendry has recognised that the vector potential would vary in the surface region but taking the exact account of spatial variation was a complex problem. Also by taking A to be a constant, it has simplified the calculation of the matrix element. This method of calculation has been successful in different cases. However, for the case of photocurren calculations from a constant initial state, the method did not give a good result especially near the plasmon energy.

Feibelman[30] has proposed that if the theory of surface electromagnetic field is to be used for interpreting the results of photoemission experiments, one should use a scheme of calculation to obtain the correct responses of the field in the presence of the surface. This concept has led Feibelman to introduce the *Random Phase Approximation* (RPA) dielectric tensor to study the plasmon dispersion and the microscopic refraction problem. In the RPA calculation, the surface is considered smooth and the dielectric response naturally includes the effect of electron spill-out in the region of the dipolar layer. The only inputs are the electron radius (r_s) and the one-electron surface potential barrier. The potential barrier completely determines the electronic structure of the surface. This can be taken to be the output of a self-consistent jellium ground state calculation. The RPA is exact for the bulk electron

gas ($r_s = 0$) where it assumed that the one-electron wavefunction and the energies are based on a Hartree-Fock type calculation. As the electron gas is not infinite, therefore, RPA is not only unreal but also not clear for the first correction to apply. The significance of RPA lies in the fact that it incorporates many electron effects that are expected to be important. The prediction of RPA agrees well with the photoemission experiments that describe the nature of electromagnetic field in the case of free electron metal surfaces. Feibelman assumed that the spatial variation parallel to the surface is negligible as compared to that perpendicular to the surface. He evaluated A_z within the RPA using $r_s = 2$ and incorporated this to the calculation of photocurrent matrix element using the Lang-Kohn potential for the initial and final states. It was found that his calculated data of jellium was in good agreement with the experimental data of Levinson *et. al.*[31]. However, the calculations of Feibelman[30,31] which has the most accurate description of the field variation could be applied only to metals which may be represented by jellium model[32]. Mukhopadhayay and Lundqvist[33] and Bagchi[34] have also proposed similar methods for calculating the electromagnetic fields near the surface.

Kliewer[35] considered the *semi-classical infinite barrier* (SCIB) model which has a sharp surface, but it did not take into account the particle-hole and plasmon excitations. The surface is taken to be an abrupt discontinuity between the vacuum and the electron gas. In this model, the structure in A_z found in Feibelman's calculation that results from a varying ground state charge density is not reproduced. As the electron cannot tunnel out of the solid due to infinite barrier, therefore, SCIB power absorptance is assumed to represent the photocurrent in this model. For example, the photocurrent is larger above the plasmon energy and below it is in contrast to the experimental data of Levinson *et al* [31]. The *semi-classical infinite barrier* model did

not reproduce the Friedel oscillations that extrend tens of angstroms into the solid, but these appear to have a small effect on photoemission cross section

Forstman and Stenschke[36] have developed the *hydrodynamical model* which considered the electron-hole spectrum. The dielectric function used is very simple so that one can easily evaluate the photon field **A**. Kempa and Forstman[37] have done the detailed calculations of the electromagnetic field using the hydrodynamical model and has incorporated the electric field for the calculations of the photoyield. This was applied to the case of aluminium and was found that the frequency dependence of the surface photoyield is due to the behaviour of the electric field. Photoyield results obtained by them had shown similar experimental behaviour as obtained by Levinson *et al*[31]. Barberan and Inglesfield[38] also have done a detailed calculation on photoemission using the hydrodynamical screening of the photon field. They had shown that the constant vector potential and the Fresnel field are inadequate to explain the photoemission results arising out of the screened electromagnetic field inside the metal. They found that below plasmon frequency (ω_p), A_z rises rapidly near the surface due to the polarisation charge but at ω_p , there are plasma oscillations. A_z is almost zero inside the metal at ω_p , which means that E_z is also zero inside the metal. These results of Barberan and Inglesfield[38] is in good agreement with that of Feibelman *et. al.*[30] for the case of aluminium, apart from the oscillations in A_z below plasmon frequency (ω_p). This had been attributed to the excitations in A_z below ω_p due to Friedel type of oscillations from the electron-hole excitation which were not included in the hydrodynamic calculation.

Maniv and Metiu[24] also have made progress in the calculation of electromagnetic field in the metal-vacuum interface region. They mainly considered the fields in the immediate vicinity of the interface and developed a scheme for a more general solution of the Feibelman's model. The plot of the photoyield against the photon energy did not show the behaviour as obtained by Feibelman[30] and Levinson *et. al.*[31] in the case of aluminium. They found that the model was true for photon energy above the plasmon energy and was applicable only to free electron type of solids.

A detailed investigation of variation of electromag netic field was also done by Thapa[39]. He applied the dielectric model developed by Bagchi and Kar[40] to various metals like aluminium, nickel, silver, etc. Thapa and others[41,42] have also calculated photocurrent in the case of aluminium by using the dielectric model of Bagchi and Kar which showed good agfreement with the experimental results[31]. The photocurrent calculations by using the Kronig-Penney model [43] in the case of a number of metals and semiconductors was also done by Thapa *et. al.*[41,42].

A realistic type of calculations for the surface state has been done by Levine[44], using the Mathieu potential model which was proposed at first by Statz[45]. In this type of potential which is given by $V = V_0 \cos(\frac{2\pi x}{a})$, where the amplitude V_0 is a measure of the crystal potential strength in a mono-atomic crystal, and the ionicity in a di- atomic one. When V_0 is small (large), the Mathieu potential model approaches the Nearly Free Electron (Tight Binding Approximation) limit, and thus acts as a bridge between these two extreme conditions. Davison and Levine[46], Slater[47] and Carver[48] have also used the Mathieu potential to describe the energy bands in a realistic crystal. We, therefore, find that no such calculations have been done in photoemission

which incorporates both the photon field variation and the initial state wave function derived by using the Mathieu potential model.

In this thesis, we have developed a simple formalism for photoemission calculation in which the electron states are derived by using the Mathieu potential. The Mathieu potential has been at first used by Statz[45] for surface state calculation. Levine[44] had also used Mathieu potential for calculating the condition for arbitrary surface termination. We have used in this formalism, the Mathieu potential model as described by Davison and Steslicka[49] for describing the crystal potential which was then used for deriving the initial state wavefunction for photocurrent calculations. In this formalism, we have used the simple model of Bagchi and Kar[40] for evaluating the photon fields. To determine the inital state wavefunction ψ_i, we have considered an empty lattice with a finite step potential and a strong periodic lattice[46,49]. The photocurrent was calculated as a function of photon energy($\hbar\omega$). The formalism was then applied to the case of metals like aluminium, beryllium, tungsten, molybdenum and semiconductor silicon.

The topics in this thesis are arranged as follows : In Chapter 2, we shall discuss the model of dielectric response function used for the calculation of the electromagnetic field (photon field vector) for the vacuum, surface and bulk regions of the metals like beryllium, molybdenum, tungsten and silicon. In Chapter 3, photoemission calculations using the Kronig-Penney model will be discussed. The dielectric model of Bagchi and Kar and also Lorentz-Drude dielectric model will be used to calculate the electromagnetic fields which were then applied to calculate the photocurrent in the case of metals like molybdenum, copper, tungsten and semiconductors silicon and gallium arsenide. The effect of inclusion of relativity in

photoemission by using the Kronig-Penney model is also discussed in Chapter 3. The relativistic Kronig-Penney is then applied to the case of heavy solids like tungsten and silicon. In Chapter 4, we shall discuss the formulation of the initial state wavefunction by using the Mathieu potential model, in the case of an empty lattice with a finite step potential and a strong periodic lattice and discuss a number of applications to metals and semiconductors.

CHAPTER 2

DIELECTRIC MODEL AND ELECTROMAGNETIC FIELD

In this chapter, we shall discuss the dielectric model used and the calculation of electromagnetic field in a solid when electromagnetic radiation is incident on it. The calculation of the fields near a surface is a complex problem and *ab initio* calculations have been done only for jellium[32]. However, these calculations have not been extended to other metals where the jellium model is not applicable. Further, if one wants to consider the field variation in the presence of surface for metals, e.g. d-band metals like tungsten, molybdenum, palladium,etc., one has to use simpler models. The dielectric model used by Bagchi and Kar[40] for the case of tungsten has been used for the calculation of the electromagnetic field in the bulk, surface and vacuum regions. This model involves the linear interpolation in the surface region between the bulk dielectric function and the vacuum value. Though it has some deficiencies, it is important to note that it is a local response function and also gives good results in agreement with the experimentally determined value[50]. Since the bulk dielectric value required for this model is obtained experimentally, the field calculation can be extended to the case of semiconductors. We, describe the dielectric model used and the calculation of the electromagnetic fields from it.

2.1 Calculation of Dielectric Model and Electromagnetic Field :

The dielectric model used for the calculation of electromagnetic fields is shown in Fig. (2.1). The metal is assumed to occupy the space to the left of the z-plane. In the region $-a \leq z \leq 0$, the dielectric constant is chosen to be a local function which

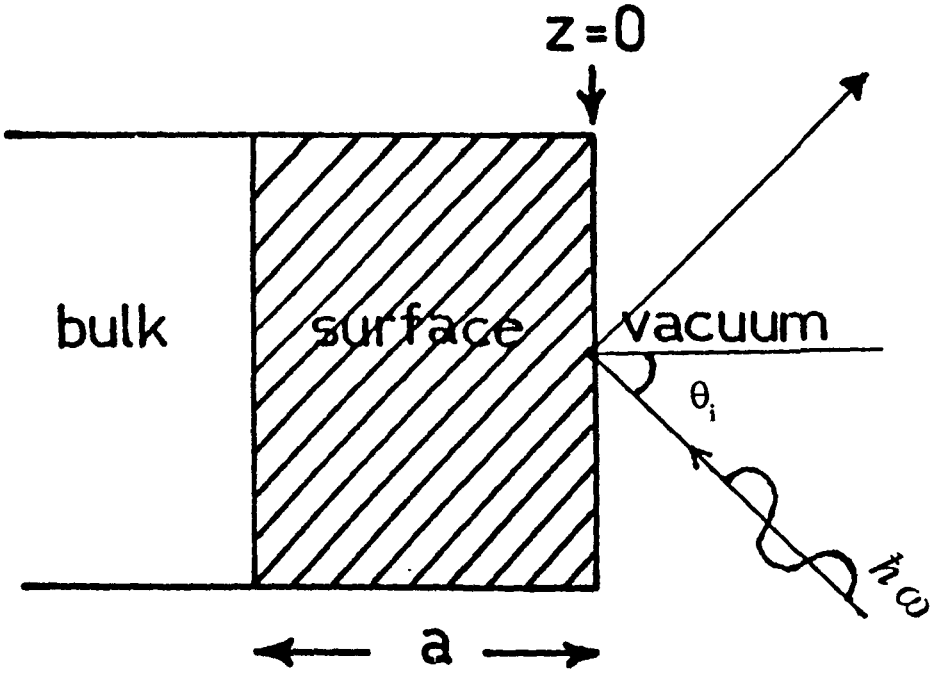

Figure 2.1

interpolates linearly between the bulk value inside the metal and the vacuum value (unity) outside. The model frequency-dependent dielectric function is, therefore, given by

$$\varepsilon(\omega,z) = \begin{cases} \varepsilon_1(\omega) + i\varepsilon_2(\omega), & \text{for} \quad z < -a \\ 1 + [1 - \varepsilon(\omega)]\frac{z}{a} & \text{for} \quad -a \le z \le 0 \\ 1, & \text{for} \quad z > 0. \end{cases} \qquad (2.1)$$

The incident radiation is taken to be p-polarised light of frequency ω and incident on the surface at an angle of incidence θ_i. A gauge was chosen in which the scalar potential A is set equal to zero and the electromagnetic field $E(Q,\omega,z)$ is expressed in terms of the vector potential as

$$E(Q,\omega,z) = \frac{i\omega}{c} A(Q,\omega,z) \qquad (2.2)$$

where $Q = \frac{\omega}{c}\sin\theta_i$. The magnetic field B(z) = $A(Q,\omega,z)$ points in the y-direction and it follows that :

$$\frac{d}{dz}\left(\frac{1}{\varepsilon}\frac{dB}{dz}\right) + \left(\frac{\omega^2}{c^2} - \frac{Q^2}{\varepsilon}\right) B = 0 \qquad (2.3)$$

where the value of ε is given by $\varepsilon = \varepsilon(\omega,z)$

The electric field components can be obtained from the magnetic field as

$$E^x(Q,\omega,z) = \frac{c}{i\omega\varepsilon}\frac{dB}{dz}$$
$$E^z(Q,\omega,z) = -\frac{\sin\theta_i}{\varepsilon}\,\mathrm{B} \qquad (2.4)$$

To solve Eq. (2.3), a new variable u(z) was introduced according to the discussion of Landau and Lifshitz[55] which is given by $B(z) = u(z)\sqrt{\varepsilon}$. Then u(z) satisfies the equation :

$$\frac{d^2u}{dz^2} + \frac{\omega^2}{c^2}(\varepsilon - \sin^2\theta_i)\,u + [\frac{1}{2\varepsilon}\frac{d^2\varepsilon}{dz^2} - \frac{3}{4}\frac{1}{\varepsilon^2}(\frac{d\varepsilon}{dz})^2]\,u = 0 \qquad (2.5)$$

For the dielectric model used, $\frac{d\varepsilon}{dz}$ is finite only in the region $-a \le z \le 0$ and $\frac{d^2\varepsilon}{dz^2}$ vanishes everywhere except for singularities at $z = \pm a$. The normal component of the electric field vector potential in the long wavelength limit $(\omega\frac{a}{c}) \to 0$ is then given by :

$$\tilde{A}_\omega(z) = \frac{E^z_\omega(z)}{E_o}$$

$$-\frac{\sin 2\theta_i}{[\varepsilon(\omega)-\sin^2\theta_i]^{\frac{1}{2}}+\varepsilon(\omega)\cos\theta_i} \qquad z < -a$$

$$-\frac{\sin 2\theta_i}{[\varepsilon(\omega)-\sin^2\theta_i]^{\frac{1}{2}}+\varepsilon(\omega)\cos\theta_i}\cdot\frac{a\varepsilon(\omega)}{[1-\varepsilon(\omega)]z+a} \qquad -a \le z \le 0$$

$$-\frac{\varepsilon(\omega)\sin 2\theta_i}{[\varepsilon(\omega)-\sin^2\theta_i]^{\frac{1}{2}}+\varepsilon(\omega)\cos\theta_i} \qquad z > 0. \qquad (2.6)$$

The electromagnetic fields have been calculated for photon energy below and above the plasmon energy of the metals and semiconductors. We have considered the plasmon energy to be the energy at which the real part of dielectric constant of the solids is minimum i.e. $\varepsilon_1 \rightarrow 0$. In calculating the electromagnetic field, the value of the dielectric constant $\varepsilon(\omega)$ is unity for vacuum region. For the bulk and the surface region, we have used the experimental data for $\varepsilon(\omega)$ as given by Weaver[50] and Edwards[51] and have calculated the frequency dependence of the magnitude of $\tilde{A}_\omega(z)$ and $|\tilde{A}_\omega(z)|^2$ for a number of cases. The solids whose dielectric functions were used are the free electron metal beryllium, transition metals molybdenum, tungsten and semiconductor silicon. $|\tilde{A}_\omega(z)|^2$ has been plotted against photon energy($\hbar\omega$) for different planes in the surface region by changing the values of z/a. The thickness of the surface is a parameter in our calculations. However, it has been found by Appelbaum[56] that for most metals, the surface width a ~ 15 $\mathring{A}$ with respect to the last plane of the atoms beyond which the electronic properties are independent of the presence of the surface and hence we have taken the value of a ~ 10 $\mathring{A}$.

2.2 **Evaluation of the Electromagnetic Fields** :

In this section, we shall discuss the electromagnetic fields calculated by using the formula in Eq. (2.6) for beryllium, molybdenum, tungsten and silicon. We have plotted $|\tilde{A}_\omega(z)|$ as a function of photon energy ($\hbar\omega$) and the distance (z/a) from the surface of the solids.

(a) **Beryllium** :

Fig. (2.2) shows the plot of variation of $|\tilde{A}_\omega(z)|^2$ against the photon energy in the case of beryllium for different locations of the surface planes at z/a = -1 (bulk),

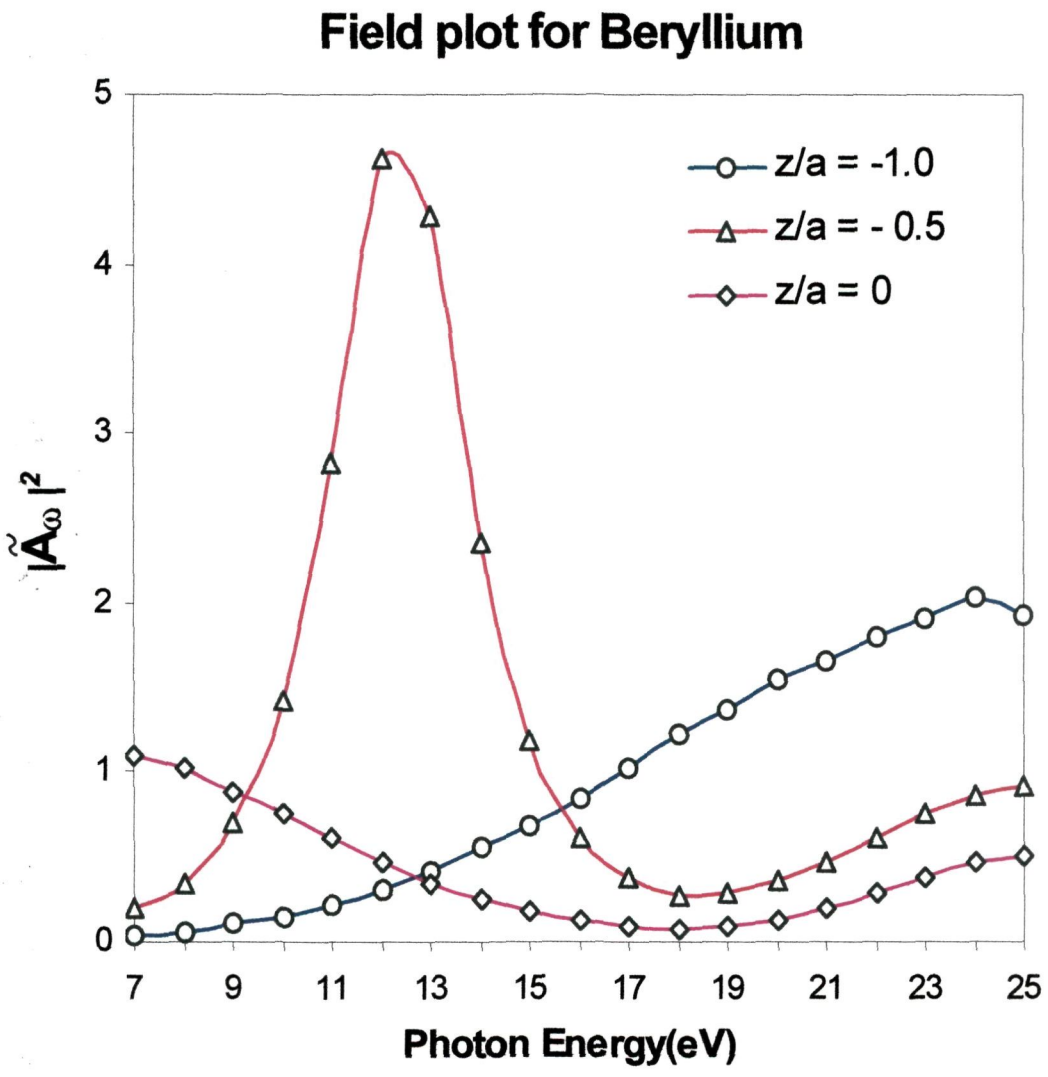
Field plot for Beryllium
z/a = -1.0
z/a = - 0.5
z/a = 0
$|\tilde{A}_\omega|^2$
0
1
2
3
4
5
7
9
11
13
15
17
19
21
23
25
Photon Energy(eV)

Figure 2.2

z/a = - 0.5 (surface) and z/a = 0 (vacuum). Here 'a' is the thickness of the surface. For regions at the surface, we find that the peak occurred at 12 eV and shows a minimum at 19 eV (the plasmon energy of Be is 19.5 eV). For regions in the vacuum side, we find that the graph shows a broad peak at photon energy larger than the plasmon energy. The behaviour of $d\tilde{A}_\omega/dz$ calculated for the surface region has shown that maximum occurs at photon energy 12 eV (Fig. 2.3). The fact that the peak is localised in the surface region means that photoemission from the surface of metal is dependent on the spatial variation of the electromagnetic fields. As the square of $\tilde{A}_\omega(z)$ is directly involved in the matrix element for photocurrent calculations, Thapa and Kar[52] and Bartynski *et. al.*[53] have obtained similar trends in the behaviour of photocurrent in the case of beryllium. In the case of $\hbar\omega$ = 7 eV and 18 eV, we find that in the plot of $d\tilde{A}_\omega/dz$ against surface location the peaks are localised more towards the vacuum region and the bulk region respectively.

(b) **Molybdenum** :

Fig.(2.4) shows the variation of $|\tilde{A}_\omega(z)|^2$ against photon energy for molybdenum for three locations of the planes at z/a = -1 (bulk), z/a = - 0.5 (surface region) and z/a = 0 (vacuum). The figure has a number of structures[57] in the curves. The plot for z/a = - 0.5 shows two prominent peaks at photon energies 9.2 eV and 9.6 eV (Fig. 2.5a). We found that for each of these energies, there is a peak in the surface region. Also there is a peak in the surface region for energies at 19.6 eV, 20 eV and 20.6 eV as shown in Fig. (2.5c). The photon energy dependence of $|\tilde{A}_\omega(z)|$ and $|\tilde{A}_\omega(z)|^2$ on both the sides of the interface (z/a = -1 and z/a = 0) is clearly seen in Fig. (2.4). Our calculated data of molybdenum showed qualitative features with the experimental data of Weng *et. al.*[58] who had also calculated the photon energy

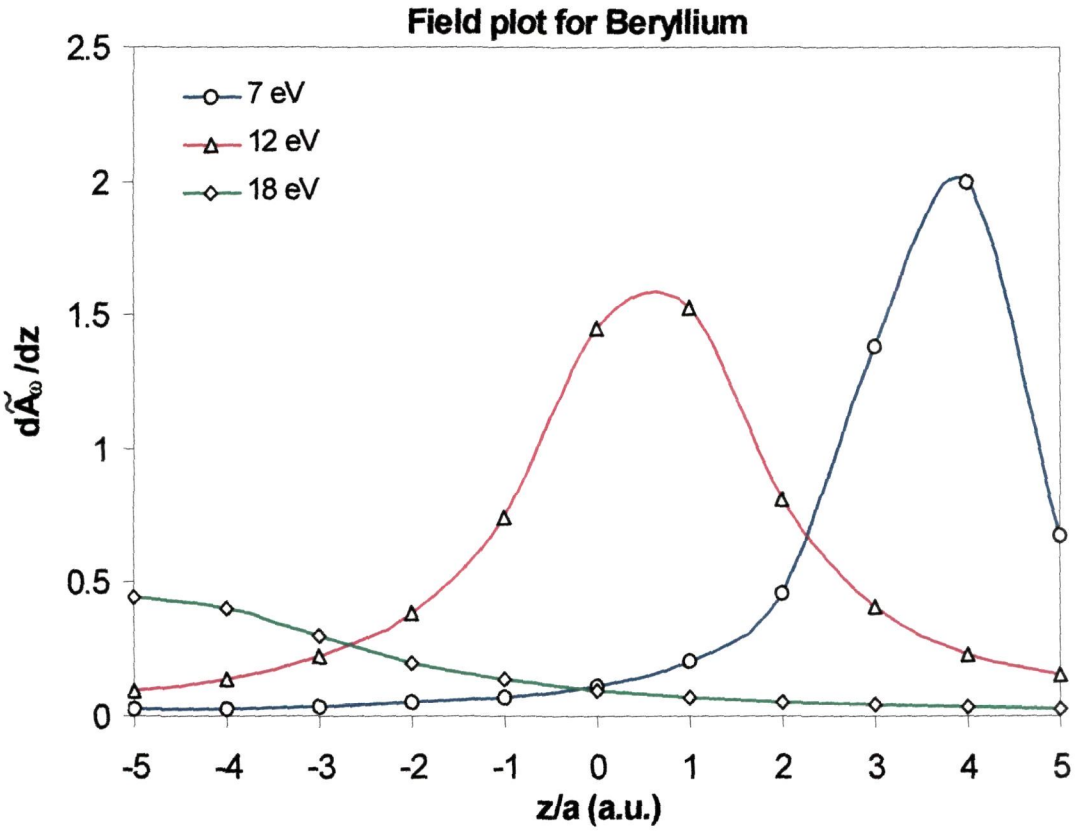
Field plot for Beryllium
7 eV
12 eV
18 eV
2.5
2
1.5
1
0.5
0
-5
-4
-3
-2
-1
0
1
2
3
4
5
z/a (a.u.)
dÃω/dz

Figure 2.3

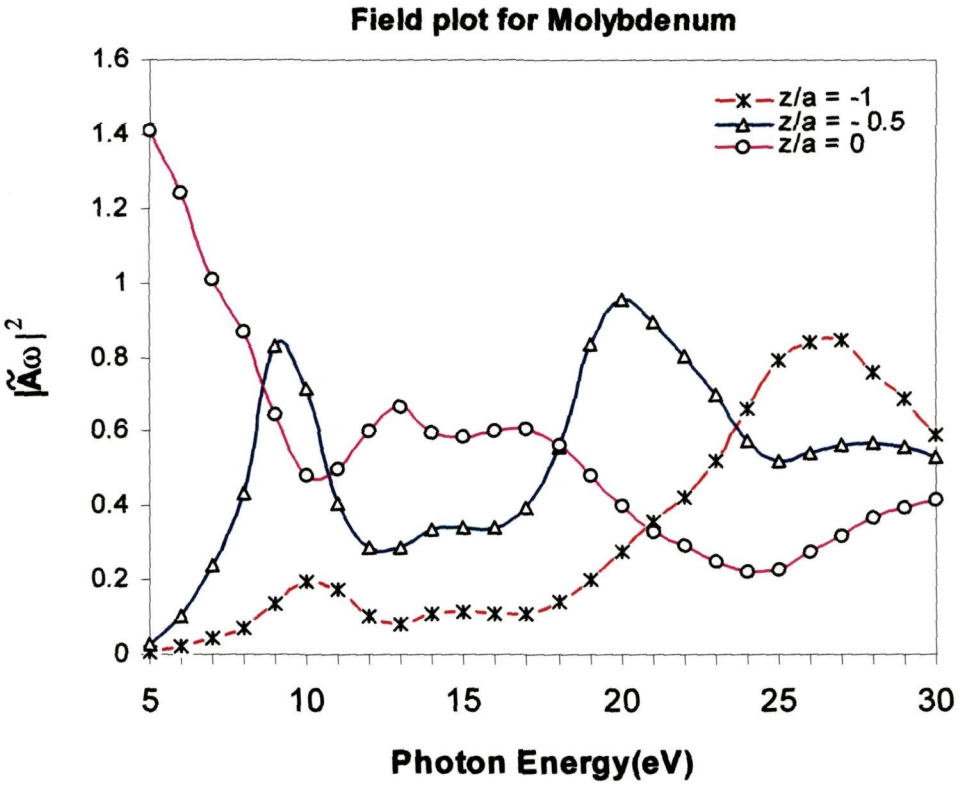
Field plot for Molybdenum
z/a = -1
z/a = - 0.5
z/a = 0
1.6
1.4
1.2
1
0.8
0.6
0.4
0.2
0
5
10
15
20
25
30
Photon Energy(eV)
$|\tilde{A}\omega|^2$

Figure 2.4

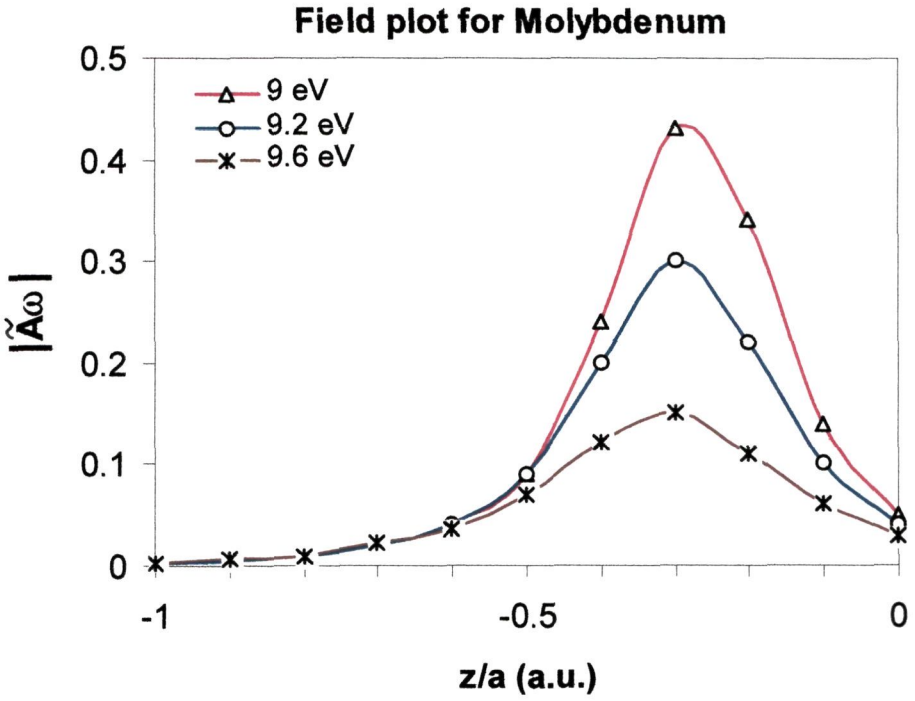
Field plot for Molybdenum
9 eV
9.2 eV
9.6 eV
0.5
0.4
0.3
0.2
0.1
0
|Ãω|
-1
-0.5
0
z/a (a.u.)

Figure 2.5(a)

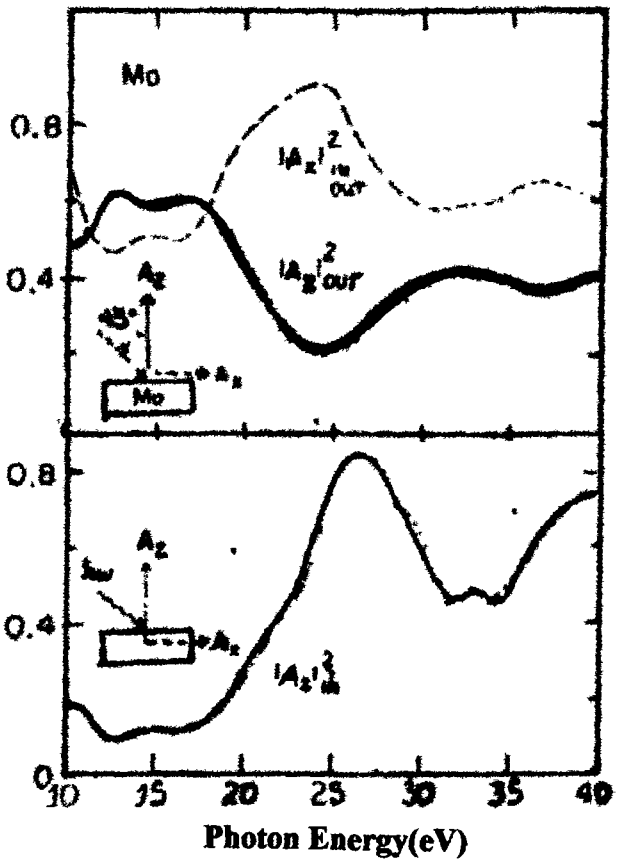

Figure 2.5(b)

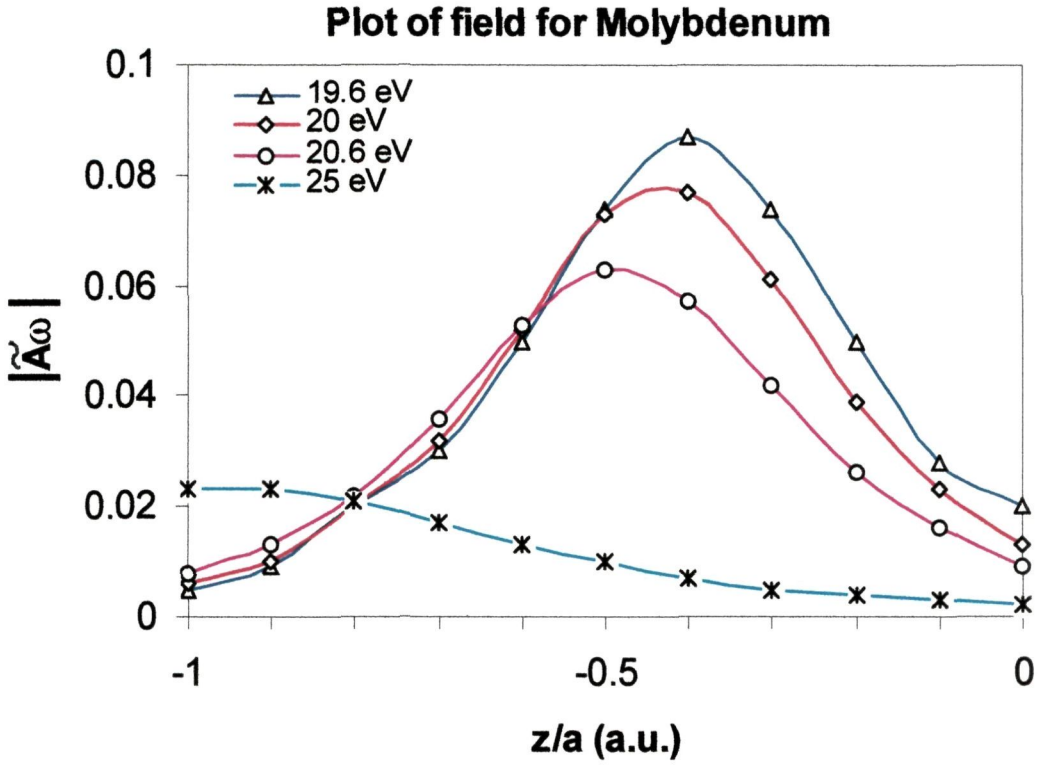
Plot of field for Molybdenum
0.1
0.08
0.06
0.04
0.02
0
|Ãω|
19.6 eV
20 eV
20.6 eV
25 eV
-1
-0.5
0
z/a (a.u.)

Figure 2.5(c)

dependence of the field. They found that the field just outside the surface has a minimum near 25 eV and inside the surface, it has a maximum at around 27 eV. For photon energy greater than 27 eV, it decreases rapidly(slowly) towards the low (high) photon energy side. Similar feature has been shown by our calculated data of the field for region within and outside the surface (Fig. 2.4). We found that there is a peak at 9.5 eV for the surface region (z/a = - 0.5). This may be attributed to the high lying resonance for molybdenum as shown in the photoemission calculation of Weng *et. al.*[58].

(c) **Tungsten** :

Fig. (2.6) shows the variation of $|\tilde{A}_{\omega}(z)|^2$ against photon energy in the case of tungsten for three locations of the planes at z/a = -1 (bulk), z/a = -0.5 (surface region) and z/a = 0 (vacuum). The figure has a number of structures in the curves. The plot for z/a = - 0.5 shows a prominent peak at photon energy 21 eV. The photon energy dependence of $|\tilde{A}_{\omega}(z)|$ and $|\tilde{A}_{\omega}(z)|^2$ on both the sides of the interface (z/a = -1 and z/a = 0) is seen from the Fig. (2.6). We found that for the field in the surface region, there is a minimum at $\hbar\omega = \hbar\omega_p$ (the plasmon energy of tungsten i.e. 26 eV) and on the vacuum region, it has a minimum at around 25 eV. Our calculated data of the field for region within and outside the surface has the same feature as shown by Weng *et. al.*[58]. We also found that there are two peaks at 9 eV and 14.5 eV for z /a = - 0.5 . This may be attributed to high lying resonance for tungsten as shown in the photoemission calculation of Weng *et. al.*[58].

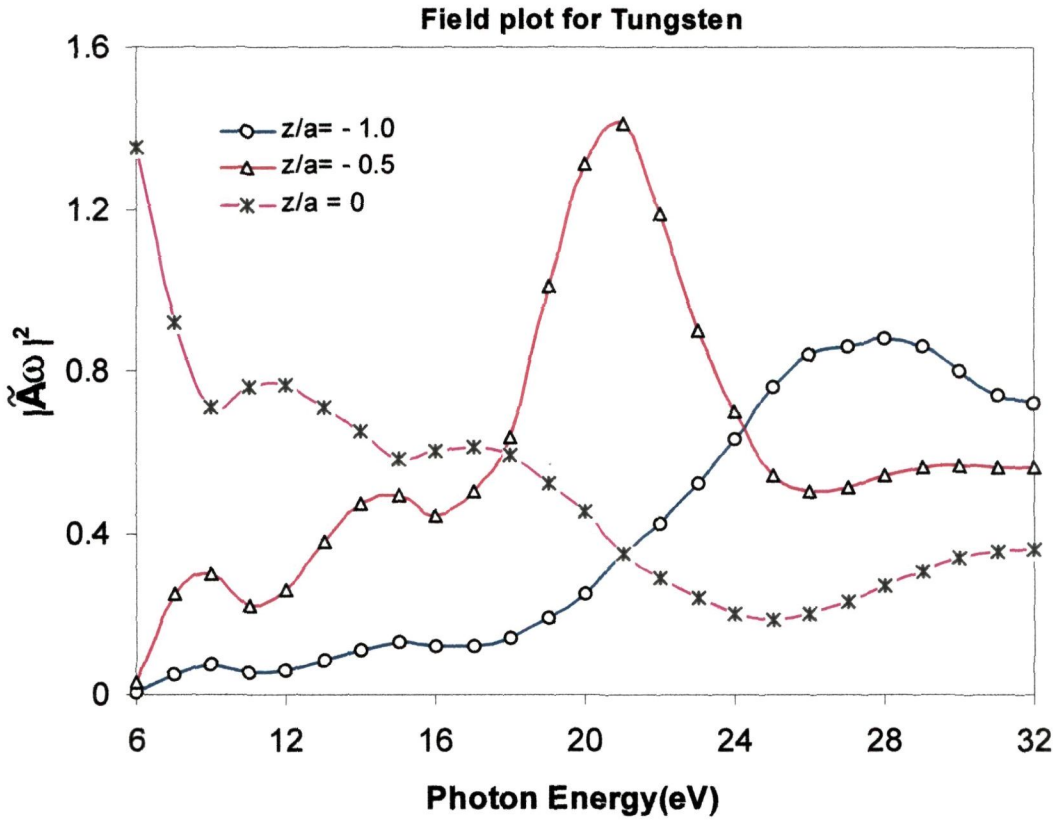
Field plot for Tungsten
z/a= - 1.0
z/a= - 0.5
z/a = 0
1.6
1.2
0.8
0.4
0
6
12
16
20
24
28
32
Photon Energy(eV)
|Ã(ω)|²

Figure 2.6

(d) **Silicon** :

The presence of the surface states on the semiconductor surfaces was earlier verified by using the method of angle integrated photoemission[59,60]. In bulk semiconductors, the Fermi level shifts depend upon the doping level from the top of the valence band to the bottom of the conduction band. But the early results of angle integrated photoemission and work function measurements[61,62] showed that the Fermi level is pinned at the surface, almost independent of the doping level. Though the existence of surface states on semiconductors was confirmed early[63], yet little is known about these states compared to the surface states on metals.

The interesting feature in semiconductors is that most of the semiconductor surfaces reconstruct. The best known example is that of Si(111) surface. A freshly cleaved surface structure can be prepared by the rapid quenching from a high temperature which stabilises the surface[64]. The Si(111) surface is only an example of a variety of reconstructed semiconductor surfaces. The models for these have been developed mostly on the basis of dynamical LEED calculations. Calculations have shown that semiconductor surfaces are rather localised within certain bonds which are shown by the dangling bond structure of surface states.

Since the field calculations with respect to the photon energy give us the first hand information about the photoemission cross - section, we have calculated $|\tilde{A}_{\omega}(z)|^2$ and $|\tilde{A}_{\omega}(z)|$ against photon energy also in the case of silicon. The plot of the field against the photon energy is shown in Figs. (2.7) and (2.8) for three different planes located at z/a = -1.0 (bulk), z/a = -0.5 (surface) and z/a = 0 (vacuum). We find that at the surface, there is a strong peak at 12 eV followed by a minimum at the

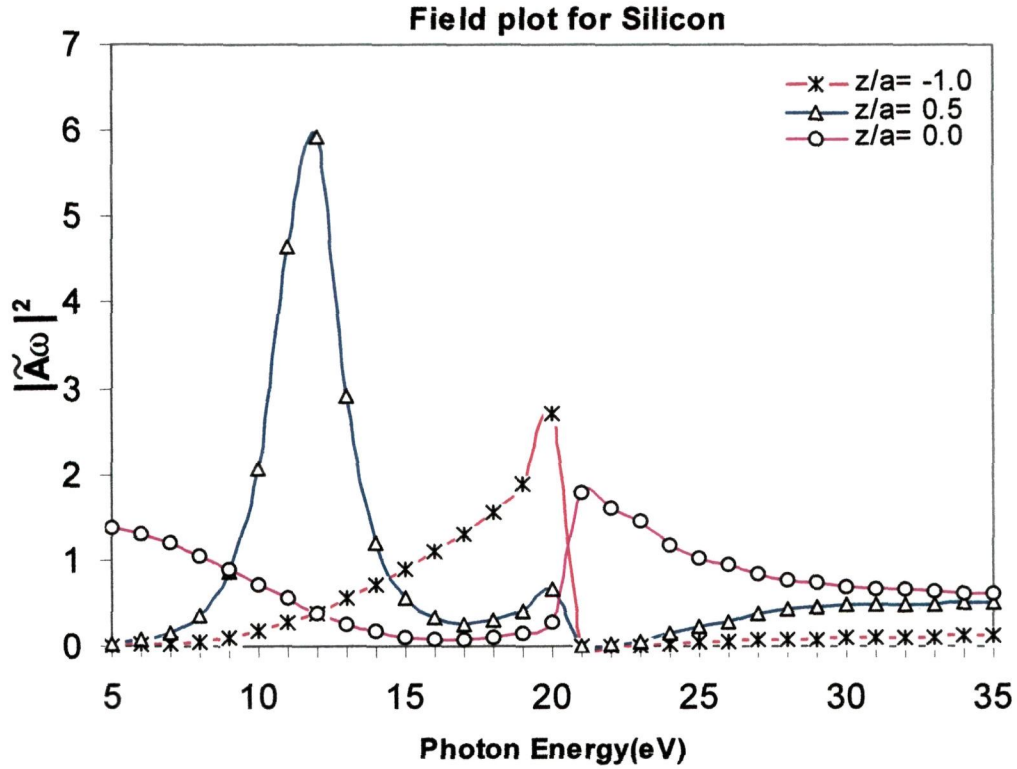
Field plot for Silicon
z/a= -1.0
z/a= 0.5
z/a= 0.0
$|\tilde{A}\omega|^2$
0
1
2
3
4
5
6
7
5
10
15
20
25
30
35
Photon Energy(eV)

Figure 2.7

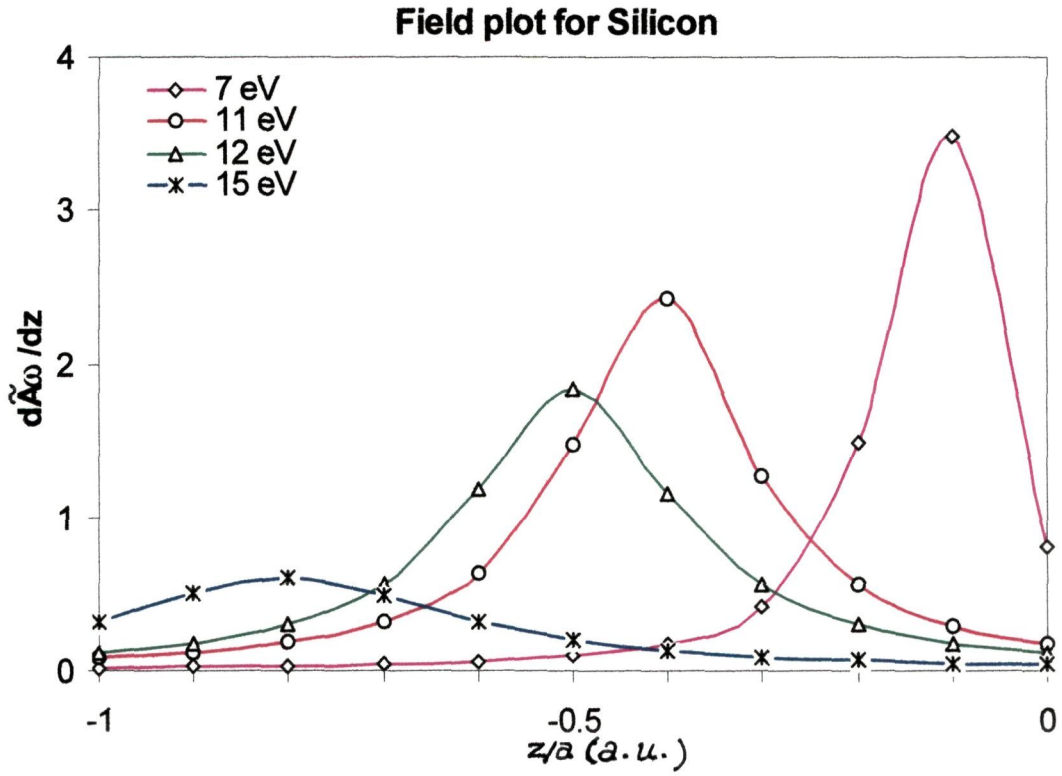
Field plot for Silicon
7 eV
11 eV
12 eV
15 eV
dÃω /dz
z/a (a.u.)
4
3
2
1
0
-1
-0.5
0

plasmon energy 16 eV. The field then increases again but at photon energy 21 eV, it becomes very small. We found that this is the region where the dielectric function for silicon shows a resonance. This behaviour is also reflected in the field data for the bulk (z/a = -1.0) which again becomes very small around 21 eV, although it does not show minimum at the plasmon energy. The field on the vacuum region (z/a = 0) on the other hand shows a maximum at 21 eV and a minimum at the plasmon energy 16 eV, which is in contrast to the bahaviour of the field in the bulk-surface boundary plane. This shows that the variation of the field in the surface region of a semiconductor is going to be quite important on the photoemission calculations.

CHAPTER 3

PHOTOCURRENT CALCULATIONS USING KRONIG-PENNEY MODEL

The calculations of photocurrent from the band state(Fermi level) and surface state of free electron metals have been extensively done by Thapa *et. al.*[41,42] in the case of aluminium. Since aluminium is a weakly-bonded metal, they used a free electron initial state wavefunction ψ_i for the calculation of band state photoemission. The initial state wavefunction ψ_i was formulated by the method of normal matching of the wavefunctions at the boundary surface of the solid. The photocurrent was then calculated by using the electromagnetic fields developed by Bagchi and Kar[40].

The free electron(FE) model has been successful in explaining the photoemission phenomena from free electron metals. However, it has drawback in explaining the band structure effects of solid. We will present in this chapter the Kronig-Penney(K-P) model which has been used for the calculations of surface electronic states by several authors[45,65-67]. Schaich and Ashcroft[18] have calculated numerically the photoyield by using the modified form of the Kronig-Penney model and also including the band structure effects. They used the wavefunction of Mitchell[3] for free electron gas in a semi-infinite box and considered the photon field vector $\tilde{A}_{\omega}(z)$ to remain constant. The numerical data as obtained by them in the case of potassium was quite realistic. The nature of photocurrent data obtained by them from various planes below the surface has clearly shown the success of their model. Steslicka[68] had done a detailed calculations of the surface states using the Kronig-Penney model both for the semi-infinite and infinite crystals. Eldib *et. al.*[69]

has also applied the Kronig-Penney model to one dimensional crystal. They had calculated only the electronic energy bands for mono and poly-atomic cystals and compared the data with the one computed by using the Linear Combinations of Atomic Orbitals(LCAO) method.

3.1 **Kronig-Penney potential model :**

In this section, we shall discuss the Kronig-Penney(K-P) model as developed by Thapa *et. al.*[42] for the calculation of photocurrent from metals and semiconductors. The K-P model was used to represent the crystal potential field by a linear array of rectangular well (Fig. 3.1), which was later transformed into a chain of δ- function potential well such that the area of each well remains constant. The initial state wavefunction was obtained by matching at the surface.

To evaluate the initial state wavefunction $\psi_i(z)$, one can solve the one-dimensional Schroedinger's equation given by :

$$\frac{d^2\psi(z)}{dz^2} + k_i^2(z) = -2V(z)\psi(z), \qquad (3.1)$$

where $k_i^2 = 2E_i$ and $V(z)$ is the δ-function potential of the K-P model.

Let $\phi(z)$ denote the Bloch wavefunction deep inside the metal and $\phi^*(z)$ the time reversal of $\phi(z)$. The eigenfuction in the semi-infinite solid ($z < 0$) was chosen to have the form[70] as :

$$\psi_i(z) = \phi(z) - P\phi^*(z) \qquad (3.2)$$

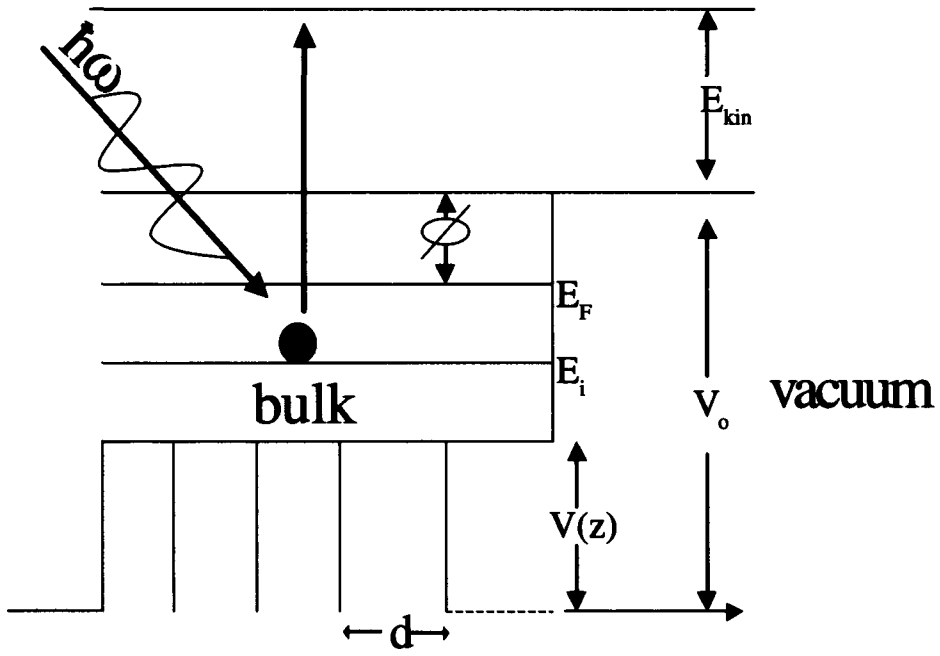

Figure 3.1

where P is the reflection coefficient obtained by matching the wavefunction and its derivative at z = 0. The potential $V(z)$ was considered to be one-dimensional Kronig-Penney type given by :

$$V(z) = = \Sigma g\ \delta[z - (2n+1)\tfrac{d}{2}] \tag{3.3}$$

One can then show[42] that the initial state wavefunction for the bulk, surface and vacuum regions may be written as

$$\psi_i = \begin{cases} (1 - iPe^{-i\delta}\sin\delta)e^{ik_i z} - (P - ie^{i\delta}\sin\delta)e^{-ik_i z}, & z \le 0 \\ \text{(bulk \& surface)} & \\ Te^{-\kappa z}, & z < 0 \text{ (vacuum)} \end{cases} \tag{3.4}$$

where $\cot\delta = -\frac{k_i}{g}$, δ is the phase shift introduced in the transmitted wave, g is the strength of the δ - potential which describes the bulk potential, T being the transmission coefficient across the boundary plane and $\kappa^2 = 2(V_o - E_i)$, where V_o is the potential at the surface which an electron encounters while transmitting through the boundary surface. From the matching conditions at z = 0, one can easily deduce the values of P and T in Eq. (3.4) which is given by :

$$P = \frac{(\kappa - ik_i) - (k_i - i\kappa)e^{i\delta}\sin\delta}{(\kappa - ik_i) - (k_i - i\kappa)e^{-i\delta}\sin\delta} \tag{3.5}$$

and

$$T = \frac{2k_i \sin 2\delta}{(\kappa - ik_i) + (k_i - i\kappa)e^{-i\delta}\sin\delta} \tag{3.6}$$

The proper evaluation of P and T with the correct numerical values for other factors enables one to write the most explicit form of initial state wavefunction $|\psi_i>$ The photo emission cross-section was obtained by using the formula

$$\frac{d\sigma}{d\Omega} = \frac{k^2}{\omega} \Sigma | < \psi_f | H' | \psi_i > |^2 \qquad (3.7)$$

The matrix element given in Eq. (3.7) can be written as

$$I = \int_{-\infty}^{-d} \psi_f^* \tilde{A}_\omega(z) \frac{d\psi_i}{dz} dz + \int_{-d}^{0} \psi_f^* \tilde{A}_\omega \frac{d\psi_i}{dz} dz$$

$$+\frac{1}{2} \int_{-d}^{0} \psi_f^* \frac{d\tilde{A}_\omega}{dz} \psi_i dz + \int_{0}^{\infty} \psi_f^* \tilde{A}_\omega(z) \frac{d\psi_i}{dz} dz. \qquad (3.8)$$

In Eq. (3.8), the final state wavefunction $\psi_f(z)$ is the scattering state of the step potential V(z) given by $V(z) = - V_o \theta(z)$. Here $V_o = E_F + \phi$, where E_F is the Fermi level and ϕ is the work function. The final state wavefunction can be written as (in atomic units) :

$$\psi_f(z) = \begin{cases} \left(\frac{1}{2\pi q_f}\right)^{\frac{1}{2}} \frac{2q_f}{q_f + k_f} e^{ik_f z} e^{-\alpha|z|}, & z \le 0 \text{ (bulk \& surface)} \\ \left(\frac{1}{2\pi q_f}\right)^{\frac{1}{2}} \left[e^{iq_f z} + \left(\frac{q_f - k_f}{q_f + k_f}\right) e^{-iq_f z}\right], & z > 0 \text{ (vacuum)} \end{cases} \qquad (3.9)$$

where $k_f^2 = 2E_f$, $q_f^2 = 2(E_f - V_o)$ and $E_f = E_i + h\omega$ In Eq. (3.9), the factor $e^{-\alpha|z|}$ (α is the scattering factor) is included on the surface and bulk side to take into account the inelastic scattering of the electrons. The photocurrent was calculated numerically by evaluating (3.8) . In our calculations, we have used the dielectric functions corresponding to different solids as given by Weaver[50] and Edwards[51].

(a) **Molybdenum and Copper :**

Photocurrent was calculated for these metals for two values of the surface widths, namely a = 0 (narrow surface width) and a = 10 a.u. for the same values of surface state energy (10.24 eV), potential barrier height (14.99 eV) and $\theta_i = 45^o$. Figure (3.2) shows the plot of photocurrent as a function of photon energy ($\hbar\omega$) in the case of molybdenum. We find that for a = 10 a.u., a maxima in the value of photocurrent occurred at $\hbar\omega$ = 10 eV. With further increase of the photon energy, the photocurrent decreased to a minimum value at $\hbar\omega$ = 12 eV and showed a small hump at $\hbar\omega$ = 14 eV. But for the case of a narrow surface width (a = 0), the behavior of photocurrent is quite different as shown in Figure (3.2). We did not find any peak for values of photon energy below and above 10 eV photon energy.

Figure (3.3) shows the plot of variation of photocurrent as a function of photon energy in the case of copper. For the surface width a = 10 a.u., the peak in the value of photocurrent occurred at $\hbar\omega$ = 20 eV and decreased to minimum at 26 eV photon energy. A second peak is also seen in the case of copper at $\hbar\omega$ = 30 eV. Copper also showed totally different behaviour for the narrow surface width (a = 0) which is evident from Figure (3.3).

We find that both metals Mo and Cu have shown atleast the qualitative features with the behavior of photocurrent as indicated also by other metals like Pd[71], W[72], Si[72] etc. in which the Kronig-Penney potential model was used. However, we see that the model employed do not exactly reproduce the earlier reported results. For example, in the case of molybdenum, Weng *et. al.*[58] have shown that for high lying surface state, photoemission intensity was maximum at

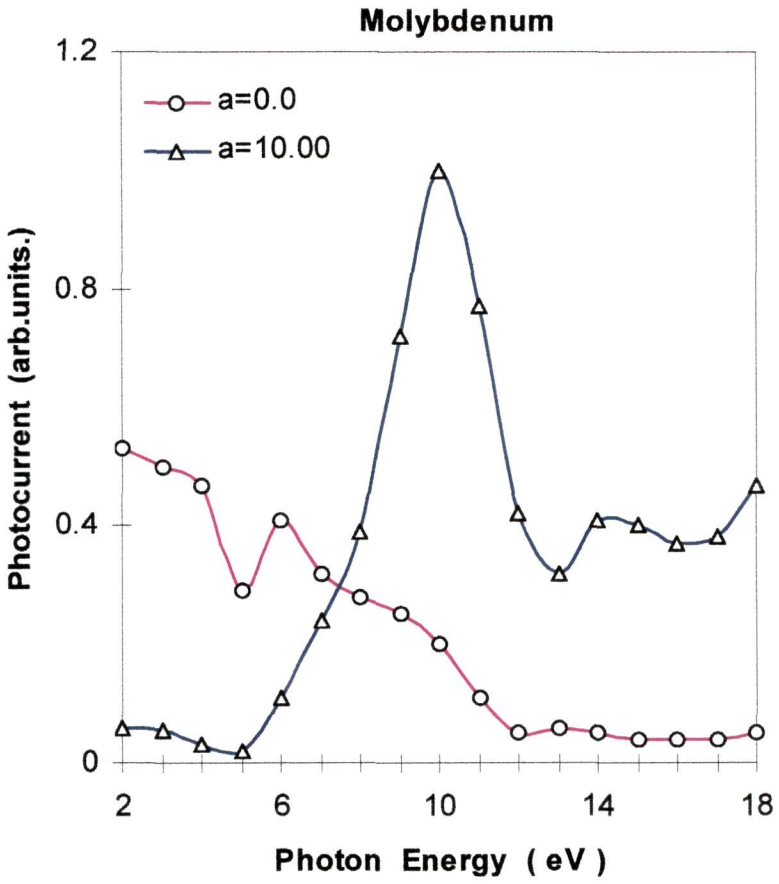
Molybdenum
1.2
0.8
0.4
0
a=0.0
a=10.00
Photocurrent (arb.units.)
2
6
10
14
18
Photon Energy (eV)

Figure 3.2

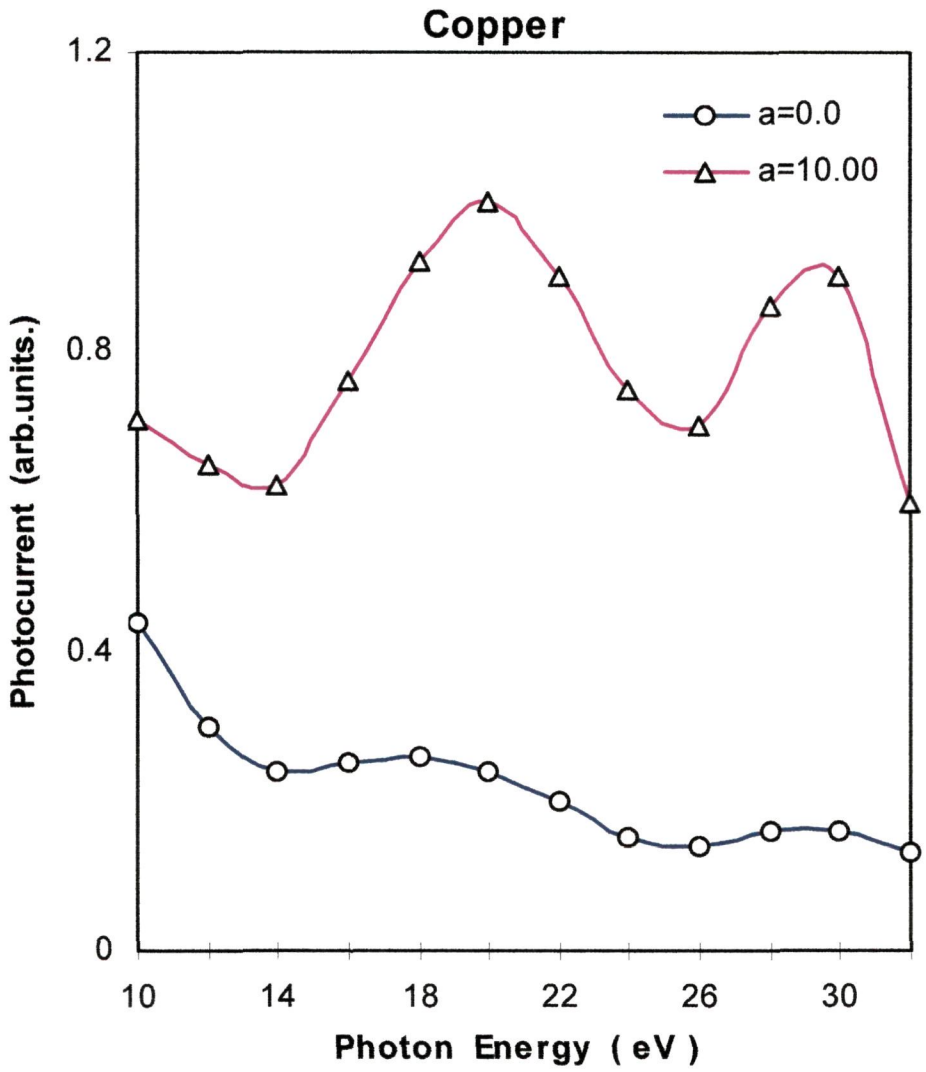
Copper
1.2
0.8
0.4
0
a=0.0
a=10.00
Photocurrent (arb.units.)
10
14
18
22
26
30
Photon Energy (eV)

Figure 3.3

photon energy 15 eV, then tends toward a minimum at 25 eV photon energy followed by a hump at $\hbar\omega$ = 30 eV. Our result did not show minimum in photocurrent at plasmon energy of molybdenum *i.e.* 24.4 eV. The reasons for not exactly conforming to other models and the experimentally measured data[16] may be attributed to the fact that our model is quite poor. For example, it is not considering the detail of the band structure effects. Also the matrix element is mainly dependent on the variation of the vector potential as evidenced in previous cases[71,72]. The variation of the vector potential mainly monitors the matrix element which causes the change in photocurrent. This fact had been also discussed by Weng *et. al.*[58] that the causes in the occurrence of peak in photoemission intensity for molybdenum is due to excitation of electrons by A_z componenet of the vector potential perpendicular to the surface plane.

(b) **Silicon** :

We have also used the Kronig-Penney model[42] in conjunction with the dielectric function $\varepsilon(\omega)$ for a semiconductor silicon as given by Edwards[51]. Using the same Kronig-Penney parameters and the same value of initial energy E_i as used in the case of Mo and Cu, the photocurrent result for a = 10 a.u. is shown in Fig. (3.4). We found that there is a minimum at 16 eV, the plasmon energy ($\hbar\omega_p$) of silicon. There is a peak below the plasmon energy and the photocurrent also rises above $\hbar\omega_p$. But in this case, another minimum occurs at 21 eV. This can be attributed to the behaviour of $\varepsilon(\omega)$ for silicon[39] which has a resonance at 21 eV (Fig. 3.5). As a result of this, the fields inside the solid become very small and hence the photocurrent shows a minimum. The photocurrent calculated with no surface region i.e. with Fresnel fields shows no minimum at 16 eV or at 21 eV (Fig. 3.4). This again shows that the photocurrent behaviour with and without the surface region is quite different.

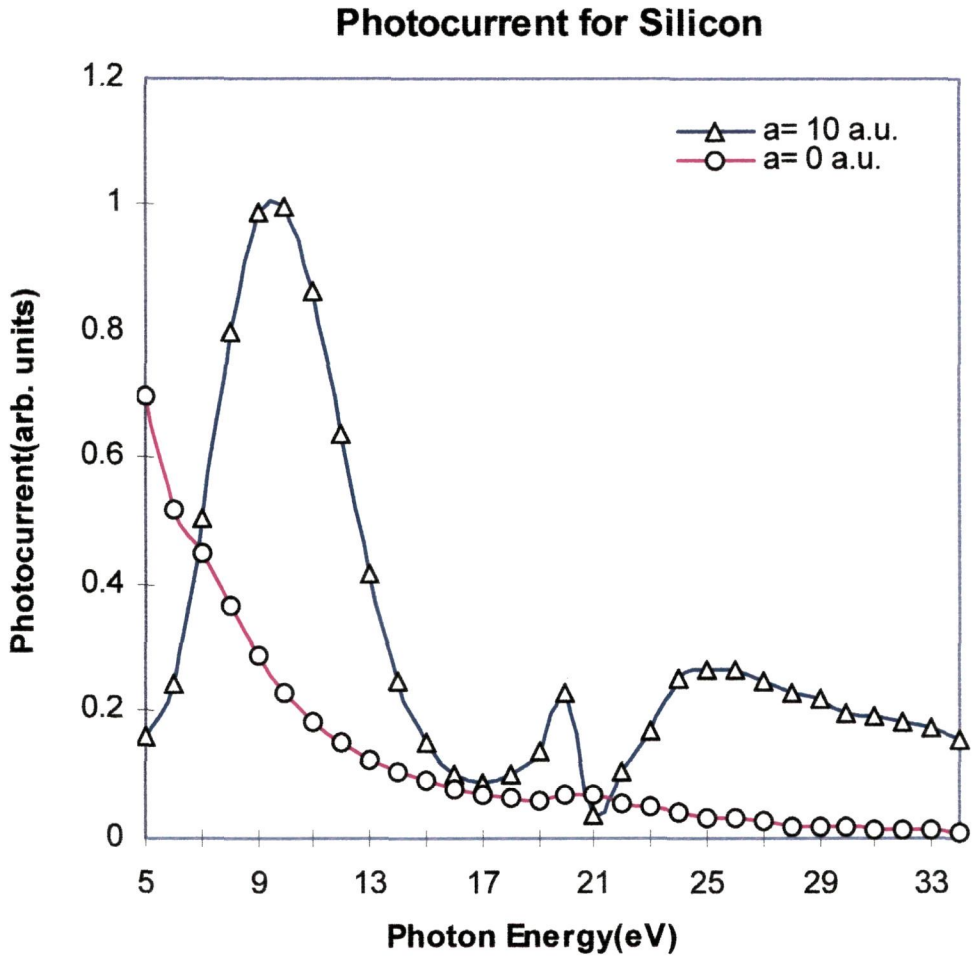
Photocurrent for Silicon
a= 10 a.u.
a= 0 a.u.
Photocurrent(arb. units)
1.2
1
0.8
0.6
0.4
0.2
0
5
9
13
17
21
25
29
33
Photon Energy(eV)

Figure 3.4

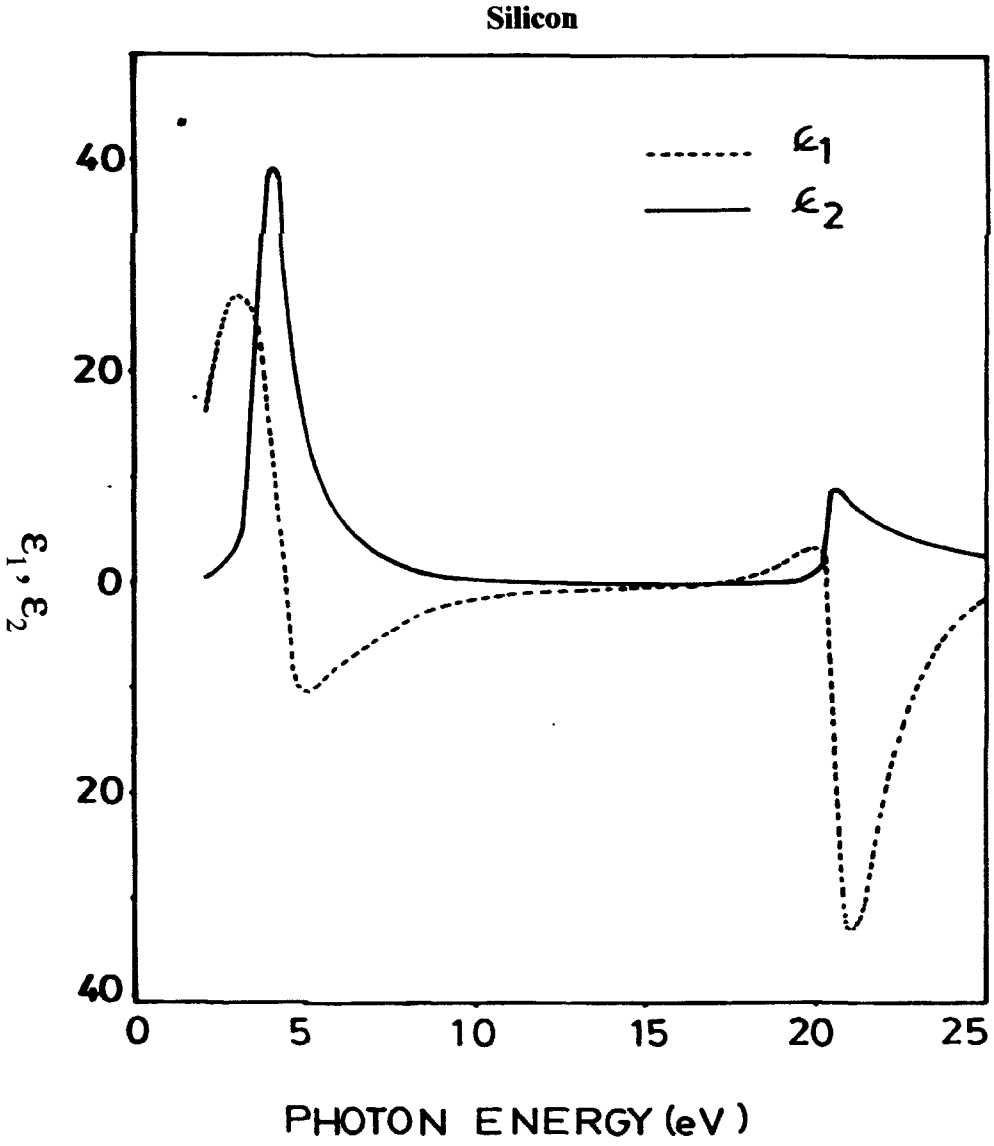
Silicon
ϵ_1
ϵ_2
40
20
0
20
40
$\varepsilon_1, \varepsilon_2$
0
5
10
15
20
25
PHOTON ENERGY (eV)

Figure 3.5

3.2 **Kronig-Penney model calculations using Lorentz-Drude dielectric model** :

In this section, we show the behaviour of photocurrent calculated by using the Lorentz-Drude model for the dielectric constant in the case of semiconductors. As discussed in the previous chapter, the existence of surface states on semiconductor surfaces was experimentally verified by using the angle integrated photoemission[73]. The semiconductor surfaces are more complex than metal surfaces for the reason that semiconductor surfaces reconstruct[74]. The presence of these reconstructed ions and atomic displacements on semiconductor surfaces makes the studies of electronic structure a very interesting topic. Of the various tools and techniques, angle resolved photoemission studies has also been widely used in understanding the surface states of semiconductors. Various type of structural models of semiconductors have been proposed[75]. In this section, we will be mainly concerned with the photoemission calculations by using the Lorentz-Drude dielectric model for metals. Then initial state wavefunctions will be the one described in the previous section, by using the Kronig-Penney model and applied it to the case of silicon and gallium arsenide.

The Drude-Lorentz model for calculating the frequency dependent dielectric constants which is given by :

$$\varepsilon(\omega) = \varepsilon_\infty[1 - \frac{\omega_p^2}{\omega(\omega+i\gamma_1)}] + \frac{(\varepsilon_0-\varepsilon_\infty)\omega_0^2}{(\omega_0^2-\omega^2-i\gamma_2\omega)} \qquad (3.10)$$

In Eq. (3.10) above, ε_0 and ε_∞ are the static and high frequency dielectric constants. By using the appropriate values of constants ε_0 , ε_∞ , γ_1, γ_2 etc. respectively for silicon and gallium arsenide. the real and imaginary parts of $\varepsilon(\omega)$ were calculated.

Using the electromagnetic fields for p-polarized radiation, we calculate the photoemission cross-section by evaluating the matrix element in Eq. (3.7)

In Fig. (3.6), we have shown the plot of photocurrent as a function of photon energy ($\hbar\omega$) for silicon. For the surface width a = 10 a.u., we find that at $\hbar\omega$ = 12 eV, photocurrent peak is maximum. It shows a minimum at $\hbar\omega$ = 16 eV followed by a small hump at 17 eV. Further, the increase of $\hbar\omega$ causes the photocurrent to decay towards a minimum value. We have taken the plasmon energy ($\hbar\omega_p$) of silicon to be 16 eV. The interesting feature that is seen here in the case of silicon is that photocurrent data[76] showed similar behaviour at least qualitatively with the earlier results[77] when fields were calculated by using the experimentally measured dielectric constants. For example, the maxima in photocurrent was obtained at $\hbar\omega < \hbar\omega_p$ i.e., at 12 eV photon energy followed by a minima occurring at $\hbar\omega = \hbar\omega_p$. For the case of narrow surface width (a = 0), the behaviour in photocurrent is completely different. We find that a peak of low height in photocurrent occurred near the plasmon energy of silicon. This is quite different behaviour obtained than with the one calculated by using the experimentally determined dielectric constants.

In Fig. (3.7), the plot of photocurrent as a function of photon frequency in the case of gallium arsenide is shown for two different surface widths a = 10 a.u and a = 0 respectively. The same values of Kronig-Penney parameters were used as in the case of silicon. The photocurrent structures of gallium arsenide data[76] showed three peaks at $\hbar\omega$ = 10 eV, 12 eV and 15 eV respectively but showing a minimum at $\hbar\omega$ = 16 eV (the assumed plasmon energy of gallium arsenide). Another hump in the photocurrent is seen at 17 eV beyond which the photocurrent decreases gradually. The photocurrent data for narrow surface width (a = 0) is found to be similar as in the

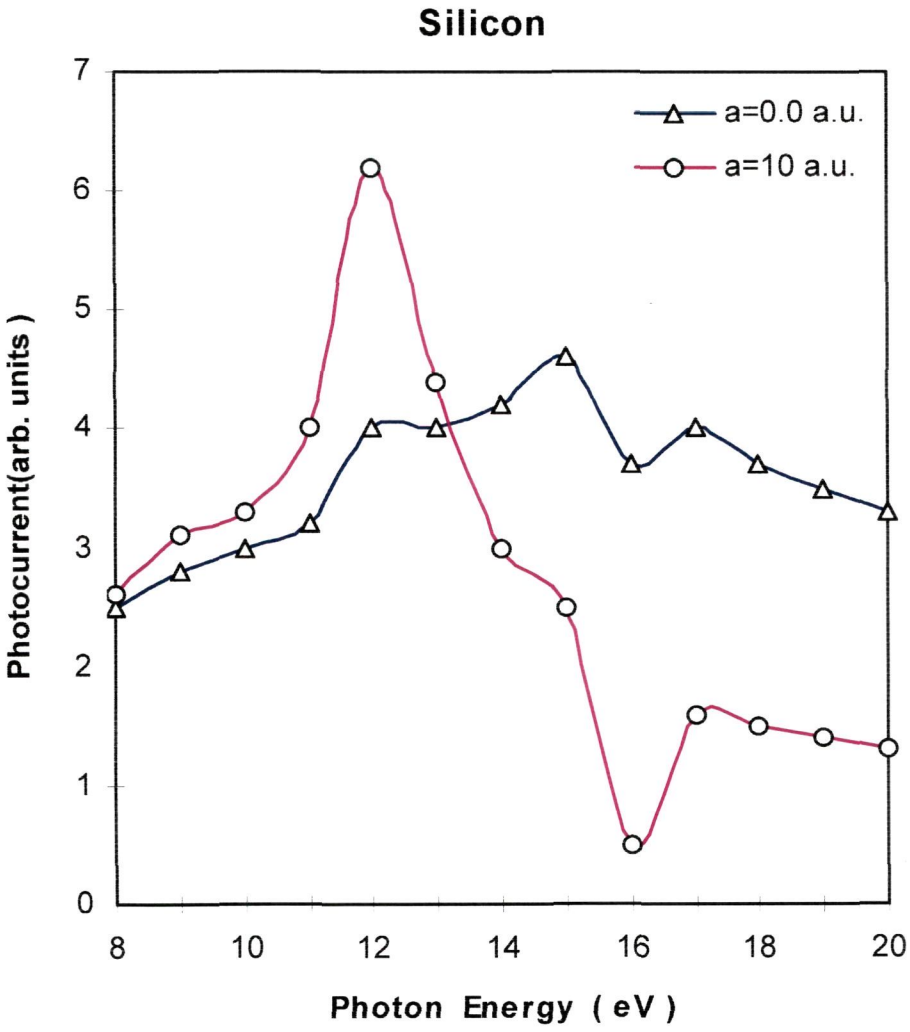
Silicon
a=0.0 a.u.
a=10 a.u.
Photocurrent(arb. units)
Photon Energy (eV)
0
1
2
3
4
5
6
7
8
10
12
14
16
18
20

Figure 3.6

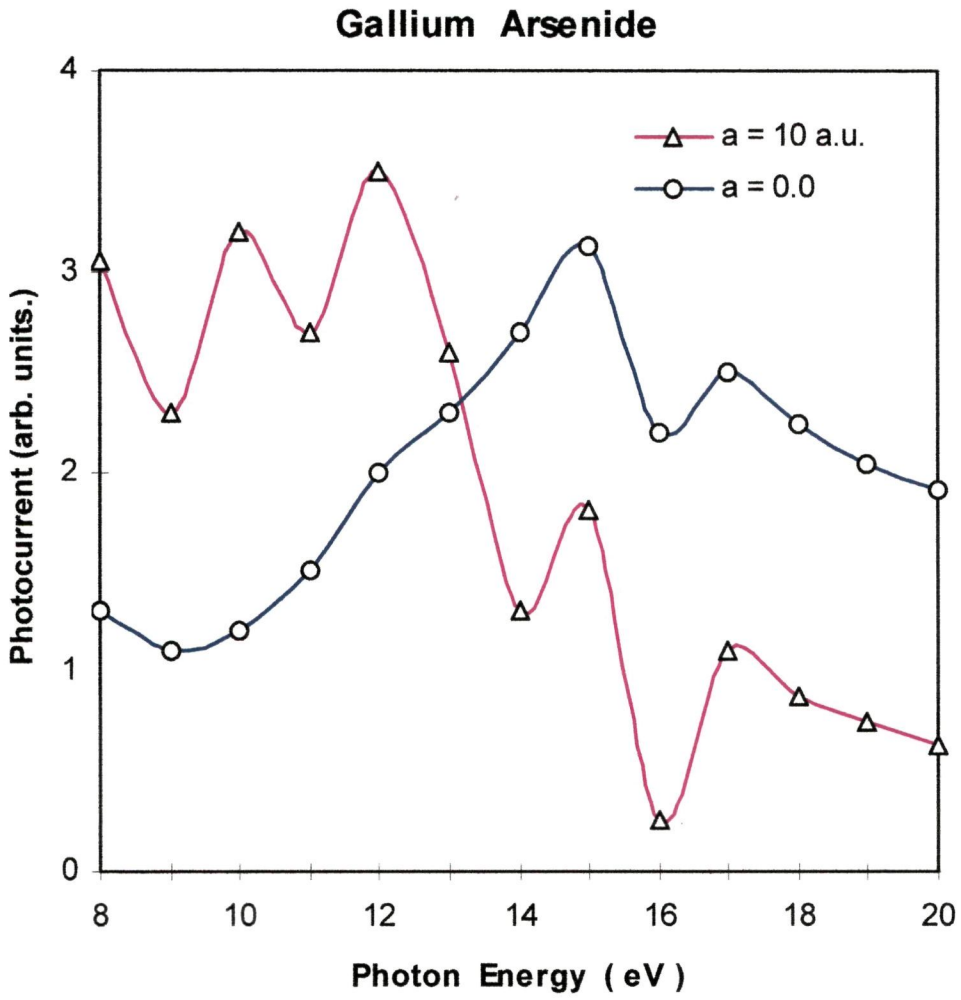
Gallium Arsenide
a = 10 a.u.
a = 0.0
Photocurrent (arb. units.)
Photon Energy (eV)
0
1
2
3
4
8
10
12
14
16
18
20

Figure 3.7

case of silicon. The reason for this being that for a = 0, both silicon and gallium arsenide had almost same values of dielectric constants as calculated by using the Drude-Lorentz formula.

We find, therefore that in the case of silicon, the model dielectric response function of Drude-Lorentz seems to work quite well for values of photon energies below and above the plasmon energy. However, a different behaviour is seen in photocurrent in the case of gallium arsenide(GaAs). For example, we find three peaks occur in photocurrent for $\hbar\omega < \hbar\omega_p$, a result seen quite different from that of silicon[77] and other metals like aluminium[41], palladium[71], tungsten[77] etc. The reason for this may be attributed to the fact that the Drude-Lorentz model for the calculation of dielectric constants is not applicable to the case of gallium arsenide. The other reason for the occurrence of such peaks may be that for $\hbar\omega < \hbar\omega_p$, the photon field vector as deduced by using the model of Bagchi and Kar[40] is not applicable to the case of compound semiconductor. We cannot rule out the weakness of the K-P model potential as used by Thapa and Kar[42] for deducing the initital state wavefunction ψ_i. The effect of the surface was not taken into consideration while formulating ψ_i for a semi-infinite solid. However, the occurrence of peaks at $\hbar\omega < \hbar\omega_p$ both for silicon and gallium arsenide can be attributed to the spatial variation of vector potential.

Lapeyre and Anderson[78] had also experimentally found the existence of surface state in gallium arsenide from the constant initial state spectroscopy. The complicated lines shapes in their measurement for the surface states were not fully understood. However, the conclusion found in their measurement was that the photoemission intensity was strongly a polarization dependent. Though we have not

taken into consideration the effect of type of semiconductor, density, etc., we find that in the case of semiconductors, the spatial dependence of vector potential is an essential ingredient in photoemission calculations. Instead of using the simple type of dielectric formula like that of Drude-Lorentz type, it would be more realistic if one can employ the method as developed by Cappellini *et. al.*[79] which is specifically defined only for the semiconductors. Further, the inclusion of crystal structure into this type of calculations will enable one to compare the data with experiment in a more realistic way. For example, a detailed study of photoemission from gallium arsenide by using the one-step model of photoemission had been done by Schattke[80]. He had used the Green function formalism to define the valence states in terms of LCAO basis functions by taking photon field vector as constant in dipole approximation. The photoemission data for the ideal gallium arsenide surface agreed well with the experimental data.

3.3 Relativistic Kronig-Penney potential model calculation of photoemission :

In the above treatments of photoemission calculations both in the case of metals and seminconductors, the spin of the electrons in the formulations of the initial state wavefunctions were not taken into considerations. This implied that the relativistic effects were omitted and it was purely a non-relativistic type of calculations. We have considered in the same way the variations of the dielectric functions for the calculations of the photon fields but adopted the wavefunctions for the initial state of the electrons as developed by Davison and Steslicka[81]. We have introduced the surface of width '*d*' into the potential model and used the wavefunctions for the evaluation of the matrix elements for photocurrent calculations. The model was applied to the case of heavy atomic solids like tungsten and silicon.

It has been seen that most of the authors have not taken into consideration the effect of relativity while applying the Kroning-Penney(KP) model to band structure studies in photoemission. For example, Thapa and others[41,71,76,77] have applied it to study the photoemission from metals like W, Si, Al, Pd, etc. But in their studies the relativistic effect on the motion of the electron in the potential well was not taken into consideration while deriving[42] the initial state wavefunction ψ_i of the electron. A detailed energy band calculations using relativistic Kronig-Penney(RKP) have been done by Davison and Steslicka (DS) by solving the Dirac equation for bulk spinors for which the surface state calculations was also given. In this section, we are discussing a simple relativistic approach to photoemission study by using the wavefunction as deduced by DS[81] for the electronic states and then applied it to the case of W and Si.

The crystal potential model as used by DS[81] for deriving ψ_i is shown in Fig. (3.8) which has a surface width d. The crystal potential is given by $Lt V_3 b = a_o$ with b as thewidth of the potential barrier and (a+b) the period of
$V_3 \to 0$
$b \to 0$
the potential, a_o being a positive quantity. The crystal surface potential is such that $V_1 > \varepsilon_o$ where ε_o is the kinetic energy related to the energy (E) of the electron given by the relation $E = \varepsilon_o + m_o c^2$, m_o being the rest mass of the electron. In the k- region of constant potential V_k, the one-dimensional time-independent Dirac equation can be written as :

$$ihc\frac{d\phi_k^{(1)}}{dx} = (\varepsilon_o - V_k)\phi_k^{(2)} \tag{3.11}$$

$$ihc\frac{d\phi_k^{(2)}}{dx} = \{(\varepsilon_o - V_k) + 2m_o c^2\}\phi_k^{(1)} \tag{3.12}$$

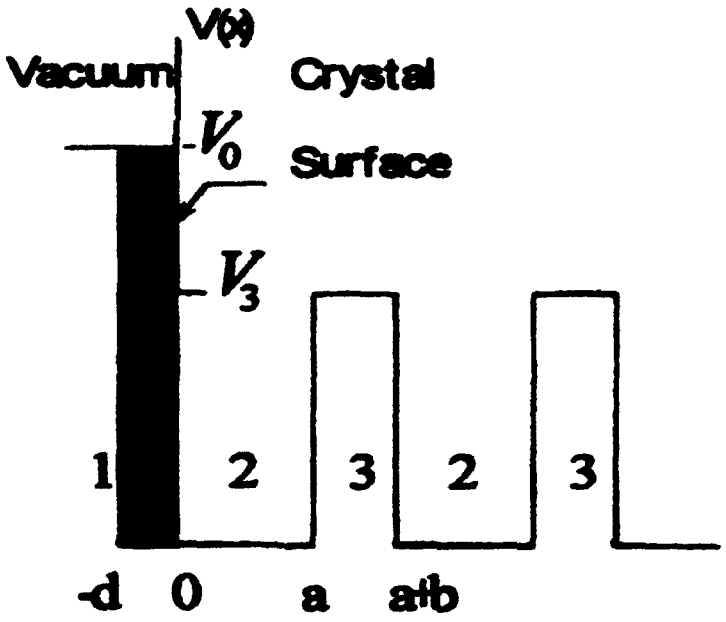

Figure 3.8

Decoupling Eqs. (3.11) and (3.12) leads to

$$ihc\frac{d\phi_k^{(j)}}{dx} = -\rho_k^2\phi_k^{(j)}, \qquad j = 1,2 \qquad (3.13)$$

where wave vector $\rho_k^2 = (\varepsilon_o - V_k)[(\varepsilon_o - V_k) + 2m_oc^2]/\hbar^2c^2$.

The plane wave solution of Eq. (3.13) for bulk (x > 0) and vacuum (x < 0) regions can be written as :

$$\psi_i(x) = \begin{cases} \phi_2(x) = a_2^{(2)}\left\{\begin{pmatrix} -\gamma_2 \\ 1 \end{pmatrix}e^{i\rho_2 x} + \lambda\begin{pmatrix} \gamma_2 \\ 1 \end{pmatrix}e^{-i\rho_2 x}\right\}, & x > 0 \\ \phi_1(x) = \begin{pmatrix} \gamma_1 \\ 1 \end{pmatrix}\beta_1^{(2)}e^{l_1 x}, & x < 0 \end{cases} \qquad (3.14)$$

where $l_1 = -i\rho_1 > 0$ and is real. The constants in Eq. (3.14) are defined as :

$$\varepsilon_o = \varepsilon - m_oc^2, \qquad a_k^{(1)} = -\gamma_k a_k^{(2)},$$

$$\beta_k^{(1)} = \gamma_k\beta_k^{(2)}, \qquad \gamma_k = \frac{\varepsilon_o - V_k}{hc\rho_k},$$

and $\lambda = \frac{\beta_2^{(2)}}{a_2^{(2)}} = \frac{1-e^{i(\rho_2-\mu)a}}{e^{-i(\rho_2+\mu)a}-1}$.

μ is the wave number and is given by $\mu = \frac{n\pi}{a} + i\zeta$ where ζ is real and $\zeta > 0$.

The final state wavefunction ψ_f which is correctly normalized in energy will be the scattering state of the step potential $V_1 = -V_o\theta(x)$, where $\theta(x)$ is a unit function. The vector potential A is assumed to be a constant in the bulk and vacuum regions but in the surface region, it is a function of x. The formula for the vector potential in one-dimension following the model of Bagchi and Kar[40] is given by

$$A_\omega(x) = \begin{cases} A_1, & x < 0 \text{ (bulk)} \\ \dfrac{A_1 \epsilon(\omega) d}{[\epsilon(\omega)-1]x+d}, & -d \leq x \leq 0 \text{ (surface)} \\ A_1 \epsilon(\omega), & x > 0 \text{ (vacuum)} \end{cases} \qquad (3.15)$$

where A_1 is a constant depending on dielectric function $\epsilon(\omega)$, photon energy $h\omega$ and angle of incidence θ_i. Such models have been used in photoemission calculation with simple forms of initial state wavefunction[41,71,76,77]. We have used the expansion of the matrix element in Eq. (3.8) for evaluation of the photocurrent. Since the integrals in the matrix element cannot be solved analytically, FORTRAN programs are developed to evaluate for computing photocurrent as a function of photon energy.

We have used the experimentally determined dielectric functions $\epsilon(\omega)$ corresponding to W and Si as given by Weaver[50]. Since it is a model calculation, we have chosen the same values of the following data (in atomic units) :

Fermi energy(E_f) = 0.3768, Potential strength(V_o) = 0.5864,

Work functon(Φ) = 0.1746, Potential width(a) = 6 a_0 (a_0 = Bohr radius)

Velocity of light(c) = 137, Surface width(d) = 10

The relativitistic parameter used in the calculations are given by :

$$\rho_1 = i0.4178, \rho_2 = 0.613$$

$$l_1 = 0.4178, \gamma_1 = -i0.001525, \quad \gamma_2 = 0.00224, \eta = 6x10^{-4}$$

The values of relativitistic Kronig-Penney(RKP) parameters like β_1, β_2, $\alpha_1, \alpha_2^{(2)}$, α_2 and λ were calculated for each values of band index number n. These values were subsituted into the matrix element for the evaluation of photocurren by using Eq. (1.3). We have calculated photocurrent against the incident photon energy ($\hbar\omega$) as a function of the band number (n) in the case of W and Si [82] for n = 2,4,6,8,10. There is no specific reason for the choice of even values of n as the photocurrent data for odd values showed similar trends[83]. In Fig. (3.9), the plot of photocurrent in the case of W is shown. We find that for all the band numbers, the peaks in photocurrent data occurred at photon energies $\hbar\omega$ = 10,18,26 eV respectively. The photocurrent peak was minimum at $\hbar\omega$ = 14 eV and maximum at $\hbar\omega$ = 26 eV. We have also calculated photocurrent in the case of silicon which is a heavy diatomic solid. The photocurrent data for silicon is shown in Fig. (3.10). We find that for all the band numbers, maxima occurred at photon energy $\hbar\omega$ = 11 eV and 20 eV respectively, but for $\hbar\omega$ > 20 eV, the peak went down drastically to a minimum and then decayed.

The photoemission calculations in the case of W and Si using the non-relativistic Kronig-Penney (NR-KP) model have been done earlier[41,76,77]. It has been observed that in the non-relativistic case, the photocurrent showed maxima at values of $\hbar\omega < \hbar\omega_p$ and a minimum occurred at $\hbar\omega \sim \hbar\omega_p$ for both W and Si. For example, in the case[41] of W maxima occurred at $\hbar\omega$ = 21 eV and a minimum at 26 eV (for tungsten, $\hbar\omega_p$ = 25.3 eV). However, in the case[41] of Si the photocurrent data

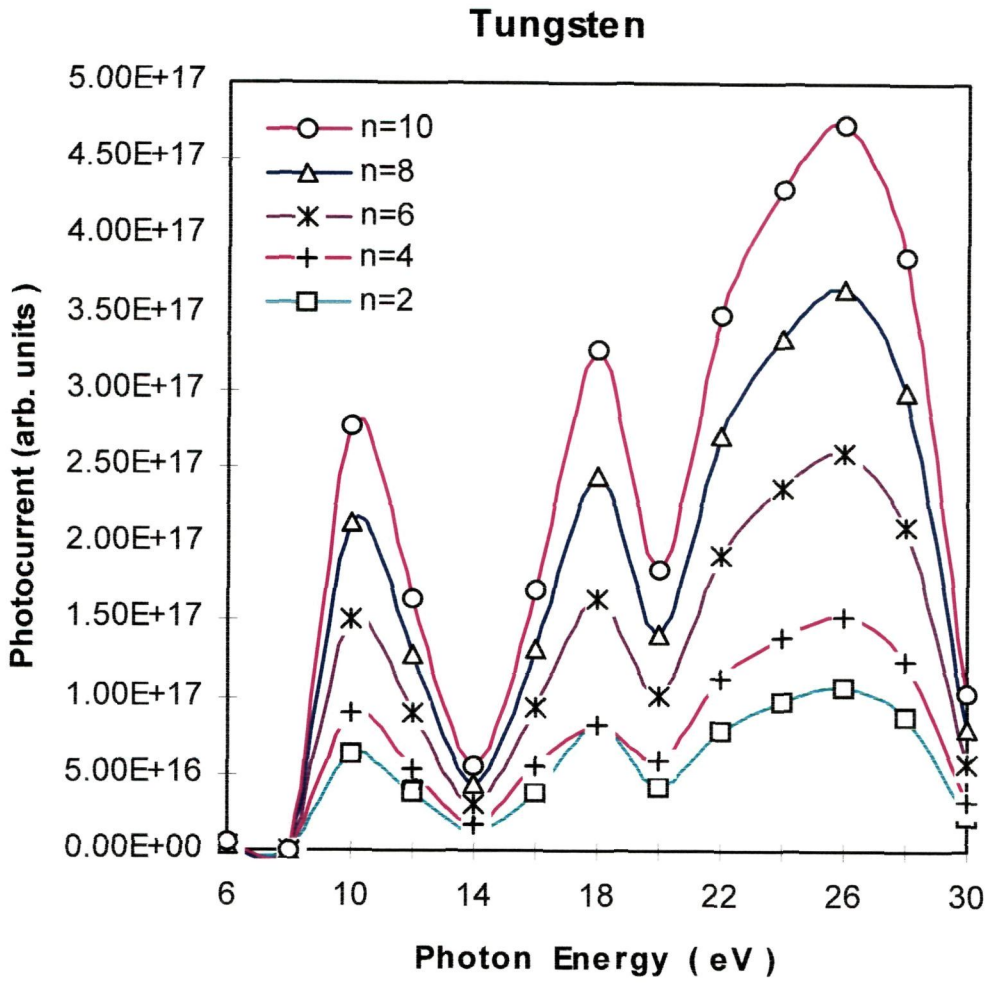
Tungsten
5.00E+17
4.50E+17
4.00E+17
3.50E+17
3.00E+17
2.50E+17
2.00E+17
1.50E+17
1.00E+17
5.00E+16
0.00E+00
Photocurrent (arb. units)
n=10
n=8
n=6
n=4
n=2
6
10
14
18
22
26
30
Photon Energy (eV)

Figure 3.9

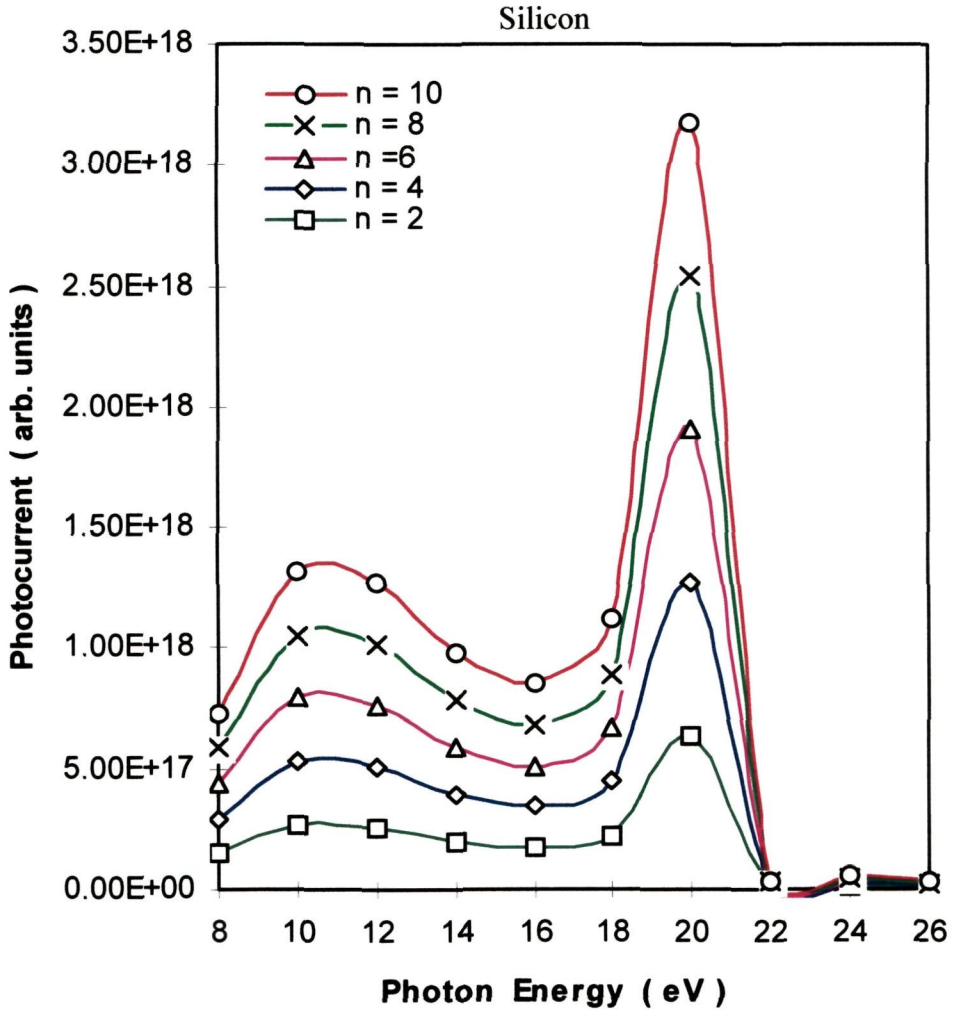
Silicon
3.50E+18
3.00E+18
2.50E+18
2.00E+18
1.50E+18
1.00E+18
5.00E+17
0.00E+00
Photocurrent (arb. units)
n = 10
n = 8
n =6
n = 4
n = 2
8
10
12
14
16
18
20
22
24
26
Photon Energy (eV)

Figure 3.10

showed a lot of structures instead of a single maximum at $\hbar\omega < \hbar\omega_p$. It also did not show a minimum at $\hbar\omega_p$(for silicon, $\hbar\omega_p$ = 16 eV). The reason has been attributed to the behaviour of the dielectric function $\epsilon(\omega)$. The behaviour of photocurent data in RKP case is completely different from that of NR-KP model. For example, in the case of W, we find that for the values of photon energies greater than 20 eV, the plot showed a peak in photocurrent data at $\hbar\omega$ = 26 eV, very close to $\hbar\omega_p$. This is in fact in contrast to the data obtained earlier by other methods[40,41,58,76] where a minimum was observed at $\hbar\omega = \hbar\omega_p$. Also for the values of $\hbar\omega < \hbar\omega_p$, we find two peaks in photocurrent at $\hbar\omega$ = 10 and 18 eV with a minimum at $\hbar\omega$ = 14 eV. Similarly, in the case of Si as shown in Fig. (3.10), we find that for a lower photon energy range the behaviour of photocurrent data showed features similar to that obtained in surface photoeffect. For example, a maximum was observed at $\hbar\omega$ = 10 eV followed by a minimum at $\hbar\omega$ = 16 eV (the plasmon energy of Si). There is increase in photocurrent for $\hbar\omega > \hbar\omega_p$ and a maximum is observed at photon energy of 20 eV for all the band numbers. The graphs showed a minima again at $\hbar\omega$ = 22 eV and decreased down towards a minimum for all the band numbers for further increase of photon energies.

The interesting feature which is seen in both the case of W and Si is that for the increase in band numbers the peak in photocurrent also goes on increasing. The only difference is that in the case of W, the highest peak on photocurrent is observed at $\hbar\omega = \hbar\omega_p$, whereas for Si it is obtained at photon energy 20 eV which is greater than its plasmon energy. This can be attributed to the fact that the band width ΔE_b goes on decreasing for the increase in band number. In other words, the relativistic correction[84] reduces ΔE_b which causes the electrons to gain sufficient momenta due to rapid spatial variation of the incident radiation to be photoexcited.

This causes the enhancement of photocurrent with the increase in n in both the cases of W and Si. In both the NR-KP and RKP treatment of photoemission, we find that only in the low frequency region photoemission is dominant due to spatial variation of the photon field vector. The evidence for this is the occurrence of peaks for the value of $\hbar\omega < \hbar\omega_p$, which has been already observed experimentally by Levinson and others[31]. But the occurrence of peaks in photoemission by using the RKP model may be described as the manifestation of band structure effects in photoemission which has not been observed in the NR-KP cases.

In the case of the relativistic treatment of photoemission (Figs. 3.9 and 3.10) by incorporating the spatially dependent vector potential, we find that the features seen in the behavior of photocurrent is quite different from the one obtained by using the NR-KP model. We did not find any peak in photocurrent for values of $\hbar\omega$ below and above the plasmon energies. Such deviation both in the case of W and Si may be due to the fact that the initial state wavefunction ψ_i as deduced by DS[81] is not applicable to photoemission calculations although the spatially varying photon field is used. We have in fact just attempted to include the effect of relativity also in photoemission calculations. We find from the data that both in the case of W and Si for RKP model, minima is seen at around the plasmon energies. The occurrence of peaks in photocurrent data is attributed mainly due to inclusion of relativistic effects in photoemission.

The main drawback of including the initial state wavefunction ψ_i as derived by DS[81] is that it does not take into account the surface width. It has been well defined for both the vacuum and bulk regions. Further, we have not done any detailed calculations to derive the initial state wavefunction ψ_i. What we are trying

to do here is that we have just used the wavefunction as derived by DS for the band state calculations using the K-P model potential. We also conclude from this study that the incorporation of the spatially variant vector potential is not sufficient. Further, the measured ultraviolet photoemission spectra(UPS) data have shown that effects due to spin-orbit coupling[84] cannot be omitted in photoemissin spectra[85-87]. Also the solution of Schrodinger's equation without the inclusion of spin-orbit interaction will become more and more inadequate[88] in photoemission spectral measurements. One has to also modify the calculation for vector potential keeping in view the relativistic effects. There is, therefore, a need for relativistic theory of photoemission for accurate presentation of the UPS data.

CHAPTER 4

PHOTOCURRENT CALCULATIONS USING MATHIEU POTENTIAL MODEL

In the last few decades, interests in detailed understanding of the physical properties of condensed materials and their surfaces have grown up fastly. Further, the development in micro-electronics have reached a point where surface properties have become very much dominant. Several developments has been made in the production of two dimensional structures like multilayers or thin films, which have new and fascinating features. For investigating the electronic properties of clean and adsorbate covered surfaces and thin films, angle resolved ultraviolet photoemission spectroscopy (ARUPS) has become one of the important tools as it allows to measure the dispersion of the bands for both occupied and unoccupied bands. Therefore, it revealed the electronic structure around the Fermi level with high amount of accuracy[29,89,90]. In order to interpret the experimental spectra, it is useful to have a quantitative comparison between the theoretical and experimental photoemission data. This demand has led to the developments of various approaches for calculating photocurrent which ranges from accurate many-body theories[91] to one-electron formulations.

In the previous chapters, we have seen that photocurrent calculations was done by using various potential models in the case of metals and semiconductors. For example, free electron[41,92] and Kronig-Penney potential[71,76,77] models were used in

the case of beryllium, tungsten, copper, silicon, etc. Photoemission studies were also carried out in the case of tungsten and silicon by using the relativistic Kronig-Penney model. We found that in the case of copper (as shown in Fig. 3.3) , Kronig-Penney model did not fit well since the plot did not show peak in photocurrent below the plasmon energy. With the increase of photon energy, the photocurrent also did not show a minimum at the plasmon energy. In the case of copper, maxima in photocurrent was measured at $\hbar\omega = 20$ eV with a minimum at $\hbar\omega = 26$ eV. Also, the application of relativistic Kronig-Penney model to W and Si showed too many peaks in photocurrent with the increase of photon energy. This is quite a different trend in the behaviour of photocurrent. These results do not conform to the calculated and measured data in photoemission when one is usually concerned with the variation of photocurrent against photon energy especially from the surface of metals. For this reason, we have applied Mathieu potential model to evaluate the initial state wavefunction to calculate the matrix element in photocurrent by using the same dielectric model as used in the earlier chapters. The photocurrent data obtained in this formalism could explain the behaviour of photocurrent also in the case of copper.

In this chapter, we shall use the Mathieu Potential model to represent the crystal potential. In this model, the potential is represented by a periodic sinusoidal wave in one-dimensional crystal. For such a potential, the Schrodinger equation reduces to the *Mathieu equation* whose solutions have been discussed in detail by McLachlan[93]. The Mathieu potential had been used early by Brillouin[94] and Morse[95]. Brillouin had used this model as an appropriate model for developing the energy band theory of solids, while Morse used it in his study of electron diffraction. Slater[96] used the Mathieu potential problem in one, two and three dimensions to describe the energy bands in a realistic crystal. Then Carver[48] has discusssed the symmetries of

Mathieu functions, and the relations between the functions and the electron wave functions at the centres and edges of the crystal bands. The Mathieu potential has been at first used by Statz[45] for surface state calculation. Levine has used Mathieu potential for calculating the condition for arbitrary surface termination. In this chapter, we will discuss a formalism developed for photoemission calculations in which the electron states are derived by using the Mathieu potential[44]. Two cases will be discussed namely, the effects of the empty lattice and strong periodic lattice potential on the electronic states for deriving the initial state wavefunctions as discussed by Davison and Steslicka[49].

4.1 Empty Potential with Finite Surface :

Let us consider a one - dimensional crystal whose potential is represented by a sinusoidal potential given by

$$V(x) = V_o \cos(\frac{2\pi x}{a}) \qquad (4.1)$$

where 'a' is the period of the potential having a maximum value V_o at x = 0. The one-dimensional Schrodinger equation can be written as

$$\psi''(z) + (a - 2q\cos 2z)\psi(z) = 0 \qquad (4.2)$$

where $z = \frac{\pi x}{a}, T = \frac{\pi^2}{a^2}, a = \frac{E}{T}$ and $2q = \frac{V_o}{T}$.

Eq. (4.2) is the *Mathieu equation* and its solution is derived for free electron or nearly empty potential (q ~ 0) when the crystal potential is flat as shown in Fig. (4.1). To

determine the initial state wavefunction $\psi_i(x)$ in Eq. (4.2), we have included a surface of width (d) in the crystal potential. The initial state wavefunction for the bulk and surface and for the vacuum region is calculated[97] as :

$$\psi_i(x,q) = \begin{cases} (\frac{1}{4\pi k_i})^{\frac{1}{2}} \phi(x_0,q) e^{-\mu(x_o - x)} & x \leqslant 0 \\ (2\xi)^{\frac{1}{2}} e^{-\xi(x - x_o)} & x > 0 \end{cases} \qquad (4.3)$$

where x_0 = location of the crystal surface. In Eq. (4.3) above, we have $k_i = \sqrt{2E_i}$ and

$$\phi(x_0,q) = \lambda \cos m'x - \sin m'x,$$
$$\lambda = \tan m'(x_0 - \xi^{-1}) \qquad (4.4)$$

such that $m' = \frac{m\pi}{a}$, m being the band gap index, ξ is the height of step potential and λ is the hybridization parameter.

Using the final state wavefunction ψ_f as the scattering state[40] of the step potential as used in the case of Kronig-Penney model, the photocurrent density is calculated by using the Fermi golden rule formula[25] as

$$\frac{dj(E)}{d\Omega} = \frac{2\pi}{\hbar} \Sigma | < \psi_f | H' | \psi_i > |^2 \delta(E - E_f) \delta(E_f - E_i - \hbar\omega) f_o(E - \hbar\omega)[1 - f_o(E)]$$

(4.5)

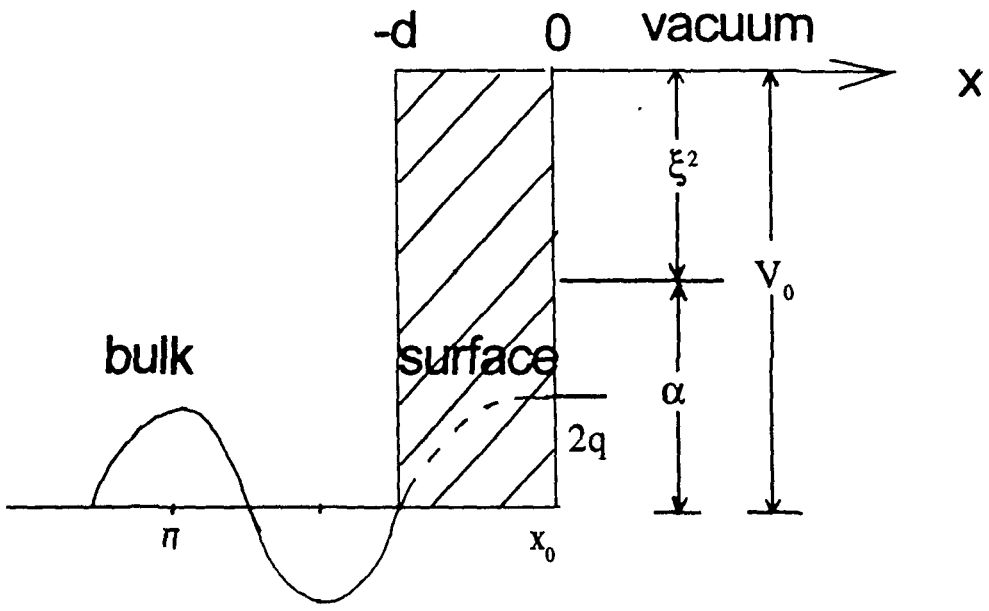

Figure 4.1

The perturbation in one dimension, H' can be written as

$$H' = \frac{e}{mc}[\tilde{A}_\omega(x)\frac{d}{dx} + \frac{1}{2}\frac{d}{dx}\tilde{A}_\omega(x)] \qquad (4.6)$$

With simple modification, the photon field used in our calculation can be written as

$$\tilde{A}_\omega(\omega,x) = \begin{cases} A_1, & x < -d \\ \frac{A_1.\varepsilon(\omega).d}{[1-\varepsilon(\omega)]x+d}, & -d \leqslant x \leqslant 0 \\ A_1.\varepsilon(\omega), & x > 0 \end{cases} \qquad (4.7)$$

where A_1 is a constant depending on the dielectric function $\varepsilon(\omega)$, photon energy $\hbar\omega$ and angle of incidence θ_i. We have chosen $x_0 = \frac{a}{2}, \xi = \frac{12}{a}$ and $m = 1$. The reason for the choice of m = 1 is that the surface state exists in the band gap[44] for finite potential case. The matrix element in Eq. (4.5) can be written as follows for calculating the photocurrent :

$$I = \int_{-\infty}^{-d} \psi_f^* \tilde{A}_\omega(x)\frac{d\psi_i}{dx}dx + \int_{-d}^{0} \psi_f^* \tilde{A}_\omega \frac{d\psi_i}{dx}dx$$

$$+\frac{1}{2}\int_{-d}^{0} \psi_f^* \frac{d\tilde{A}_\omega(x)}{dx}\psi_i dx + \int_{0}^{\infty} \psi_f^* \tilde{A}_\omega(z)\frac{d\psi_i}{dx}dx. \qquad (4.8)$$

Photocurrent was calculated as a function of photon energy ($\hbar\omega$) by evaluating the integrals in Eq. (4.8). The formalism was then applied to the case of metals Al and Be as they are free electron type of metals. For these metals, we have used the experimentally determined dielectric function[50,51] for calculating the photon fields through the subroutine of the main FORTRAN program.

The plot of photocurrent as a function of $\hbar\omega$ for normal photoemission for the case of Al and Be is shown in Fig. (4.2). We have shown here the photoemission for constant initial state for which the energy was located at the Fermi level. As it is a model calculation, we have chosen the Fermi level for both Al and Be as 0.43 Hartrees. The photocurrent data[97] for Al showed a strong photoemission at photon energy $\hbar\omega$ = 10 eV. This was followed by a suppressed photoemission and therefore photocurrent was minimum at $\hbar\omega$ = 15 eV (the plasmon energy of Al is $\hbar\omega_p$ = 15.3 eV). There is another hump in photocurrent data at $\hbar\omega$ = 18 eV. Similar trends in the behaviour of photocurrent in the case of Al were also found by using other models like free electron case[41,92] and Kronig-Penney model [98] . When the photocurrent data is compared with the experimental data of Levinson *et. al.*[31] , we find that our results atleast reproduced the measured data qualitatively. Levinson and others[31] have shown that maxima in photocurrent occurred at $\hbar\omega$ = 13 eV with the occurrence of minima at the plasmon energy of Al. The photocurrent behaviour in the case[97] of Be is also similar to that of Al. For example, it showed a maxima at $\hbar\omega$ = 10 eV followed by a minimum occurring at $\hbar\omega$ = 19 eV (the plasmon energy of Be is 19.5 eV). There was enhancement in photocurrent value for $\hbar\omega > \hbar\omega_p$. We see from the variation of photocurrent data that even in the case of Be, it has shown the qualitative behaviour as seen earlier in the theoretical results of Thapa and Kar[52] and the experimental data of Bartynski *et. al.*[53] and Plummer[99] as shown in Fig. (4.3).

The features seen in the behaviour of photocurrent in Al and Be can be attributed to the fact that in the free electron metals the change in bulk potential is too weak to impart sufficient momentum for photoexcitation[99]. The surface photo-effect is due to the rapid variation of photon field in the surface region. This is evident from the

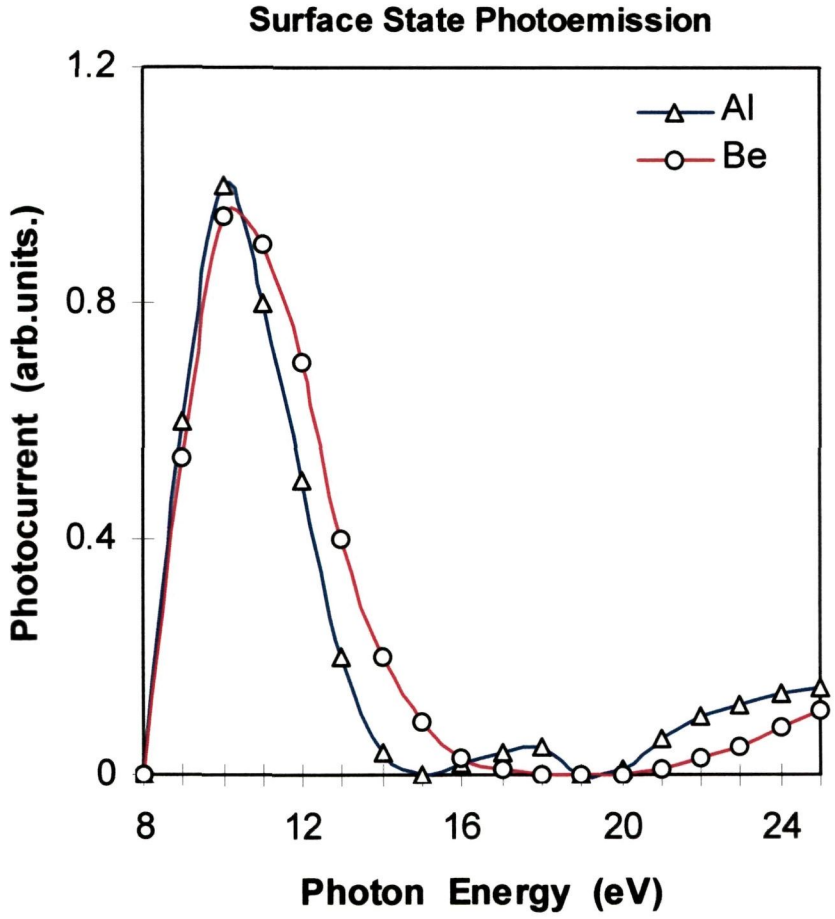
Surface State Photoemission
1.2
0.8
0.4
0
Photocurrent (arb.units.)
Al
Be
8
12
16
20
24
Photon Energy (eV)

Figure 4.2

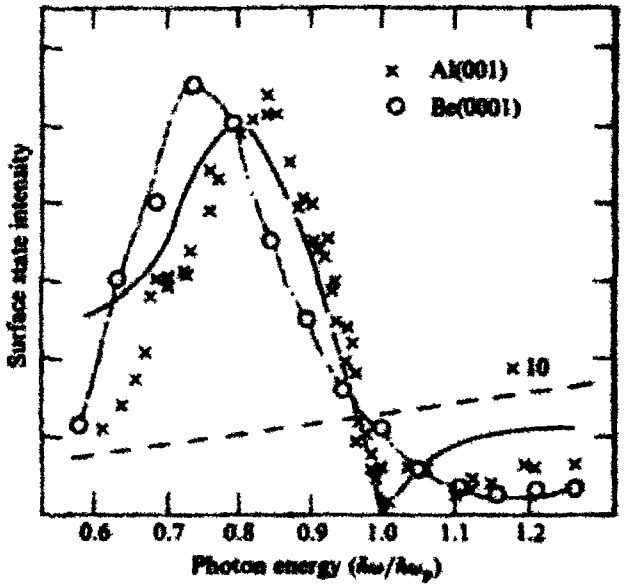
Al(001)
Be(0001)
× 10
Surface state intensity
0.6
0.7
0.8
0.9
1.0
1.1
1.2
Photon energy (ħω/ħω_p)

Figure 4.3

matrix element in Eq. (4.5) where $d\tilde{A}_{\omega}/dx$ is directly dependent on photocurrent as the photon energy passes through the threshold for plasmon excitation. Moreover, we have considered a low photon energy photoemission and hence the incident radiation is too weak to photoexcite electrons from the bulk bands. The origin of peak in photocurrent data in the case of Be for $\hbar\omega < \hbar\omega_p$ has been explained by Karlsson *et. al.*[100] from band picture. He attributed this to the existence of surface state at $\bar{\Gamma}$ with energy 2.8 eV in the bulk energy band gap $\Gamma_3^+ - \Gamma_4^-$.

4.2 **Strong Periodic Potential with Finite Surface :**

The case of empty lattice potential is not applicable to the strongly bonded metals like d-band metals or semiconductors. Hence one needs to develop the intial statre wavefunctions by solving the Mathieu equation in Eq. (4.2) by incorporating the sine and cosine elliptic functions. We have considered the same model as in the case of empty lattice potential model which is given in Fig. (4.1), but used it for strong periodic potential i.e. q > 0. The only difference with empty potential case is that we have to evaluate the function $\phi(x_0,q)$ more appropriately to define the existence of surface states.

It is therefore, necessary to find an explicit form for $\phi(x_0',q)$ in Eq. (4.4) to derive the intial state wavefunction $\psi_i(x)$. Here the coordinate $x_0' = \frac{\pi}{a}x_0$ unlike the case of empty potential. The most general form is a linear combination of all the bulk standing states $se_m(x_0',q)$ and $ce_m(x_0',q)$ for all the Fermi energy gap m. Thus the surface states will be largely a hybrid of sine and cosine elliptic functions which is given by the expression

$$\phi(x_0',q) = \lambda_m ce_m(x_0',q) - se_m(x_0',q) \qquad (4.9)$$

where λ_m is the hybridization parameter which can be written as

$$\lambda_m = \frac{se_m(x_0', q) - (\xi + \mu)^{-1} se_m'(x_0', q)}{ce_m(x_0', q) - (\xi + \mu)^{-1} ce_m'(x_0', q)} \tag{4.10}$$

The sine and cosine elliptic functions in Eq. (4.9) in expanded form can be written as

$$se_m(x_0', q) = \sin mx_0' - \frac{q}{4}\left[\frac{\sin(m+2)x_0'}{m+1} - \frac{\sin(m-2)x_o'}{m-1}\right] + \frac{q2}{32}\left[\frac{\sin(m+4)x_o'}{(m+1)(m+2)} + \frac{\sin(m-4)x_o'}{(m-1)(m-2)}\right] + ... \tag{4.11}$$

and

$$ce_m(x_0', q) = \cos mx_0' - \frac{q}{4}\left[\frac{\cos(m+2)x_0'}{m+1} - \frac{\cos(m-2)x_o'}{m-1}\right] + \frac{q2}{32}\left[\frac{\cos(m+4)x_o'}{(m+1)(m+2)} + \frac{\cos(m-4)x_o'}{(m-1)(m-2)}\right] + ... \tag{4.12}$$

For finite surface potential, surface state existence condition implies that

$$x_0' = \frac{\pi}{a}x_0,\ \xi = \frac{12}{a},\ \lambda > 0 \text{ and } m = 3, 5, .. \tag{4.13}$$

We are considering surface state occuring for m = 3 and hence from Eqs. (4.11), (4.12) and (4.13), we can write,

$$ce_3(x_o', q) = 0 \quad , \qquad ce_3'(x_o', q) = 3(1 + \frac{q}{16} - \frac{q^2}{640})$$

$$se_3(x_o', q) = -1 + \frac{q}{16} - \frac{11}{640}q^2 \quad , \qquad se_3'(x_o', q) = 0 \tag{4.14}$$

Hence, we may obtain the value of λ_3 as :

$$\lambda_3 = \frac{(\xi+\mu)\left[1 - \frac{q}{16} + \frac{11}{640}q^2\right]}{3(1 + \frac{q}{16} - \frac{q^2}{640})} \qquad (4.15)$$

Using Eqs. (4.13) and (4.14) into Eq. (4.9), the intial state wavefuntion in the case of strong periodic potential becomes

$$\psi_i(x,q) = \begin{cases} (\frac{1}{4\pi k_i})^{\frac{1}{2}}(-1 + \frac{q}{16} - \frac{11}{640}q^2)e^{-\mu(x_o'-x)} & x \leqslant 0 \\ (\frac{1}{4\pi k_i})^{\frac{1}{2}} e^{-\xi(x-x_o')} & x > 0 \end{cases} \qquad (4.16)$$

The final state wavefunction ψ_f used is the scattering state[40] of the step potential which is same as that was employed in Kronig-Penney model in Chapter 3, and the photon field is the one described in empty potential case in Section 4.1. Photocurrent was calculated[101] as a function of photon energy ($\hbar\omega$) in the case of d-band metals like molydenum, tungsten, copper and semiconductor silicon. For each of these metals, the experimentally determined dielectric function[50,51] were used for calculating the photon fields but the same surface parameters were used for all of these solids as it is a model calculation.

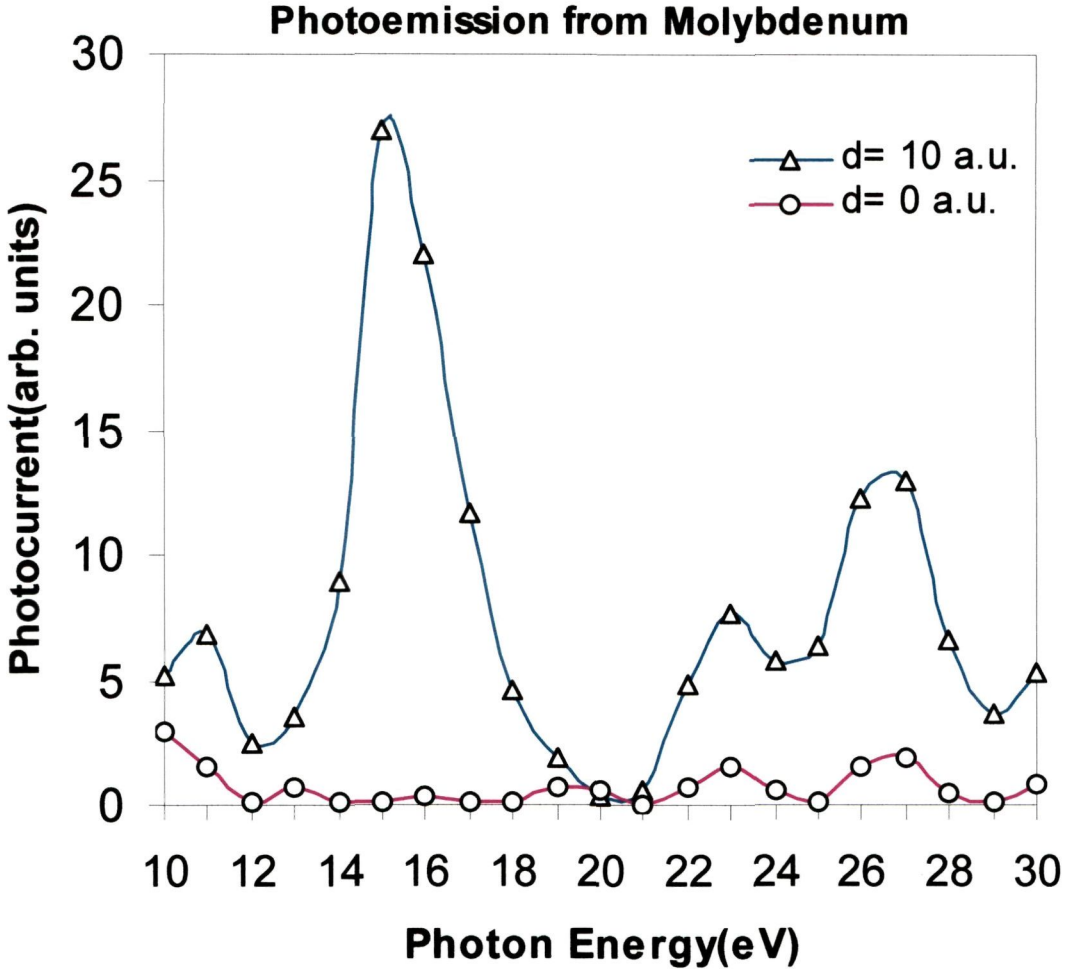
Photoemission from Molybdenum
Photocurrent(arb. units)
30
25
20
15
10
5
0
10 12 14 16 18 20 22 24 26 28 30
Photon Energy(eV)
d= 10 a.u.
d= 0 a.u.

Figure 4.4

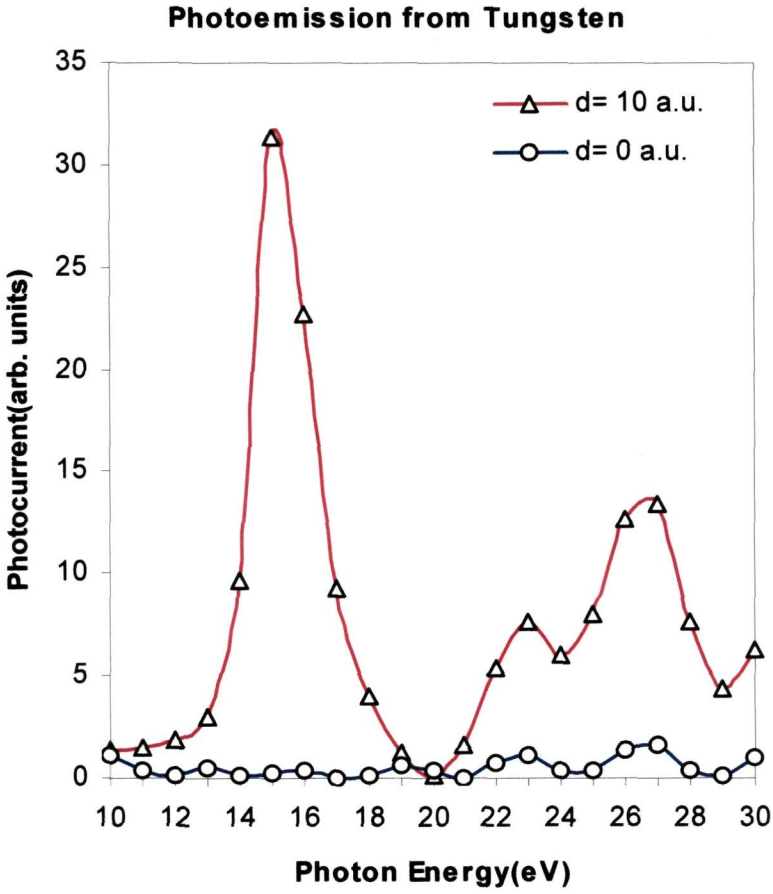
Photoemission from Tungsten
d= 10 a.u.
d= 0 a.u.
Photocurrent(arb. units)
Photon Energy(eV)
0
5
10
15
20
25
30
35
10
12
14
16
18
20
22
24
26
28
30

Figure 4.5

(a) **Tungsten(W) and Molybdenum(Mo) :**

The plot of photocurrent as a function of photon energy ($\hbar\omega$)) for W and Mo is shown in Figs. (4.4) and (4.5), both for surface width d = 10 a.u. and narrow surface width (d = 0). We have considered the case of high lying surface state as was done by Weng *et. al.*[58] which is shown in Fig. (4.6). The high lying surface state lies at - 0.4 (- 0.3 eV) for W(Mo). The peak in photocurrent occurred at $\hbar\omega$ = 15 eV in the case of both W and Mo. But as the value of photon energy increased, the photocurrent decreased and showed minimum at the photon energies 20 eV (21 eV) in the case of W (Mo). The plasmon energies of W and Mo are respectivley 25.3 eV and 24.4 eV. Both of these metals showed a shoulder in photocurrent again at $\hbar\omega$ = 23 eV followed by a peak of smaller height at $\hbar\omega$ = 27 eV. The ratio between the two peaks in photocurrent at photon energies 15 eV and 23 eV is approximately 43 % (49 %) in the case of W(Mo). However, the case of narrow surface width did not exhibit such behaviour in photocurrent both in the case of W and Mo.

The experimental data of Weng *et. al.*[58] showed that the ratio between the two peaks in photocurrent in the case of W and Mo are approximately 45 % and 54 %. This has a close approximation to our calculated data. Also the occurrence of second peak in photocurrent in our calculated data in both W and Mo is closely related to the experimental data as shown in Fig. (4.6). However, the minimum in photocurrent for W(Mo) did not occur at the plasmon energies which was clearly displayed by the experimental data. We thus find that the Mathieu potential model used in this calculation for defining the initial state wavefunction is a useful model, as the data calculated showed atleast the qualitative behaviour with the experimental results.

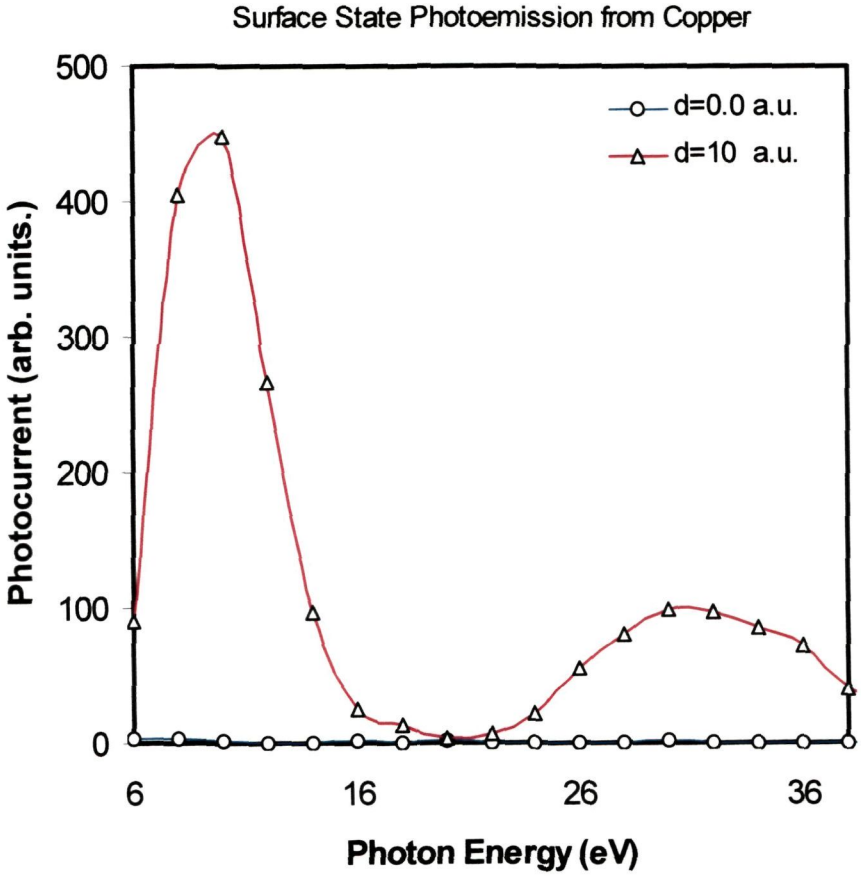
Surface State Photoemission from Copper
d=0.0 a.u.
d=10 a.u.
Photocurrent (arb. units.)
500
400
300
200
100
0
6
16
26
36
Photon Energy (eV)

Figure 4.7

(b) **Copper(Cu)** :

We have plotted the behaviour of photocurrent as a function of photon energy both for surface width d = 10 a.u. and narrow surface width for Cu (Fig. 4.7). For the surface width d = 10 a.u., the photocurrent showed a maximum at $\hbar\omega$ = 10 eV and decreased to minimum at 20 eV, the plasmon energy of Cu. At photon energy ($\hbar\omega$) = 30 eV, it showed a second peak in current but of lower height than at $\hbar\omega$ = 10 eV.

It has been reported by Himpsel and Ortega[102] that for Cu(100), Fermi level photoemission intensity when plotted as a function of photon energy, the data showed maxima at $\hbar\omega$ = 10.5 eV. Similar reports were also given by Eastman *et. al* [103]. but with maximum intensity occuring at $\hbar\omega$ = 10.6 eV. In our case, our model calculations has shown peak in photocurrent at $\hbar\omega$ = 10 eV. The occurrence of such peak in photocurrent in the band structure had been attributed to transition in energy between the lower and upper s-p bands either at the Fermi level or near it and has Δ_5 symmetry. The case of photocurent for narrow surface width just produced a linear line of very negligible magnitude in photocurrent. We find that Cu has shown atleast the qualitative feature with the behaviour of photocurrent as indicated also by other metals like Pd[71], W[72], Si[72] etc. which were calculated earlier.

(c) **Silicon** :

We have also used this model for calculating photocurrent from semiconductor Si which is shown in Fig. (4.8). For surface width d = 10 a.u., we find that photocurrent showed a maximum height at $\hbar\omega$ = 10 eV followed by a minimum at $\hbar\omega$ = 15 eV. A second peak of small magnitude was found at $\hbar\omega$ = 17 eV and decreased again to

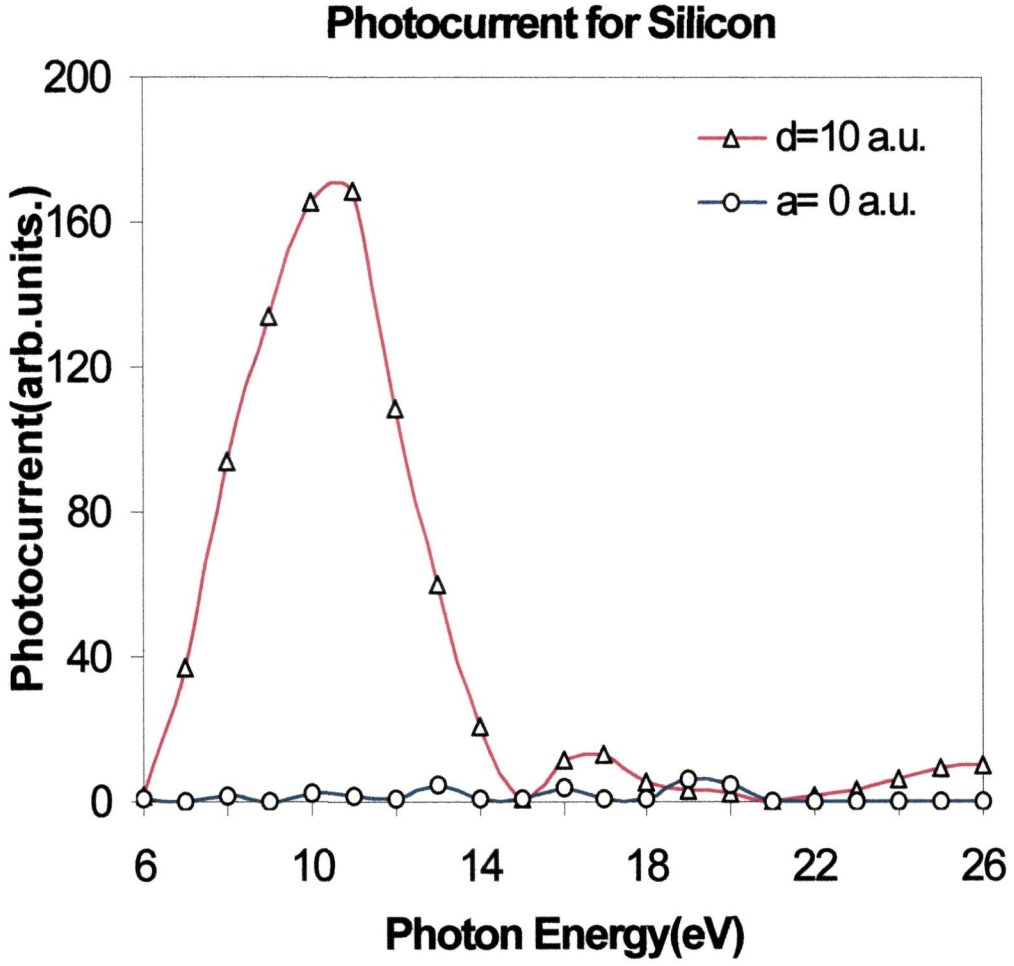
Photocurrent for Silicon
200
160
120
80
40
0
Photocurrent(arb.units.)
d=10 a.u.
a= 0 a.u.
6
10
14
18
22
26
Photon Energy(eV)

Figure 4.8

minimum at 21 eV with further increase in photon energy. This can be attributed to the behaviour of $\varepsilon(\omega)$ for silicon[39] which has a resonance at 21 eV. In the case of Si also, for the case of narrow surface width the magnitude of photocurrent is negligible for all the values of photon energy.

We also have calculated the wavefunction given in Eq. (4.15) for q = 0 to see whether this can reproduce the results calculated in the case of empty potential (q ~ 0) and for surface state condition m = 1. When this is applied to the case of Al and Be, it was seen that the photocurrent data matched exactly the earlier reported data both for Al and Be respectively, which was shown in Fig. (4.2).

A study of these cases show that one can also make use of Mathieu type of potential in photoemission calculations. Though the model used is very simple, however, the inclusion of initial state wavefunction into the matrix element appears to produce the qualitative features as observed earlier in the experimentally measured data of photocurrent. The main drawback of of the model used is that the same initial state wavefunction ψ_i is used to describe both the surface and bulk regions of the solids under study. We have used the constant initial state energy for all the cases and also kept constant other parameters as it is a model calculation. However, it is interesting to note that the wavefunctions formulated for strong periodic potential easily reproduces the wavefunctions for empty potential (free electron) cases. It would be further interesting to extend such type of model to include the band structure effects in the electronic structure calculations.

CHAPTER 5

CONCLUSION

In this thesis, we have shown the photocurrent calculations by using a modified form of simple dielectric model as given by Bagchi and Kar[40]. At first, we have calculated the variation of photon field against the photon energy for the planes located in the surface region. We have used the metals beryllium, molybdenum, tungsten and silicon for calculation of the electromagnetic fields. In our calculations, we found that there are a lot of structures associated with the variation of the photon field instead of a monotonic trend.

It was found that photoemission calculations by using the free electron model could not explain the band structure effects. Thapa *et. al*[41,42] has used the Kronig-Penney model for derivation of the initial state wavefunction ψ_i and applied it to calculations of band state photoemission from aluminium, tungsten and silicon with success. With this motivation, we have performed photocurrent calculations using the dielectric constants of molybdenum, copper, silicon and gallium arsenide but with a modofied dielectric model for the surface region. It was seen that in our calculations, the plasmon energy has effect on the photocurrent calculations. In most of the photoemission calculations, it was found that the photocurrent showed a peak at photon energy less than the plasmon energy and a minimum at the plasmon energy. We have also used the Lorentz-Drude dielectric model for the photocurrent calculations from the semiconductors to see whether it could explain the band state photoemission. We have also done the photocurrent calculations by using the constant inital state and final state wavefunction but with no surface region. In this case,

the peak below the plasmon energy was not found in the photocurrent data and also a minimum at the plasmon energy was not exhibited. Therefore, we can conclude that the inclusion of surface is important in photocurrent calculations from metals and semiconductors.

We have included the effect of relativity also in photoemission calculations. We have just used the wavefunction as derived by Davison and Steslicka[81] for the band state calculations using the KP model potential. From our calculations, we can conclude that the incorporation of the spatially variant vector potential is not sufficient. Further, the measured ultraviolet photoemission spectra(UPS) data have shown that effects due to spin-orbit coupling[84] cannot be omitted in photoemissin spectra[85-87]. One has to also modify the calculation for vector potential keeping in view the relativistic effects. There is, therefore, a need for relativistic theory of photoemission for accurate presentation of the UPS data.

Finally we have shown the application a simple potential model like Mathieu potential to the study of photoemission which has not been done so far. Davison and Steslicka(DS)[49] have used such type of sinusoidal periodic potential to the case of surface state studies. The advantage with this model is that it can monitor the situations from Nearly Free Electron(NFE) model to Tight Binding Approximation(TBA) method. One could have also used various types of potentials in such kind of studies, however, since DS has already established the fact for the existence of surface state for band index m = 1 (free electron case) and m = 3,5, etc. (tight binding case) we have chosen this potential as case study to incorporate the photoeffect. As dis cussed earlier in the case of W and Mo in chapter 4, we have observed that the model worked quite satisfactory. We have also then extended the model to the photoemission studies from

copper and silicon with the motivation by this fact. Interestingly, the results showed similar trends as was obtained in the case of W and Mo.

Howver, there are certain drawbacks in the model that we have employed i.e. Mathieu potential. For example, we paid attention only to the derivation of initial state wavefunction. We have not considered the final structural effects in which the final state wavefunction will have some important to play. This had been explained by Egelhoff *et. al.*[104] in the case of photoemission data[58] of W and Mo where macroscopic effects on final state band structure was essential. It has also been seen that dielectric response plays important role especially for surface photoemission in metals. This is required in order to describe appropriately the variation field in the bulk, surface and vacuum regions of metals. Though the dielectric model employed in our case is a simple one, howver it can be applied to the case of photoemission stuides. This has been further evidenced by the theoretical and experimental studies of resonant surface photoeffect[105] in the case of oxygen adsorbed on W(100) where such type of dielectric model was used. It would be appropriate for semiconductors, if a different model be used as proposed by Cappellini *et. al.*[79]. Further, we have not considered the role of symmetry points and the directions in the formulation of initial state wavefunction. For example, in the case of W, it is Δ_1 and Δ_5 initial states which can be excited on the (100) face of the bcc crystal (W). Moreover, it is Δ_1 symmetry (initial states) which is photoexcited by only z-component of vector potential **A** which is normal to (100) face. Δ_5 symmetry states are possible to be excited by only A_x and A_z component of vector potential **A**. Hence this do not contribute to photoemission. Thus inclusion of symmetry states would be more appropriate and exact also to generate the exact locations for electronic states.

From all these speculations, we can conclude that although the model presented here is highly simplified, however it gives first hand information on the behaviour of photocurent in the studies of metals and semiconductors. For more accurate calculations of photocurrent, one has to use the formalism of *Low Energy Electron Diffraction* (LEED) which was developed by Pendry that could lead us to explain the detailed microscopic nature and effects of photoemission in metals and semiconductors.

References :

1. R.H. Fowler, *Phys. Rev.* **38**, 45 (1931).
2. Ig. Tamm and S. Schubin, *Z. Physik*, **68**, 97 (1931).
3. K. Mitchell, *Proc. Roy. Soc.* ***A*****146**, 442 (1934), *Proc. Roy. Soc.* ***A*****153**, 513 (1935).
4. R.E.B. Makinson, *Proc. Roy. Soc.* ***A*****162**, 367 (1937).
5. L.I. Schiff and L.H. Thomas, *Phys. Rev.* **47**, 860 (1935).
6. H.Y. Fan, *Phys. Rev.* **68**, 43 (1945).
7. H. Mayer and H. Thomas, *Z. Physik*, **147**, 419 (1957).
8. H. Puff, *Phys. Stat. Sol.* **1**, 636 (1961), *Phys. Stat. Sol.* **1**, 704 (1961).
9. E.O. Kane, *Phys. Rev. Lett.* **12**, 97 (1964).
10. G.W. Gobeli, F.G. Allen and E.O. Kane, *Phys. Rev. Lett.* **12**, 94 (1964).
11. G.W. Gobeli and F.G. Allen, *Phys. Rev.* **127**, 141 (1962), F.G. Allen and G.W. Gobeli, *Phys. Rev.* **127**, 150 (1962), *ibid, Phys. Rev.* **35**, 597 (1964).
12. C.N. Berglund and W.E. Spicer, *Phys. Rev.* **136**, *A*1044 (1964).
13. W.E. Spicer, *Phys. Rev.* **112**, 144 (1959).
14. C.N. Berglund and W.E. Spicer, *Phys. Rev.* **136**, *A*1030 (1964).
15. W.E. Spicer, *Phys. Rev.* **154**, 385 (1967).
16. B.J. Waclawski and E.W. Plummer, *Phys. Rev. Lett.* **29**, 783 (1972), B. Feuerbacher and B.Fitton, *Phys. Rev. Lett.* **29**, 786 (1972).
17. N.E. Christensen and B. Feuerbacher, *Phys. Rev.* ***B*****10**, 2349 (1974), B. Feuerbacher and N.E. Christensen, *Phys. Rev.* ***B*****10**, 2373 (1974), P.J. Feibelman and D.E.Eastman, *Phys. Rev.* ***B*****10**, 4932 (1974).
18. W.L. Schaich and N.W. Ashcroft, *Phys. Rev.* ***B*****3**, 2452 (1971).
19. G.D. Mahan, *Phys. Rev. Lett.* **24**, 1068 (1970).
20. I. Adawi, *Phys. Rev.* **134**, *A*788 (1964)
21. J.B. Pendry, *Low Energy Electron Diffraction*, Academic Press, London (1974)
22. J.A. Appelbaum and D.R. Hamann, *Phys. Rev.* **B6**, 2166 (1972)
23. G.P. Alldrege and L. Klieman, *Phys. Rev.* ***B*****10**, 559 (1974)

24. T. Maniv and H. Metiu, *Phys. Rev.* ***B22***, 4731 (1980)

25. D.R. Penn, *Phys. Rev. Lett.* **28**, 1041 (1972)

26. J.G. Endriz, *Phys. Rev.* ***B7***, 3464 (1973)

27. H. Petersen and S.B.M. Hagstrom, *Phys. Rev. Lett.* **41**, 1314 (1978)

28. A. Liebsch, *Phys. Rev. Lett.* **32**, 1203 (1973).

29. J.B. Pendry, *Surf. Sci.* **57**, 679 (1976).

30. P.J. Feibelman, *Phys. Rev.* ***B12***, 1319 (1975), *Phys. Rev. Lett.* **34**, 1092 (1975).

31. H.J. Levinson, E.W. Plummer and P.J. Feibelman, *Phys. Rev. Lett.* **43**, 952 (1979).

32. A. Kiejna, *Prog. Surf. Sci.* **61**, 85 (1999).

33. G. Mukhopadhayay and S. Lundqvist, *Phys. Scripta*, **17**, 69 (1978).

34. A. Bagchi, *Phys. Rev.* ***B5***, 3060 (1977).

35. K.L. Kliewer, *Phys. Rev.* ***B14***, 1412 (1976).

36. F. Forstman and H. Stenschke, *Phys. Rev. Lett.* **38**, 1365 (1977).

37. K. Kempa and F. Forstman, *Surf. Sci.* **129**, 516 (1983).

38. N. Barberan and J.E. Inglesfield, *J. Phys.* ***C14***, 3114 (1981).

39. R.K. Thapa, *A Theoretical Study of Photon Fields near Surfaces with Application to Photoemission,* Ph.D.Thesis, North Bengal University (1993).

40. A. Bagchi and N. Kar, *Phys. Rev.* ***B18***, 5240 (1978).

41. P. Das, R.K. Thapa and N. Kar, *Mod. Phys. Lett.* ***B5***, 65 (1991), R.K.Thapa, P. Das and N. Kar, *Mod. Phys. Lett*, ***B8***, 36 (1994).

42. R.K. Thapa and N. Kar, *Indian J. Pure & Appl. Phys.* **26**, 620 (1988).

43. R. de L. Kronig and W.G. Penney, *Proc. Roy. Soc.* ***A130***, 499 (1931).

44. J.D. Levine, *Phys. Rev.* **171**, 701 (1968).

45. H. Statz, *Z. Naturforsch*, ***5A***, 534 (1950).

46. S.G. Davison and J.D. Levine, *Solid State Physics,* **25**, 1 (1970).

47. J.C. Slater and G.F. Koster, *Phys. Rev.* **94**, 1498 (1954).

48. T.R.Carver, *Am. J. Phys.* **39**, 1225 (1971).

49. S.G. Davison and M. Steslicka, *Basic Theory of Surface State*, Clarendon, Oxford (1992).

50. J.H. Weaver, *Handbook of Chemistry and Physics* ,CRC Press, Boca Raton, Ohio (1987) for optical data of Al.

51. D.F. Edwards, *Handbook of Optical Constants of Solids*, Academic (1991), E.D. Pallik (ed.), p. 429 for optical data of Be.

52. R.K. Thapa and N. Kar, *Phys. Rev.* ***B*51,** 17980 (1995).

53. R.A. Bartynski, E. Jensen, T. Gustafson and E. Plummer, *Phys. Rev.* ***B*** **32**, 952 (1985).

54. A. Bagchi, N. Kar and R.G.Barrera, *Phys. Rev. Lett.* **40**, 803 (1978).

55. L.D. Landau and E.M. Lifshitz, *Electrodynamics of Continuous Media*, (Pergamon, New York, 1970).

56. J.A. Appelbaum, *Surf. Phys. of Materials*, (ed.) J.H. Blakely, Vol. I (Academic Press, New York), 1975, p. 77.

57. R.K. Thapa, N. Kar and R.A. Lal, *Bull. Mat. Sci.*, 16, 29 (1993).

58. S.L. Weng, T. Gustaffson and E.W. Plummer, *Phys. Rev. Lett.* **39**, 822 (1978).

59. L.F. Wagner and W.E. Spicer, *Phys. Rev. Lett.* **28**, 1381 (1972).

60. D.E. Eastman and W.D. Grobman, *Phys. Rev. Lett.* 28, 1378 (1972).

61. F.G. Allen and G.W. Gobelli, *Phys. Rev.* **159**, 127 (1962).

62. J. van Laar and J.J. Scheer, *Surf. Sci.* **8**, 342 (1967).

63. R.E. Schlier and H.E. Farnsworth, *J. Chem Phys.* **30**, 917 (1959).

64. H.D. Shih, F. Jona, D.W. Jepsen and P.M. Marcus, *Phys. Rev. Lett.* **37**, 1622 (1976.)

65. Ig. Tamm., *Phys. Z. Souvjet*, **1**, 733 (1932).

66. A.W. Maue, *Z. Physik.*, **94**, 717 (1935).

67. W. Schockley, *Phys. Rev.* **56,** 317 (1939).

68. M. Steslicka, *Prog. Surf. Sci.* **5**, 157 (1974).

69. A M .E ldib, H F .H asson and M A .M ohm ad, *J.Phys.* **C20**, 3011 (1987).

70. N. W. Ashcroft and N. D. Mermin, *Solid State Physics*, CBS Publishing, Japan, (1976), p. 146.

71. R.K. Thapa, *Phys. Stat. Sol.*, ***B*179**, 621 (1993).

72. R.K. Thapa and N. Kar, *Mod. Phys. Letts.* ***B*8**, 361 (1994).

73. F. J. Himpsel, *Appl. Phys.* ***A*38**, 205 (1985), L. F. Wagner and W. E. Spicer, *Phys. Rev. Lett.* **28**, 1381 (1972).

74. G. P. Srivastava, *Rep. Prog. Phys.* **60**, 561 (1996).

75. K. C. Pandey and J. C. Phillips, *Phys. Rev. Lett.* **32**, 1433 (1974), D. Haneman, *Phys. Rev.* **121**, 1093 (1961).

76. Z. Pachuau, S. Gurung, R.K. Thapa, D.T. Khating and N. Kar, *Indian J. Phys*, **73*A***, 237 (1999).

77. R.K. Thapa and N. Kar, *Surf. Sci.*, **338**, 138 (1995).

78. G. J. Lapyere and P. J. Anderson, *Phys. Rev. Lett.* **35**, 117 (1975).

79. G. Cappellini, R. Del Sole, L. Reining and F. Bechstedt, *Phys. Rev.* ***B*47**, 9892 (1993).

80. W. Schattke, *Prog. Surf. Sci.* **54**, 211 (1997).

81. S. G. Davison and M. Steslicka, *J. Phys.* (*Sol. Stat. Phys.*) ***C*2**, 1802 (1969).

82. R. K. Thapa, S. Gurung, Z. Pachuau and D. T. Khating, *Surf. Rev. Lett.* **6**, 145 (1999).

83. R.K Thapa and Z. Pachuau (unpublished data).

84. H. Przybylski, A. Baalman, G. Borstel and M. Neumann, *Phys. Rev.* ***B*27**, 6669 (1985).

85. J. Braun, *Rep. Prog. Phys.* **59**, 1267 (1996).

86. M. Woods, P.Strange, A. Ernst and W.M. Temmerman, *YK2000 Conf.*, Aug., 2000, Daresbury Laboratory (U.K.).

87. A.C. Jenkins, *Application of spin-polarised relativistic scattering theory to the calculation of electronic properties of heavy metals and alloys*, Ph.D. Thesis, University of Keele, U.K.(1998).

88. G. Borstel, *Appl. Phys.* **A38,** 193 (1985)

89. B. Feurbacher, B. Fitton and R. F. Willis in *Photoemission and Electronic Properties of Surfaces* (Wiley, New York, 1978).

90. J. E. Inglesfield, *Rep. Prog. Phys.* **45**, 223 (1982).

91. A. Ishii and T. Aisaka, *Surf. Sci.* **242**, 250 (1991).

92. Z. Pachuau and R.K. Thapa, *Indian J. Pure & Appl. Phys.*, **34**, 843 (1996).

93. N.W. McLachlan, *Theory and Application of Mathieu Functions*, Oxford University Press, New York (1951).

94. L. Brillouin, *Wave Propagation in Periodic Structures*, Dover, New York (1953).

95. P.M. Morse, *Phys. Rev.* **35**, 1310 (1930).

96. J.C. Slater, *Phys. Rev.* 87, 807 (1952).

97. Z. Pachuau, B. Zoliana, D. T. Khating, P. K. Patra and R. K. Thapa, *Phys. Lett.* **A275,** 459 (2000).

98. P. Das, R.K. Thapa and N. Kar, *Proc. Sol. Stat. Phys. Symposium*, DAE (India), **36**, 485 (1993).

99. E. W. Plummer and W. Eberhardt, *Adv. Chem. Phys.* **49**, 533 (1982).

100. U. O. Karlsson, S. A. Flodstrom, R. Engelhardt, W. Gadeka and E. E. Koch, *Sol. Stat. Comm.* **49**, 711 (1984).

101. Z. Pachuau, B. Zoliana, P. K. Patra, D. T. Khating and R. K. Thapa, *Phys. Lett. A* (communicated).

102. F.J. Himpsel and J.E. Ortega, *Phys. Rev.* ***B46***, 9719 (1992).

103. D.E. Eastman, J.A. Knapp and F.J. Himpsel, *Phys. Rev. Lett.* **41**, 825 (1978).

104. W.F. Egelhoff, J.W. Linnet and D.L. Perry, *Phys. Rev. Lett.* **36**, 98 (1976).

105. R. Avci and G.J. Lapeyere, *Phys. Rev. Lett.* (preprint).

APPENDIX - A

CALCULATIONS OF PHOTOCURRENT USING MATHIEU POTENTIAL MODEL (EMPTY LATTICE CASE)

We will derive here the formula for calculating the photocurrent from the solids using the Mathieu potential model as described in Chapter 4 (a) for empty lattice (q ~ 0). The initial state wavefunction $\psi_i(x)$ derived by using Mathieu potential model for free electron case can be discussed as follows :

Let us consider a one-dimensional crystal whose potential is represented by a sinusoidal potential given by $V(x) = V_o\cos(\frac{2\pi x}{a})$ where 'a' is the period of the potential having a maximum value V_o at x = 0. The one-dimensional Schrodinger equation can be written as

$$\psi''(z) + (a - 2q\cos 2z)\psi(z) = 0 \qquad \text{(A-1)}$$

where $z = \frac{\pi x}{a}, T = \frac{\pi^2}{a^2}, a = \frac{E}{T}$ and $2q = \frac{V_o}{T}$

The initial state wavefunction for the bulk and surface and for the vacuum regions is given by

$$\psi_i(x) = \begin{cases} (\frac{1}{4\pi k_i})^{\frac{1}{2}}\phi(x_0,q)e^{-\mu(x_o-x)} & x \leqslant 0 \text{ (bulk \& surface)} \\ (2\xi)^{\frac{1}{2}}e^{-\xi(x-x_o)} & x > 0 \text{ (vacuum)} \end{cases} \qquad \text{(A-2)}$$

where x_0 = location of the crystal surface. In Eq. (4.2) above, we have $k_i = \sqrt{2E_i}$ and the matrix element in Eq. (4.5) can be expanded as the following for calculating the photocurrent which is given by

$$I = \int_{-\infty}^{-d} \psi_f^* \tilde{A}_\omega(x) \frac{d\psi_i}{dx} dx + \int_{-d}^{0} \psi_f^* \tilde{A}_\omega \frac{d\psi_i}{dx} dx$$

$$+\frac{1}{2} \int_{-d}^{0} \psi_f^* \frac{d\tilde{A}_{\omega}(x)}{dx} \psi_i dx + \int_{0}^{\infty} \psi_f^* \tilde{A}_\omega(z) \frac{d\psi_i}{dx} dx. \qquad \text{(A-3)}$$

$$= I_1 + I_2 + I_3 + I_4 \qquad \text{(A-4)}$$

The final state wavefunction $\psi_f(x)$ of Eq. (3.9) and photon field vector of Eq. (4.7) is used for the evaluation of the integral I in Eq. (A-3). Using Eqs. (A-2) and (3.9), the integrals in Eq. (A-3) can be expanded as follows :

$$I_1 = \int_{-\infty}^{-d} \psi_f^* \tilde{A}_\omega(x) \frac{d\psi_i}{dx} dx$$

$$= \frac{1}{\pi} \left(\frac{1}{2q_f k_i} \right) \frac{q_f}{q_f + k_f} A_1 \int_{-\infty}^{-d} e^{-ik_f x} e^{\alpha x} e^{-\frac{i\pi}{2}} \cdot \frac{d}{dx} [(\lambda \cos m'x - \sin m'x)] e^{\mu x} dx$$

$$= -\frac{1}{\pi} \left(\frac{1}{2q_f k_i} \right)^{\frac{1}{2}} \frac{q_f}{q_f + k_f} A_1 e^{-\frac{i\pi}{2}} \int_{-\infty}^{-d} e^{-ik_f x} \, e^{(\alpha+\mu)x} \cdot$$

$$[-\lambda\mu \cos m'x + \lambda m' \sin m'x + m' \cos m'x + \mu \sin m'x] dx$$

$$= -\frac{1}{a}\left(\frac{1}{2q_f k_i}\right)^{\frac{1}{2}} \frac{q_f}{q_f + k_f} A_1 . e^{-\frac{i\pi}{2}} \int_{-d}^{-d} (\cos k_f x - i \sin k_f x)\, e^{(a+\mu)x}.$$

$$\cdot[(\lambda m' + \mu)\sin m'x - (\lambda\mu - m')\cos m'x]dx \qquad \text{(A-5)}$$

$$I_2 = \int_{-d}^{0} \psi_f^* \tilde{A}_{\omega} \frac{d\psi_i}{dx} dx$$

$$= \frac{1}{2\pi}\left(\frac{1}{2q_f k_i}\right)^{\frac{1}{2}} \frac{q_f}{q_f + k_f} A_1 \varepsilon(\omega) d \int_{-d}^{0} e^{-ik_f x} e^{a} \frac{1}{[1 - \varepsilon(\omega)]x + d}.$$

$$\frac{d}{dx}[(\lambda \cos m'x - \sin m'x)e^{-\mu(x_0 - x)}]dx$$

$$= -\frac{1}{a}\left(\frac{1}{2q_f k_i}\right)^{\frac{1}{2}} \frac{q_f}{q_f + k_f} A_1 \varepsilon(\omega) d e^{-\frac{i\pi}{2}} \int_{-d}^{0} e^{-ik_f x} e^{(a+\mu)x} \frac{1}{[1 - \varepsilon(\omega)]x + d}.$$

$$[-\lambda\mu \cos m'x + \lambda m' \sin m'x + \mu \sin m'x + m' \cos m'x]dx$$

$$= -\frac{1}{a}\left(\frac{1}{2q_f k_i}\right)^{\frac{1}{2}} \frac{q_f}{q_f + k_f} A_1 \varepsilon(\omega) d e^{-\frac{i\pi}{2}} \int_{-d}^{0} (\cos k_f x - i \sin k_f x) e^{(a+\mu)x}.$$

$$\frac{1}{[1 - \varepsilon(\omega)]x + d}[(m - \lambda\mu)\cos m'x + (\lambda m + \mu)\sin m'x]dx. \qquad \text{(A-6)}$$

$$I_3 = \tfrac{1}{2}\int_{-d}^{0} \psi_f^* \tilde{A}_\omega \frac{d\psi_t}{dx} dx$$

$$= \frac{1}{2\pi}\left(\frac{1}{2q_f k_t}\right)^{\frac{1}{2}} \frac{q_f}{q_f + k_f} A_1 \varepsilon(\omega) d \int_{-d}^{0} e^{-ik_f x} e^{\alpha x} \frac{d}{dx}\left[\frac{1}{[1-\varepsilon(\omega)]x + d}\right].$$

$$[\lambda \cos m'x - \sin m'x]\, e^{-\mu(x_m - x)}\, dx.$$

$$= -\frac{1}{2\pi}\left(\frac{1}{2q_f k_t}\right)^{\frac{1}{2}} \frac{q_f}{q_f + k_f} A_1 \varepsilon(\omega)[1-\varepsilon(\omega)] d e^{-\frac{\mu\pi}{2}} \int_{-d}^{0} e^{-ik_f x} . e^{(\alpha+\mu)x}.$$

$$\frac{1}{\{[1-\varepsilon(\omega)]x + d\}^2}(\lambda \cos m'x - \sin m'x) dx.$$

$$= -\frac{1}{2\pi}\left(\frac{1}{2q_f k_t}\right)^{\frac{1}{2}} \frac{q_f}{q_f + k_f} A_1 \varepsilon(\omega)[1-\varepsilon(\omega)] d e^{-\frac{\mu\pi}{2}} \int_{-d}^{0} (\cos k_f x - i \sin k_f x) e^{(\alpha+\mu)x}.$$

$$\frac{1}{\{[1-\varepsilon(\omega)]x + d\}^2}(\lambda \cos m'x - \sin m'x) dx. \qquad \text{(A-7)}$$

$$I_4 = \int_0^r \psi_f^* \tilde{A}_\omega(x) \frac{d\psi_t}{dx} dx.$$

$$= \left(\frac{\xi}{\pi q_f}\right)^{\frac{1}{2}} A_1 \varepsilon(\omega) e^{\frac{-\pi}{2}} \int_0^{\infty} \left(e^{-iq_f x} + \frac{q_f - k_f}{q_f + k_f} e^{iq_f x}\right).$$

$$\frac{d}{dx}[e^{\alpha x}(\lambda \cos m'x - \sin m'x)] dx$$

$$= \frac{\pi}{a}\left(\frac{\xi}{\pi q_f}\right)^{\frac{1}{2}} A_1 \varepsilon(\omega) e^{\frac{\pi}{2}} \int_0^{\infty}\left(e^{-iq_f x} + \frac{q_f - k_f}{q_f + k_f} e^{iq_f x}\right).$$

$$e^{\xi x}(\lambda\xi \cos m'x - \lambda m' \sin m'x - \xi \sin m'x - m' \cos m'x)dx.$$

$$= \frac{1}{a}\left(\frac{\xi\pi}{q_f}\right)^{\frac{1}{2}} A_1 \varepsilon(\omega) e^{\frac{\pi}{2}} \int_0^{\infty}\left(e^{-iq_f x} + \frac{q_f - k_f}{q_f + k_f} e^{iq_f x}\right).$$

$$e^{\xi x}[(\lambda\xi - m')\cos m'x - (\lambda m' + \xi)\sin m'x]dx. \qquad \text{(A-8)}$$

Substituting these integrals I_1, I_2, I_3, I_4 in Eq. (A-3) the photocurrent from the solids were calculated by numerical method as some of these integrals cannot be evaluated analytically. The FORTRAN program for the evaluation of the integrals I_1, I_2, I_3, I_4 is given in Appendix-C. For the evaluation of photon fields in metals and semiconductors, we have used the experimentally determined dielectric function[50,51].

APPENDIX - B

CALCULATIONS OF PHOTOCURRENT USING MATHIEU POTENTIAL MODEL (STRONG PERIODIC LATTICE WITH FINITE POTENTIAL)

We will derive the formula for calculating the photocurrent from the solids using the Mathieu potential model as described in Chapter 4(b) in the case of strong periodic potential. The initial state wavefunction $\psi_i(x)$ derived by using Mathieu potential model for finite surface potential can be discussed as follows:

Let us consider a finite surface lattice (i.e. q > 0) with a finite step potential having surface width '*d*' and potential width '*a*'. The most general form for the initial state wavefunction will be a linear combination of sine and cosine elliptic functions for all the Fermi energy gap m which is given by

$$\phi(x_{0,}^{'}q) = \lambda_m ce_m(x_{0,}^{'}q) - se_m(x_{0,}^{'}q) \qquad \text{(B-1)}$$

where λ_m is the hybridization parameter which can be written as

$$\lambda_m = \frac{se_m(x_{0,}^{'}q) - (\xi + \mu)^{-1} se_m^{'}(x_{0,}^{'}q)}{ce_m(x_{0,}^{'}q) - (\xi + \mu)^{-1} ce_m^{'}(x_{0,}^{'}q)} \qquad \text{(B-2)}$$

The elliptic functions can be expanded as follows :

$$se_m(x_0', q) = \sin mx_0' - \frac{q}{4}\left[\frac{\sin(m+2)x_0'}{m+1} - \frac{\sin(m-2)x_o'}{m-1}\right]$$
$$+\frac{q2}{32}\left[\frac{\sin(m+4)x_o'}{(m+1)(m+2)} + \frac{\sin(m-4)x_o'}{(m-1)(m-2)}\right] + ... \qquad \text{(B-3)}$$

and $$ce_m(x_0', q) = \cos mx_0' - \frac{q}{4}\left[\frac{\cos(m+2)x_0'}{m+1} - \frac{\cos(m-2)x_o'}{m-1}\right]$$

$$+\frac{q2}{32}\left[\frac{\cos(m+4)x_o'}{(m+1)(m+2)} + \frac{\cos(m-4)x_o'}{(m-1)(m-2)}\right] +.... \qquad \text{(B-4)}$$

For finite surface potential, surface state existence condition implies that

$$x_0' = \frac{\pi}{a}x_0,\ \xi = \frac{12}{a},\ \lambda > 0 \text{ and } m = 3, 5, .. \qquad \text{(B-5)}$$

We are considering surface state occuring for m = 3 and hence from Eqs. (B-3), (B-4) and (B-5), we can write,

$$ce_3(x_o', q) = 0 \ , \qquad ce_3'(x_o', q) = 3(1 + \frac{q}{16} - \frac{q^2}{640})$$

$$se_3(x_o', q) = -1 + \frac{q}{16} - \frac{11}{640}q^2 \ , \qquad se_3'(x_o', q) = 0 \qquad \text{(B-6)}$$

Hence, we can write the value of λ_3 as :

$$\lambda_3 = \frac{(\xi + \mu)\left[1 - \frac{q}{16} + \frac{11}{640}q^2\right]}{3(1 + \frac{q}{16} - \frac{q^2}{640})} \qquad \text{(B-7)}$$

Using Eqs. (B-1), (B-2) and (B-6), the intial state wavefuntion in the case of strong periodic potential becomes

$$\psi_i(x,q) = \begin{cases} (\frac{1}{4\pi k_i})^{\frac{1}{2}}(-1+\frac{q}{16}-\frac{11}{640}q^2)e^{-\mu(x_n'-x)} & x \leqslant 0 \\ (\frac{1}{4\pi k_i})^{\frac{1}{2}} e^{-\xi(x-x_n')} & x > 0 \end{cases} \quad \text{(B-8)}$$

The photoemision cross-section formula for normal photoemission is given by :

$$\frac{d\sigma}{d\Omega} \approx \frac{k^2}{\omega}| < \psi_f|\tilde{A}_\omega(x)\frac{d}{dx} + \frac{1}{2}\frac{d}{dx}\tilde{A}_\omega(x)|\psi_i > |^2 \quad \text{(B-9)}$$

The matrix element given in Eq. (B-9) can be expanded as

$$I = \int_{-\infty}^{-d} \psi_f^* \tilde{A}_\omega(x)\frac{d\psi_i}{dx}dx + \int_{-d}^{0} \psi_f^* \tilde{A}_\omega \frac{d\psi_i}{dx}dx$$

$$+\frac{1}{2}\int_{-d}^{0} \psi_f^* \tilde{A}_\omega \frac{d\psi_i}{dx}dx + \int_{0}^{\infty} \psi_f^* \tilde{A}_\omega(x)\frac{d\psi_i}{dx}dx. \quad \text{(B-10)}$$

$$= I_1 + I_2 + I_3 + I_4 \quad \text{(B-11)}$$

The final state wavefunction in Eq. (A-4) and the photon field vector $\tilde{A}_\omega(x)$ given in Eq. (A-6) are used again for the evaluation of the integral I in Eq. (B-10). Using Eq. (B-8), the integrals in Eq. (B-10) can be expanded as follows :

$$I_1 = \int_{-\infty}^{-d} \psi_f^* \tilde{A}_\omega(x) \frac{d\psi_i}{dx} dx$$

$$= \frac{1}{2\pi}\left(\frac{1}{2q_i k_i}\right)\frac{2q_f}{q_f + k_f} A_1(2\mu + \xi) e^{-\frac{\mu\pi}{2}} \cdot \left[1 - \frac{q}{16} + \frac{11}{640}q^2\right].$$

$$\int_{-\infty}^{-d} e^{(\alpha+\mu)x} e^{-ik_f x} dx.$$

$$= \frac{1}{\pi(\alpha+\mu)}\left(\frac{1}{2q_i k_i}\right)\frac{q_f}{q_f + k_f} A_1(2\mu + \xi) e^{-\frac{\mu\pi}{2}} \left[1 - \frac{q}{16} + \frac{11}{640}q^2\right].$$

$$e^{-[\mu x_m + (\alpha+\mu)d]} \cdot \int_{-\infty}^{-d} e^{-ik_f x} dx.$$

$$= \frac{1}{\pi(\alpha+\mu)}\left(\frac{1}{2q_i k_i}\right)\frac{q_f}{q_f + k_f} A_1(2\mu + \xi) e^{-\frac{\mu\pi}{2}} \left[1 - \frac{q}{16} + \frac{11}{640}q^2\right].$$

$$e^{-[\mu x_m + (\alpha+\mu)d]} \cdot \int_{-\infty}^{-d} (\cos k_f x - i \sin k_f x) dx \qquad \text{(B-12)}$$

$$I_2 = \int_{-d}^{0} \psi_f^* \tilde{A}_\omega \frac{d\psi_i}{dx} dx$$

$$= \frac{1}{2\pi}\left(\frac{1}{2q_i k_i}\right)\frac{2q_f}{q_f + k_i} A_1(2\mu + \xi) e^{-\frac{\mu\pi}{2}} \cdot \left[1 - \frac{q}{16} + \frac{11}{640}q^2\right].$$

$$\varepsilon(\omega) d \cdot \int_{-d}^{0} \frac{1}{[1 - \varepsilon(\omega)]x + d} e^{(\alpha+\mu)x} e^{-ik_f x} dx$$

$$= \frac{1}{\pi}\left(\frac{1}{2q_i k_i}\right)\frac{q_f}{q_f + k_f} A_1(2\mu + \xi) e^{-\frac{\mu\pi}{2}} \cdot \left[1 - \frac{q}{16} + \frac{11}{640}q^2\right].$$

$$\varepsilon(\omega) d \cdot [e^{-(\alpha+\mu)d} - 1] \int_{-d}^{0} \frac{1}{[1 - \varepsilon(\omega)]x + d} e^{-ik_f x} dx$$

$$= \frac{1}{\pi}\left(\frac{1}{2q_f k_i}\right)\frac{q_f}{q_f + k_f}A_1(2\mu + \xi)e^{-\frac{\mu\pi}{2}}.\left[1 - \frac{q}{16} + \frac{11}{640}q^2\right].$$

$$\varepsilon(\omega)d.[e^{-(\alpha+\mu)d} - 1]\int_{-d}^{0}\frac{1}{[1-\varepsilon(\omega)]x + d}(\cos k_f x - i\sin k_f x)dx. \qquad \text{(B-13)}$$

$$I_3 = \frac{1}{2}\int_{-d}^{0}\psi_f^*\tilde{A}_\omega\frac{d\psi_i}{dx}dx$$

$$= \frac{1}{2\pi}\left(\frac{1}{2q_f k_i}\right)\frac{q_f}{q_f + k_f}A_1(2\mu + \xi)e^{-\frac{\mu\pi}{2}}.\left[1 - \frac{q}{16} + \frac{11}{640}q^2\right].$$

$$\varepsilon(\omega)de^{-\frac{\mu\pi}{2}}\int_{-d}^{0}e^{\alpha x}e^{-ik_f x}\frac{d}{dx}\left\{\frac{1}{[1-\varepsilon(\omega)]x + d]}e^{\mu x}\right\}dx$$

$$= \frac{1}{2\pi}\left(\frac{1}{2q_f k_i}\right)\frac{q_f}{q_f + k_f}A_1(2\mu + \xi)e^{-\frac{\mu\pi}{2}}.\left[1 - \frac{q}{16} + \frac{11}{640}q^2\right].$$

$$\varepsilon(\omega)[1-\varepsilon(\omega)]\int_{-d}^{0}e^{(\alpha+\mu)x}e^{-ik_f x}\frac{1}{\{[1-\varepsilon(\omega)]x + d\}^2}dx$$

$$= \frac{1}{2\pi}\left(\frac{1}{2q_f k_i}\right)\frac{q_f}{q_f + k_f}A_1(2\mu + \xi)e^{-\frac{\mu\pi}{2}}.\left[1 - \frac{q}{16} + \frac{11}{640}q^2\right].$$

$$= \varepsilon(\omega)[1-\varepsilon(\omega)][e^{-(\alpha+\mu)} - 1]\int_{-d}^{0}\frac{1}{\{[1-\varepsilon(\omega)]x + d\}^2}(\cos k_f x - i\sin k_f x)dx$$

(B-14)

$$I_4 = \int_0^c \psi_f^*\tilde{A}_\omega(x)\frac{d\psi_i}{dx}dx.$$

$$= \frac{1}{2\pi}\left(\frac{1}{2q_f k_i}\right)A_1\varepsilon(\omega)e^{-\frac{\mu\pi}{2}}\int_0^\infty\left[e^{-iq_f x} + \frac{q_f - k_f}{q_f + k_f}e^{iq_f x}\right].$$

$$\frac{d}{dx}[\lambda_3 ce_3(x_o, q) - se_3(x_0, q)]dx.$$

$$= \frac{1}{2\pi}\left(\frac{1}{2q_f k_i}\right) A_1 \varepsilon(\omega) e^{-\frac{i\pi}{2}} \int_0^\infty \left[e^{-iq_f x} + \frac{q_f - k_f}{q_f + k_f} e^{iq_f x} \right] \cdot$$

$$e^{-\xi_1}(2\xi + 3\mu)(1 - \frac{q}{16} + \frac{11}{640}q^2)dx$$

$$= \frac{1}{2\pi}\left(\frac{1}{2q_f k_i}\right) A_1 \varepsilon(\omega) e^{-\frac{i\pi}{2}} (2\xi + 3\mu)(1 - \frac{q}{16} + \frac{11}{640}q^2) \cdot$$

$$\int_0^\infty \left[e^{-iq_f x} + \frac{q_f - k_f}{q_f + k_f} e^{iq_f x} \right] \cdot e^{-\xi x}\, dx \qquad \text{(B-15)}$$

Substituting these integrals I_1, I_2, I_3, I_4 in Eq. (B-7), the photocurrent from the solids were calculated by numerical method by developing FORTRAN program which is given in Appendix-D.

APPENDIX - C

```
C     NAME OF PROGRAM : MATHIEU1.FOR COPY OF MATHIEU.FOR
C     WRITTEN ON 27-4-2000
C     PHOTOEMISSION CALCULATIONS USING THE MATHIEU
C     POTENTIAL MODEL
C     FREE ELECTRON CASE (Q = 0)
C     BY DR.R.K.THAPA, DEPTT. OF PHYSICS, P.U. COLLEGE, AIZAWL
      COMPLEX A1,CI,T1,T2,T3,T4,TT4,TTX,TTY,EPS,CMPLX,AQ
      COMMON AKI, AKF, AQ, CI, D, A
      CI = CMPLX(0.,1.)
      PI = 22./7.
      READ (1,*) NP,NINT
      READ(1,*)EI,THETA,D,VZ,ALPHA,NE
C     READ (1,*)EI,THETA,D,A,LAMDA,MU,XI,M,VZ,ALPHA,NE
C     WRITE (NP,2) WP,EI,THETA,D,A,LAMDA,MU,XI,M,VZ,NE,ALPHA
      AKI = SQRT(2.*EI)
      A = 6.
C     ALAMB = TAN(M*5*PI/12)
C     ALAMB = 0.02
C     AMU = 0.5
C     XI = 3.81
C     M = 1
C     M*PI/A = 0.52
C     ALPHA=AMU*PI/A=0.088
      DO 90 IE = 1,NE
      READ (1,*) W,EPS1,EPS2
      WEV = W*27.2
      AKF = SQRT(2.*(EI+W))
      EX = EI+W-VZ
      AQ = SQRT(2.*EX)
      TTX = AQ-AKF
      TTY = AQ+AKF
      TT4 = TTX/TTY
      EPS = CMPLX(EPS1,EPS2)
      CALL REFRAC (W,WP,THETA,EPS,A1)
      CALL TERM1 (A1,EPS,T1,NINT)
      CALL TERM2 (A1,EPS,T2,NINT)
      CALL TERM3 (A1,EPS,T3,NINT)
      CALL TERM4 (A1,EPS,T4,NINT)
C     WRITE (NP,3) W,AQ,T1,T2,T3,T4
```

```
      XINT = CABS(T1+T2+T3+T4)
      XCUR = XINT*XINT
      CUR = (XCUR*AKF*AKF)/W
      CUR = ALOG(CUR)
   90 WRITE (NP,5) WEV,EPS1,EPS2,CUR
C  3 FORMAT(2X,2F8.4,2X,4(F15.6,1X))
   5 FORMAT (2X,'W = ',F7.4,2X,'EPS = ',2(F10.6,2X),'CUR = ',F12.6)
C  90 CONTINUE
      STOP
      END
C
      SUBROUTINE TERM1 (A1,EPS,T1,NINT)
      COMPLEX EPS,A1,T1,R1,R2,CI,F1,F2,Q
      DIMENSION F1(701),F2(701)
      COMMON AKI,AKF,AQ,CI,D,A
      CI = CMPLX(0.,1.)
      Q = (1./A)*A1*SQRT(1./(AQ*AKI))
      AG = -5.*A
      AH = -D
      DD = (AH-AG)/(NINT-1)
      DO 10 I = 1, NINT
      X = AG+(I-1)*DD
C     ZX = 0.088*X
C     ZZ = AKF*X
      F1(I) = COS(AKF*X)-CI*SIN(AKF*X)
      F1(I) = F1(I)*EXP(0.088*X)
   10 F2(I) = 1.01*COS(0.52*X)-0.48*SIN(0.52*X)
      CALL SINT(AG,AH,F1,NINT,R1)
      CALL SINT(AG,AH,F2,NINT,R2)
      T1 = R1*R2
      T1 = -T1*Q*AQ
      T1 = T1/(AQ+AKF)
C     WRITE (NP,22)R1,R2,T1
C  22 FORMAT (2X,6F10.6,2X)
      RETURN
      END
C
      SUBROUTINE TERM2 (A1,EPS,T2,NINT)
      COMPLEX EPS,A1,T2,R1,R2,CI,F1,F2,T22
      DIMENSION F1(701),F2(701)
      COMMON AKI,AKF,AQ,CI,D,A
      CI = CMPLX(0.,1.)
      Q = -A1*(D/A)*SQRT(1./(AQ*AKI))
```

```
      AG = -D
      AH = 0.
      DD = (AH-AG)/(NINT-1)
      DO 10 I = 1, NINT
      X = AG+(I-1)*DD
C     ZX = 0.088*X
C     ZY = AKF*X
      F1(I) = COS(AKF*X)-CI*SIN(AKF*X)
      F1(I) =F1(I)*EXP(0.088*X)
      F2(I) = 1.01*COS(0.52*X)-0.48*SIN(0.52*X)
   10 F2(I) = F2(I)*EPS/((1.-EPS)*X+D)
      CALL SINT(AG,AH,F1,NINT,R1)
      CALL SINT(AG,AH,F2,NINT,R2)
      T22 = R1*R2
      T2 = T22*Q
      T2 = T2*AQ/(AQ+AKF)
C     WRITE (NP,22)R1,R2,T2
C  22 FORMAT (2X,4F10.6,2X,2E16.6,6X)
      RETURN
      END

C
      SUBROUTINE TERM3 (A1,EPS,T3,NINT)
      COMPLEX EPS,A1,T3,R1,R2,CI,F1,F2,CMPLX,Q
      DIMENSION F1(701),F2(701)
      COMMON AKI,AKF,AQ,CI,D,A
      CI = CMPLX(0.,1.)
      Q = A1*D*SQRT(1./AQ*AKI)
      Q = Q*(1./2.*PI)
      AG = -D
      AH = 0.
      DD = (AH-AG)/(NINT-1)
      DO 10 I = 1, NINT
      X = AG+(I-1)*DD
C     ZX = 0.088*X
C     ZZ = AKF*X
      F1(I) = COS(AKF*X)+CI*SIN(AKF*X)
      F1(I) = F1(I)*EXP(0.088*X)
      F2(I) = 0.022*COS(0.52*X)-SIN(0.52*X)
   10 F2(I) = F2(I)*EPS*(1.-EPS)/((1.-EPS)*X+D)**2.
      CALL SINT(AG,AH,F1,NINT,R1)
      CALL SINT(AG,AH,F2,NINT,R2)
      T3 = R1*R2
```

```
      T3 = T3*AQ
      T3 = -T3/(AQ+AKF)
C     WRITE (NP,22) R1,R2,T3
C  22 FORMAT (2X,6F10.6,2X)
      RETURN
      END
C
      SUBROUTINE TERM4 (A1,EPS,T4,NINT)
      COMPLEX EPS,A1,T4,R1,R2,CI,F1,F2,Q,TT4,CMPLX
      DIMENSION F1(701),F2(701)
      COMMON AKI,AKF,AQ,CI,D,A
      CI = CMPLX(0.,1.)
      Q = 0.5*A1*EPS/A
      Q = Q*SQRT(1./(AQ*AKI))
      AG = 0
      AH = 2.*A
      DD = (AH-AG)/(NINT-1)
      DO 10 I = 1, NINT
      X = AG+(I-1)*DD
C     ZX = 0.088*X
C     ZZ = AQ*X
      F1(I) = COS(AQ*X)-CI*SIN(AQ*X)+TT4*(COS(AQ*X)+CI*SIN(AQ*X))
      F1(I) = F1(I)*EXP(-6.)
      F2(I) = -0.92*COS(0.52*X)+3.7977*SIN(0.52*X)
   10 F2(I) = F2(I)*EXP(2.*X)
      CALL SINT(AG,AH,F1,NINT,R1)
      CALL SINT(AG,AH,F2,NINT,R2)
      T4 = R1*R2
      T4 = Q*T4
C     WRITE (NP,22) R1,R2,T4
C  2  FORMAT (2X,6E12.6,4X)
      RETURN
      END
C
      SUBROUTINE REFRAC (W,WP,THETA,EPS,A1)
      COMPLEX A1,CX,CSQRT,EPS,CI,CMPLX,CY
      S2 = SIN(2.*THETA)
      S1 = SIN(THETA)
      C1 = COS(THETA)
C     B1 = 1.-EPS
C     B1 = 1./(B1*X+D)
      CY = EPS-S1*S1
      CX = CSQRT(CY)
```

```
      A1 = -S2/(CX+EPS*C1)
      RETURN
      END
C
      SUBROUTINE SINT (A,B,F,N,R)
C     INTEGRATION BY SIMPSON'S ONE-THIRD RULE
      COMPLEX F,R,S
      DIMENSION F(N)
      H = (B-A)/(N-1)
      S = 0.0
      S = S+F(1)+F(N)
      M = N-1
      DO 10 I = 2,M,2
   10 S = S+4.*F(I)+2.*F(I+1)
      R = H*S/3
      RETURN
      END
```

APPENDIX - D

```
C     NAME OF PROGRAM : ZPMATH3. FOR WRITTEN ON 20-02-2001
C     PHOTOEMISSION CALCULATIONS USING THE MATHIEU
C     POTENTIAL MODEL
C     ( FINITE SURFACE &  STRONG POTENTIAL, Q > 0 )
C     BY ZAITHANZAUVA PACHUAU, DEPTT.OF PHYSICS, GAC,AIZAWL
      COMPLEX A1,CI,T1,T2,T3,T4,EPS,CMPLX,AQF,EX,TTF,TTX,TTY
      COMMON AKI,AKF,AQF,CI,D,A
      CI=CMPLX(0.,1.)
      PI=22./7.
      READ (1,*) NP,NINT
      READ(1,*) EI,THETA,D,VZ,ALPHA,NE
C     READ (1,*) EI,THETA,D,A,MU,XI,VZ,ALPHA,NE
C     WRITE (NP,2) EI,THETA,D,A,MU,XI,VZ,ALPHA,NE
      AKI=SQRT(2.*EI)
      A=6.
C     ALAMB3 = (XI+MU)*0.295
C     ALAMB3 = 1.275
C     MU=0.5
C     XI=2.0
C     M=3.
C     QM=1.
      DO 90 IE=1,NE
      READ (1,*) W,EPS1,EPS2
      WEV=W*27.2
      AKF=SQRT(2.*(EI+W))
      EX=EI+W-VZ
      AQF=SQRT(2.*EX)
      TTX=AQF-AKF
      TTY=AQF+AKF
      TTF=TTX/TTY
      EPS=CMPLX(EPS1,EPS2)
      CALL REFRAC (W,WP,THETA,EPS,A1)
      CALL TERM1 (A1,EPS,T1,NINT)
      CALL TERM2 (A1,EPS,T2,NINT)
      CALL TERM3 (A1,EPS,T3,NINT)
      CALL TERM4 (A1,EPS,T4,NINT)
C     WRITE (NP,3) W,AQF,T1,T2,T3,T4
      XINT=CABS(T1+T2+T3+T4)
      XCUR=XINT*XINT
      CUR=(XCUR*AKF*AKF)/W
```

```
C       CUR=ALOG(CUR)
        WRITE (NP,5) WEV,EPS1,EPS2,CUR
C  3    FORMAT(2X,2F8.4,2X,4(F15.6,1X))
   5    FORMAT (2X,'W=',F7.4,2X,'EPS=',2(F10.6,2X),'CUR='F12.6)
  90    CONTINUE
        STOP
        END
C
        SUBROUTINE TERM1 (A1,EPS,T1,NINT)
        COMPLEX EPS,A1,T1,R1,R2,CI,F1,F2,Q,AQF,XX
        DIMENSION F1(700),F2(700)
        COMMON AKI,AKF,AQF,CI,D,A
        CI=CMPLX(0.,1.)
C       Q=A1*SQRT(1./(2.*AQF*AKI))*0.912
        Q=A1*SQRT(1./(2.*AQF*AKI))
        AG=-10.*A
        AH=-D
        DD=(AH-AG)/(NINT-1)
        DO 10 I=1, NINT
        X=AG+(I-1)*DD
   10   F1(I)= COS(AKF*X)-CI*SIN(AKF*X)
C  10   F1(I)=F1(I)*EXP(-(1.5 + D))
C  10   F2(I)= COS(AKI*X)-CI*SIN(AKI*X)
        CALL SINT(AG,AH,F1,NINT,R1)
        CALL SINT(AG,AH,F2,NINT,R2)
        T1 =R1
        XX=AQF+AKF
        T1=T1*Q*AQF/XX
C       WRITE (NP,22)R1,R2,T1
C  22   FORMAT (2X,6F10.6,2X)
        RETURN
        END
C
        SUBROUTINE TERM2 (A1,EPS,T2,NINT)
        COMPLEX EPS,A1,T2,T22,XY,R1,R2,CI,F1,F2,Q,AQF
        DIMENSION F1(700),F2(700)
        COMMON AKI,AKF,AQF,CI,D,A
        CI=CMPLX(0.,1.)
C       Q=A1*D*SQRT(1./(2.*AQF*AKI))*0.203
        Q=A1*D*SQRT(1./(2.*AQF*AKI))
        AG=-D
        AH=0.
        DD=(AH-AG)/(NINT-1)
        DO 10 I=1, NINT
```

```
      X=AG+(I-1)*DD
      F1(I)= COS(AKF*X)-CI*SIN(AKF*X)
C     F1(I)=F1(I)*EXP((-D)- 1.)
      XY=AQF+AKF
   10 F2(I)=EPS/((1.-EPS)*X+D)
      CALL SINT(AG,AH,F1,NINT,R1)
      CALL SINT(AG,AH,F2,NINT,R2)
      T22 =R1*R2
      T2=T22*Q*AQF/XY
C     WRITE (NP,22)R1,R2,T2
C  22 FORMAT (2X,4F10.6,2X,2E16.6,6X)
      RETURN
      END


C
      SUBROUTINE TERM3 (A1,EPS,T3,NINT)
      COMPLEX EPS,A1,T3,AXY,R1,R2,CI,F1,F2,CMPLX,Q,AQF
      DIMENSION F1(700),F2(700)
      COMMON AKI,AKF,AQF,CI,D,A
      CI=CMPLX(0.,1.)
      Q=A1*D*SQRT(1./(2.*AQF*AKI))
C     Q=Q*0.035
      AG=-D
      AH=0.
      DD=(AH-AG)/(NINT-1)
      DO 10 I=1,NINT
      X=AG+(I-1)*DD
      F1(I)= COS(AQF*X)-CI*SIN(AQF*X)
C     F1(I)=F1(I)*EXP((-D)-1.)
      AXY=AQF+AKF
   10 F2(I)= EPS*(1.-EPS)/((1.-EPS)*X+D)**2.
C  10 F2(I)= F2(I)*EXP(0.5*D - 1.)
      CALL SINT(AG,AH,F1,NINT,R1)
      CALL SINT(AG,AH,F2,NINT,R2)
      T3 =R1*R2
      T3=T3*Q*AQF/AXY
C     WRITE (NP,22) R1,R2,T3
C  22 FORMAT (2X,6F10.6,2X)
      RETURN
      END
C
```

```
      SUBROUTINE TERM4 (A1,EPS,T4,NINT)
      COMPLEX EPS,A1,T4,R1,R2,CI,F1,F2,Q,CMPLX,AQF
      DIMENSION F1(700),F2(700)
      COMMON AKI,AKF,AQF,CI,D,A
      CI=CMPLX(0.,1.)
      Q=A1*EPS*0.835
C     Q=A1*EPS
      Q=Q*SQRT(1./(2.*AQF*AKI))
      AG=0
      AH=10.*A
      DD=(AH-AG)/(NINT-1)
      DO 10 I=1, NINT
      X=AG+(I-1)*DD
      F1(I)=COS(AQF*X)-CI*SIN(AQF*X)
C     F1(I)=F1(I)*EXP(6.)*EXP(-2.*X)
      F1(I)=F1(I)*EXP(6.)
   10 F2(I)=(COS(AQF*X)+CI*SIN(AQF*X))*TTF
      CALL SINT(AG,AH,F1,NINT,R1)
      CALL SINT(AG,AH,F2,NINT,R2)
      T4 =R1*R2
      T4=Q*T4
C      WRITE (NP,22) R1,R2,T4
C  2 FORMAT (2X,6E12.6,4X)
      RETURN
      END
C
        SUBROUTINE REFRAC (W,WP,THETA,EPS,A1)
        COMPLEX A1,CX,CSQRT,EPS,CI,CMPLX,CY
        S2=SIN(2.*THETA)
        S1=SIN(THETA)
        C1=COS(THETA)
C       B1=1.-EPS
C       B1=1./(B1*X+D)
        CY=EPS-S1*S1
        CX=CSQRT(CY)
        A1=-S2/(CX+EPS*C1)
        RETURN
        END
C
```

```
      SUBROUTINE SINT (A,B,F,N,R)
C     INTEGRATION BY SIMPSON'S ONE-THIRD RULE
      COMPLEX F,R,S
      DIMENSION F(N)
       H=(B-A)/(N-1)
       S=0.0
      S=S+F(1)+F(N)
      M=N-1
      DO 10 I=2,M,2
   10 S=S+4.*F(I)+2.*F(I+1)
      R=H*S/3
      RETURN
      END
```

APPENDIX - E

```
C     MAIN PROGRAM FOR PHOTOEMISSION CALCULATIONS USING
C      KRONIG-PENNEY  MODEL
C     SURFACE WIDTH IS  Z= - A  TO  0.
C     B1 = 1. - EPS AND UPDATED ON 19.9.1999
      COMPLEX A1,CI,T1,T2,T3,T4,EPS,B1,ASP,AST,SP1,SP2,SPA,SPB,AQ,EX
      COMMON AKI,AKP,AKF,AQ,AG,A,ALPHA,CI,DELTA,ASP
      CI = (0.,1.)
      READ (1,*) NP
C     WRITE (1,*) 'WP,EI,THETA,A,ALPHA,DELTA,AG,VZ,NE'
      READ (1,*)  WP,EI,THETA,A,ALPHA,DELTA,AG,VZ,NE
C     READ (1,*) W,EPS1,EPS2
      WRITE (NP,2) WP,EI,THETA,A,ALPHA,DELTA,AG,VZ,NE
      AKI = SQRT(2.*EI)
      AKP = SQRT(2.*(VZ-EI))
      SP1 = AKP-CI*AKI
      SP2 = AKI-CI*AKP
      SPA = (COS(DELTA)+CI*SIN(DELTA))*SIN(DELTA)
      SPB = (COS(DELTA)-CI*SIN(DELTA))*SIN(DELTA)
      ASP = (SP1-SP2*SPA)/(SP1+SP2*SPB)
      AST = 2.*AKI*SIN(2.*DELTA)/(SP1+SP2*SPB)
      DO 90 IE=1,NE
C     WRITE (1,*) 'W,EPS1,EPS2'
      READ (1,*) W,EPS1,EPS2
      W = 27.2*W
      AKF = SQRT(2.*(EI+W))
      EX=EI+W-VZ
      AQ = SQRT(2.*EX)
C     WRITE (NP,3) W,AKI,AKF,AG,DELTA,AKP,ASP,AST,AQ
      EPS = CMPLX (EPS1,EPS2)
      CALL REFRAC (W,WP,THETA,EPS,A1,B1)
      CALL TERM1 (A1,APA,APB,EPS,T1)
      CALL TERM2 (A1,B1,EPS,T2)
      CALL TERM3 (A1,B1,EPS,T3)
      CALL TERM4 (A1,EPS,AST,T4)
      T2 = R1 *APA-R2*APB
      T2 = CI*A1*Q*T2*2.
C     WRITE (6,91)AG
C 91  FORMAT(3X,'TERM2 COMPUTED',F10.2,/)
      RETURN
      END
```

```
C
      SUBROUTINE INT2 (N,R1,R2,B1)
      COMPLEX R1,R2,CI,CMPLX,Z1,Z2,B1
      COMMON AKI,AKP,AKF,AQ,AG,A,ALPHA,CI,DELTA,ASP
      R1 = CMPLX (0.,0.)
      R2 = CMPLX (0.,0.)
      D = A/FLOAT(N-1)
      X = -A
      I = 0
    2 I = I+1
      IF (I.GT.N) GO TO 10
      E = EXP(ALPHA*X)
      Z1 = (COS(AKI-AKF)*X + CI* SIN(AKI-AKF)*X)/(B1*X+A)
      Z2 = (COS(AKI-AKF)*X - CI* SIN(AKI-AKF)*X)/(B1*X+A)
      Z1 = E*Z1
      Z2 = E*Z2
      R1 = R1+Z1
      R2 = R2+Z2
      IF (I.EQ.1) R1 = R1-0.5*Z1
      IF (I.EQ.N) R1 = R1-0.5*Z1
      IF (I.EQ.1) R2 = R2-0.5*Z2
      IF (I.EQ.N) R2 = R2-0.5*Z2
      X = X+D
      GO TO 2
   10 R1=R1*D
C     WRITE(6,91)AG
C 91  FORMAT(4X,'INTEGRAL-2 COMPUTED',F10.2,/)
      RETURN
      END
C
      SUBROUTINE TERM3 (A1,B1,EPS,T3)
      COMPLEX A1,R1,R2,CI,T3,B1,EPS,APA,APB,Q,AQ
      COMMON AKI,AKP,AKF,AQ,AG,A,ALPHA,CI,DELTA,ASP
      N = 201
      CALL INT3 (N,R1,R2,B1)
      Q = (SQRT(AQ)*EPS)/(AQ+AKF)*EPS*A
      APA = 1.-ASP*(SIN(DELTA))**2 -CI*ASP*SIN(DELTA)*COS(DELTA)
      APB = ASP + (SIN(DELTA))**2 -CI*(SIN(DELTA))**2
      T3 =R1*APA - R2*APB
      T3 =T3*Q*A1
C     WRITE (6,91)AG
C 91  FORMAT(5X,'TERM3 COMPUTED',F10.2,/)
      RETURN
```

```
      END
C
      SUBROUTINE INT3 (N,R1,R2,B1)
      COMPLEX R1,R2,CMPLX,Z1,Z2,B1,EPS,APA,APB,CI
      COMMON AKI,AKP,AKF,AQ,AG,A,ALPHA,CI,DELTA,ASP
      R1 = CMPLX(0.,0.)
      R2 = CMPLX(0.,0.)
      D = A/FLOAT(N-1)
      X=-A
      I=0
    2 I=I+1
      IF (I.GT.N) GO TO 10
      C = COS(AKI-AKF)*X
      S = SIN(AKI+AKF)*X
      CP=COS(AKI+AKF)*X
      SP=SIN(AKI+AKF)*X
      E=EXP(ALPHA*X)
      Z1=(C+CI*S)/((B1*X+A)**2.)
      Z2=(CP-CI*SP)/((B1*X+A)**2.)
      Z1=E*Z1
      Z2=E*Z2
      R1=R1+Z1
      R2=R2+Z2
      IF (I.EQ.1) R1=R1-0.5*Z1
      IF (I.EQ.N) R1=R1-0.5*Z1
      IF (I.EQ.1) R2=R2-0.5*Z2
      IF (I.EQ.N) R2=R2-0.5*Z2
      X=X+D
      GO TO 2
   10 R1=R1*D
      R2=R2*D
C     WRITE (6,91)AG
C 91  FORMAT(6X,'INTEGRAL-3 COMPUTED',F10.2,/)
      RETURN
      END
C
      SUBROUTINE REFRAC (W,WP,THETA,EPS,A1,B1)
      COMPLEX A1,CX,CSQRT,EPS,B1,CI,CMPLX,CY
      S2=SIN (2.*THETA)
      S1=SIN(THETA)
      C1=COS(THETA)
C     EPS=1.-(WP/W)**2.
      B1= (1.-EPS)
```

```
      CY = EPS - S1*S1
      CX=CSQRT(CY)
      A1=-S2/(CX+EPS*C1)
      RETURN
      END
C
        SUBROUTINE TERM4 (A1,EPS,AST,T4)
        COMPLEX A1,R1,R2,CI,T4,EPS,AST,QF,Q,AQ
        COMMON AKI,AKP,AKF,AQ,AG,A,ALPHA,CI,DELTA,ASP
        QF=AKP*AST
        Q=(QF*A1*EPS)/SQRT(AQ)
        R1=(AQ-AKF)/((AQ+AKF)*(CI*AQ-AKP))
        R2=1./(CI*AQ+AKP)
        T4=-Q*(R1-R2)
C       WRITE (6,91)AG
C 91    FORMAT(7X,'TERM4 COMPUTED',F10.2,/)
        RETURN
        END
```

APPENDIX F

```
C     PROGRAM WRITTEN BY DR.R.K.THAPA,DEPTT. OF PHYSICS,
C     PUC, AIZAWL.
C     NAME OF FILE: SRLTRA1.FOR (14-6-98)
C     LAST UPDATED ON 12-06-1998 BY DR. R.K.THAPA, PUC, AIZAWL.
C     PROGRAM TO COMPUTE PHOTOCURRENT USING K-P MODEL
C     MAIN PROGRAM TO STUDY PHOTOEMISSION INCORPORATING
C     RELATIVITY.
      COMPLEX A1,B1,CI,GAMMA1,BETA12,BETA22,AQ,RHO1,EX,EPS
      COMPLEX ALPHA22,CMPLX,LAMDA,AMU,T1,T2,T3,T4,CSQRT
      COMMON A,CI,AQ,AKF,ALPHA
      CI=CMPLX(0.,1.)
      READ (1,*) NP
      READ (1,*) WP,EI,THETA,A,ALPHA,VZ,C,NE
      READ(1,*) AA,RHO2
      WRITE(NP,2) WP,EI,THETA,A,ALPHA,VZ,C
C     EK=EI-VZ
C     EK1=EK+2.*C*C
C     EK1=EK*EK1/C
C     RHO1=CSQRT(EK1)
C     EK2=EI+2.*C*C
C     EK2=EI*EK2/C
C     RHO2=SQRT(EK2)
C     GAMMA1=EK/C*RHO1
C     GAMMA2=EI/C*RHO2
C     AL1=-CI*RHO1
C     BETA12=-2.*SIN(RHO2*AA)*(SIN(AMU*AA)+CI*COS(AMU*AA))
C     BETA22=1.-(COS(RHO2-AMU)*AA+CI*SIN(RHO2-AMU)*AA)
C     ALPHA22=(COS(RHO2+AMU)*AA-CI*SIN(RHO2+AMU)*AA)-1.
C     LAMDA=BETA22/ALPHA22
C     AA=3.
C     AMU=(NN*PI/AA)+CI*ETA
      DO 99 IE=1,NE
      READ (1,*) W,EPS1,EPS2
      WX=W*27.2
      AKF=SQRT(2.*(EI+W))
      EX=EI+W-VZ
      AQ=CSQRT(2.*EX)
      EPS=CMPLX(EPS1,EPS2)
      CALL REFRAC (W,THETA,EPS,A1,B1)
      CALL TERM1 (A1,B1,EPS,T1)
      CALL TERM2 (A1,B1,EPS,T2,N)
```

```
      CALL TERM3 (A1,B1,EPS,T3,N)
      CALL TERM4 (A1,B1,EPS,T4)
      CALL TERM5 (A1,B1,EPS,T5,N)
C     WRITE (NP,5) W,AKF,AQ,A1
C     WRITE (NP,7) W,T1,T2,T3,T4
      CUR=CABS(T1+T2+T3+T4)
      XCUR=CUR*CUR*AKF*AKF/W
      CURMAX=XCUR/0.368163E+18
C     X=LOG10(XCUR)
   99 WRITE (NP,6)WX,W,EPS1,EPS2,XCUR,CURMAX
    2 FORMAT (2X,F6.3,2X,6(F8.4,1X))
C 5  FORMAT(  2F10.6,1X,4(F12.6))
C 7  FORMAT (2X,F7.4,8(E12.6),2X)
    6 FORMAT (2X,2(F7.4),2X,2(F10.6,1X),E14.6,2X,F10.6)
      STOP
      END
C
        SUBROUTINE TERM1 (A1,B1,EPS,T1)
        COMPLEX AL11,T1A,T1,AQ,CI,AT1,BETA12,GAMMA1,AKQ,T11,AT2
        COMPLEX AL12,T12,T1B,CMPLX,EPS
        COMMON A,CI,AQ,AKF,ALPHA
        CI=CMPLX(0.,1.)
        AL1=0.5909
        GAMMA1=CMPLX(0.,0.002156)
C       BETA12=CMPLX(-0.00006486,-0.8784878)
        AL11=AL1-CI*AKF
        AT1=COS(AKF)-CI*SIN(AKF)
        T11=AT1/AL11
        AKQ=(AKF-AQ)/(AKF+AQ)
        AT2=COS(AKF)+CI*SIN(AKF)
        AL12=AL1+CI*AKF
        T12=AKQ*AT2/AL12
        CALL TERM5 (A1,B1,EPS,T5,N)
        T1A=A1*EPS*BETA12
        T1B=T1A*AL1*(1.+GAMMA1)/SQRT(AKF)
        T1=T1B*(T11+T12)
        T1=T1*EXP(AL1*A)
C       WRITE (NP,11) T1
   11   FORMAT (2X,10F12.6)
        RETURN
        END
C
```

```
      SUBROUTINE REFRAC (W,THETA,EPS,A1,B1)
      COMPLEX A1,CX,CSQRT,EPS,B1,CMPLX
      S2=SIN(2.*THETA)
      S1=SIN(THETA)
      C1=COS(THETA)
C     EPS=1.-(WP/W)**2
      B1=EPS-1.
      CX=EPS-S1*S1
      CX=CSQRT(CX)
      A1=-S2/(CX+EPS*C1)
      RETURN
      END

C
        SUBROUTINE TERM2 (A1,B1,EPS,T2,N)
        COMPLEX EPS,A1,B1,T2,CI,T2A,T2B,T2C,R1,R2,AQ,AQR,ALPHA22,
        COMPLEX LAMDA, CMPLX
        COMMON A,CI,AQ,AKF,ALPHA
        CI=CMPLX(0.,1.)
        N=201
        RHO2=0.8681
        GAMMA2=0.003168
C       ALPHA22=CMPLX(-1.901744,-0.439176)
C       LAMDA=CMPLX(-0.898692,0.438541)
        AQR=(SQRT(AKF))/(AKF+AQ)
        T2A=-2.*A1 *EPS*A*AQR
        CALL TERM5 (A1,B1,EPS,T5,N)
        T2B=ALPHA22*(1.-GAMMA2)*CI*RHO2
        T2C=CI*RHO2*LAMDA*(1.+GAMMA2)
        CALL INT2 (R1,R2,A1,B1)
        T2=T2B*R1+T2C*R2
        T2=T2A*T2
        RETURN
        END
C
        SUBROUTINE TERM3 (A1,B1,EPS,T3,N)
        COMPLEX A1,B1,EPS,CI,T3A,T3B,T3C,R1,R2,AQ,AQS,ALPHA22,
        COMPLEX  LAMDA,  CMPLX
        COMMON A,CI,AQ,AKF,ALPHA
        CI=CMPLX(0.,1.)
        GAMMA2=0.003168
C       ALPHA22=CMPLX(-1.901744,-0.439176)
C       LAMDA=CMPLX(-0.898692,0.438541)
```

```
      AQS=(SQRT(AKF))/(AKF+AQ)
      T3A=A1*EPS*A*B1
      T3A=-2.*AQS*T3A
      T3B=ALPHA22*(1.-GAMMA2)
      T3C=LAMDA*(1.+GAMMA2)
      CALL INT3 (N,R1,R2,A1,B1)
      T3=(T3B*R1+T3C*R2)
      T3= T3*T3A
      RETURN
      END
C
       SUBROUTINE TERM4 (A1,B1,EPS,T4)
       COMPLEX A1,B1,EPS,T4A,T4B,T4C,T4,CI,AQ,AQS,ALPHA22
       COMPLEX  LAMDA,CMPLX
       COMMON A,CI,AQ,AKF,ALPHA
       CI=CMPLX(0.,1.)
       RHO2=0.8681
       GAMMA2=0.003168
C      ALPHA22=CMPLX(-1.901744,-0.439176)
C      LAMDA=CMPLX(-0.898692,0.438541)
       AQS=(SQRT(AKF))/(AKF+AQ)
       T4A=2.*AQS*A1
       CALL TERM5 (A1,B1,EPS,T5,N)
       T4B=CI*RHO2*ALPHA22*(1.-GAMMA2)
       F4A=1./(ALPHA-CI*(RHO2-AQ))
       T4C=CI*RHO2*LAMDA*(1.+GAMMA2)
       F4B=1./(ALPHA+CI*(RHO2+AQ))
       T4=(T4B*F4A-T4C*F4B)
       T4=T4*T4A
C      WRITE (NP,44)
  44   FORMAT (2X,2F12.6)
       RETURN
       END
C
       SUBROUTINE INT2 (R1,R2,A1,B1)
       COMPLEX R1,R2,Z1,Z2,AQ,B1,CMPLX,CI,EPS
       COMMON A,CI,AQ,AKF,ALPHA
       CI=CMPLX(0.,1.)
       N=201
       RHO2=0.8681
       R1=CMPLX(0.,0.)
       R2=CMPLX(0.,0.)
       D=A/FLOAT(N-1)
```

```
      X=-A
      I=0
    2 I=I+1
      IF (I.GT.N) GO TO 10
      E=EXP(-ALPHA*X)
      Z1=(COS((RHO2-AQ)*X)+CI*SIN((RHO2-AQ)*X))/(B1*X+A*EPS)
      Z2=(COS((RHO2-AQ)*X)-CI*SIN((RHO2-AQ)*X))/(B1*X+A*EPS)
      Z1=E*Z1
      Z2=E*Z2
      R1=R1+Z1
      R2=R2+Z2
      IF (I.EQ.1) R1=R1-0.5*Z1
      IF (I.EQ.N) R1=R1-0.5*Z1
      IF (I.EQ.1) R2=R2-0.5*Z2

      IF (I.EQ.N) R2=R2-0.5*Z2
      X=X+D
      GO TO 2
   10 R1=R1*D
      R2=R2*D
      RETURN
      END
C
        SUBROUTINE INT3 (N,R1,R2,A1,B1)
        COMPLEX R1,R2,Z1,Z2,AQ,B1,CI,CMPLX,EPS
        COMMON A,CI,AQ,AKF,ALPHA
        CI=CMPLX(0.,1.)
        N=201
        RHO2=0.8681
        R1=CMPLX(0.,0.)
        R2=CMPLX(0.,0.)
        D=A/FLOAT(N-1)
        X=-A
        I=0.
    2   I=I+1
        IF (I.GT.N) GO TO 10
        E=EXP(-ALPHA*X)
        Z1=(COS((RHO2-AQ)*X)+CI*SIN((RHO2-AQ)*X))/(B1*X+A*EPS)**2
        Z2=(COS((RHO2-AQ)*X)-CI*SIN((RHO2-AQ)*X))/(B1*X+A*EPS)**2
        Z1=E*Z1
        Z2=E*Z2
        R1=R1+Z1
        R2=R2+Z2
```

```
      IF (I.EQ.1) R1=R1-0.5*Z1
      IF (I.EQ.N) R1=R1-0.5*Z1
      IF (I.EQ.1) R2=R2-0.5*Z2
      IF (I.EQ.N) R2=R2-0.5*Z2
      X=X+D
      GO TO 2
   10 R1=R1*D
      R2=R2*D
      RETURN
      END
C
      SUBROUTINE TERM5 (A1,B1,EPS,T5,N)
      COMPLEX CI,AMU,AX,AB,AC,AD,BETA12,BETA22,Y,CMPLX,CCOS,
      COMPLEX CSIN,ALPHA22,LAMDA,AX1,AB1,AC1,AD1,AX2,AY2,AXX
C     AA=3.
C     RHO2=0.8961
      PI=3.1416
      NN=0
      DO 9 J=1,10
      NN=NN+1
      ETA=0.001
      AMU=(NN*PI/AA)+CI*ETA
      Y=AMU*AA
      AX2=CSIN(Y)
      AY2=CCOS(Y)
      AXX=AX2+CI*AY2
      BETA12= -2.*AXX*SIN(RHO2*AA)
      AX=(RHO2-AMU)
      AX=AX*AA
      AB=CCOS(AX)
      AC=CSIN(AX)
      AD=AB+CI*AC
C     AD=CABS(AD)
      BETA22=1.-AD
C     BETA22=CABS(BETA22)
      AX1=RHO2+AMU
      AX1=AX1*AA
      AB1=CCOS(AX1)
      AC1=CSIN(AX1)
      AD1=AB1-CI*AC1
      ALPHA22=AD1-1.
C     ALPHA22=CABS(ALPHA22)
      LAMDA=BETA22/ALPHA22
```

```
C     LAMDA=CABS(LAMDA)
C   9 WRITE(6,3) NN,AMU,BETA12,BETA22,ALPHA22,LAMDA
C   3 FORMAT (I4,2(F8.4,1X),2(F20.8,2X),6(F20.6,1X))
C     STOP
    9 CONTINUE
      RETURN
      END
```

Biodata

Name	:	Zaithanzauva Pachuau
Father's Name	:	Lalsangluaia
Date of Birth	:	29.06.1966
Age	:	34 yrs
Institution Address	:	Department of Physics, Govt. Aizawl College, Aizawl-796001, Mizoram
Home Address	:	Ramhlun Venglai, B-12/1, Aizawl-796012 Mizoram.
E-mail Address	:	zpc1@sancharnet.in zaiapachuau@rediffmail.com
Designation	:	Lecturer (Physics)
Year of entry into Service	:	1994
Teaching Experience	:	7 years
Research Experience	:	5 years
Publications	:	Four (4) papers published, two (2) papers communicated and three (3) conference papers.
Research Work and Knowledge	:	I have been given a Minor Research Project by UGC(NER) from the academic year 2000-2001 and the project work is under progress. I have the knowledge of programs and languages like Fortran77, Lotus SmartSuite, MS Office, Adobe Pagemaker, MS-DOS, Internet Explorer, Netscape, etc.

Research Publications :

1. *Photocurrent behaviour in free electron metals*, Zaithanzauva and R. K. Thapa, Indian J. Pure and Appld. Phys. **34**, 843 (1996).

2. *Relativistic treatment of photoemission incorporating the spatially dependent photon fields*, R. K. Thapa, Shivraj Gurung, Zaithanzauva Pachuau and D. T. Khating, Surf. Rev. Letts. **6[1]**, 145 (1999).

3. *Photocurrent calculations in semiconductor using Kronig-Penney model*, Zaithanzauva Pachuau, Shivraj Gurung, R. K. Thapa, D. T. Khating and N. Kar, Indian J. Phys. **73A**, 237 (1999).

4. *Application of Mathieu potential to photoemission from metals*, Zaithanzauva Pachuau, B. Zoliana, D. T. Khating, P. K. Patra and R. K. Thapa, Phys. Lett. ***A*275**, 459 (2000)

5. *A Simple Study of Photoemission from metals*, B. Zoliana, Z. Pachuau, P. K. Patra, S. Srivastava, R.C. Tewari and R. K. Thapa, Indian J. Phys. (accepted)

6. Zaithanzauva Pachuau, B. Zoliana, P. K. Patra, D. T. Khating and R. K. Thapa, *Phys. Lett. A* (communicated)

Conference Papers :

1. *Photoemission from Free Electron Metals* : Aluminium, Beryllium and Potassium, Zaithanzauva, R. K. Thapa and N. Kar, National Conf. Dev. Elect. Mat. and Applications, Shivaji University, Kolhapur, May 6 - 8, 1995.

2. *Photocurrent calculations in beryllium using Kronig - Penney model potential*, Zaithanzauva, Shivraj Gurung, R. K. Thapa and N. Kar, National Conf. Sci. Technol. Surfaces and Interfaces, I.I.T, Kharagpur, December 16 - 18, 1996.

3. *Calculations of photon field in an adsorbate of oxygen on tungsten*, Shivraj Gurung, Zaithanzauva and R. K. Thapa, National Conf. Sci. Technol. Surfaces and Interfaces, I.I.T, Kharagpur, December 16 - 18, 1996

Indian Journal of Pure & Applied Physics
Vol. 34, October 1996, pp. 843-844

Photocurrent behaviour in free electron metals

Zaithanzauva
Department of Physics, Government Kolasib College, Kolasib 796 081, Mizoram
and
R K Thapa
Department of Physics, Pachhunga University College, Aizwal 796 001, Mizoram

Received 19 July 1995; revised 6 May 1996; accepted 8 May 1996

Photoemission from the band states of free electron metals aluminium, beryllium and potassium has been discussed. Free electron wavefunctions are used for the evaluation of the photocurrent by incorporating the *locally variant spatially dependent vector potential of the* incident photon radiation.

Much of the current qualitative understanding of the bulk effects on photoemission is based on the free-electron (FE) model of the semi-infinite metal. In this simplest model, the surface barrier confining the electrons in the metal is represented by a step-function discontinuity in the potential. In bulk photoemission, the necessary momentum is provided by the lattice and surface induces the surface photoeffect as the incident photon carries too little momentum to be able to photoexcite electrons. The perpendicular component of the electromagnetic field undergoes a rapid spatial variation in the surface region of a metal and this is the main factor responsible for the cause of the surface photoemission. In this note, we will discuss the photoemission from the free electron metals aluminium, beryllium and potassium.

We considered a *p*-polarised radiation in the long wavelength limit with *z*-component of vector potential $\tilde{A}_\omega(z)$. The relevant expressions for the electromagnetic field for the bulk ($z \le -a/2$), surface ($-a/2 \le z \le a/2$) and vacuum ($z \ge a/2$) regions are:

$$\tilde{A}_\omega(z) = \begin{cases} A & z \le -a/2 \\ A \cdot \dfrac{\varepsilon(\omega)/[1-\varepsilon(\omega)]}{z/a+B} & -a/2 \le z \le a/2 \\ A\varepsilon(\omega) & z \ge a/2 \end{cases} \quad \ldots (1)$$

where

$$A = -\sin 2\theta/[\varepsilon(\omega) - \sin^2\theta]^{1/2} + \varepsilon(\omega)\cos\theta$$

$$B = [1+\varepsilon(\omega)]/2[1-\varepsilon(\omega)]$$

The photoemission cross-section (PEC) was calculated by using the formula:

$$\frac{d\sigma}{d\Omega} = \frac{k^2}{\omega} |\langle \psi_f | \mathcal{H} | \psi_i \rangle|^2 \quad \ldots (2)$$

in which the perturbation $\mathcal{H}$ due to the incident photon radiation in one dimension is given by

$$\mathcal{H} = \frac{e}{mc}\left[\tilde{A}_\omega(z)\frac{d}{dz} + \frac{1}{2}\frac{d}{dz}\tilde{A}_\omega(z)\right] \quad \ldots (3)$$

The initial and final state wavefunctions ψ_i and ψ_f in Eq. (2) are derived by using the free electron model, the detailed discussion of which is given elsewhere[1,2]. A factor $e^{-\alpha|z|}$ is introduced in the calculation of the matrix element for the region $z<0$. This is done to take into account the inelastic scattering of the electrons. The matrix element in Eq. (2) can be expanded as

$$\begin{aligned} \langle \psi_f | \mathcal{H} | \psi_i \rangle &= \int_{-\infty}^{\infty} \psi_f^*(z) \mathcal{H} \psi_i(z)\, dz \\ &= \int_{-\infty}^{-a/2} \psi_f^* \tilde{A}_\omega(z) \frac{d\psi_i}{dz} dz \\ &+ \int_{-a/2}^{0} \psi_f^* \tilde{A}_\omega(z) \frac{d\psi_i}{dz} dz \\ &+ \frac{1}{2}\int_{-a/2}^{0} \psi_f^* \frac{d\tilde{A}_\omega(z)}{dz} \psi_i\, dz \\ &+ \int_{0}^{a/2} \psi_f^* \tilde{A}_\omega(z) \frac{d\psi_i}{dz} dz \\ &+ \frac{1}{2}\int_{0}^{a/2} \psi_f^* \frac{d\tilde{A}_\omega(z)}{dz} \psi_i\, dz \\ &+ \int_{a/2}^{\infty} \psi_f^* \tilde{A}_\omega(z) \frac{d\psi_i}{dz} dz \end{aligned} \quad \ldots (4)$$

Photoemission cross-section was calculated from the band state (Fermi level) of these metals by evaluating the integrals in Eq. (4). These integrals cannot be solved analytically and hence Fortran

programs were developed for numerical evaluation.

Photocurrent for normal photoemission ($\mathbf{k}_{\parallel}=0$) was calculated as a function of photon energy ($\hbar\omega$) from the band state (Fermi level) of metals under study for the same value of the surface thickness ($a=10$ a.u.) and the scattering factor ($\alpha=0.35$). The angle (θ) made by the incident photon with the surface normal is taken as 45°. The field $\tilde{A}_{\omega}(z)$ was calculated by using the experimentally measured optical data for these metals[3,4].

In Fig. 1, we show the plot of photocurrent from the Fermi level ($E_F=11.7$ eV) of aluminium. The plasmon energy of aluminium is 16 eV ($\hbar\omega_p$). We find that the graph has sharp peak at $\hbar\omega=11$ eV and is followed by a minimum at 15 eV. A second broad peak is obtained at $\hbar\omega=20.5$ eV. The detailed photoemission study of aluminium has been reported elsewhere[1,2].

In Fig. 2, the plot of photocurrent against photon energy from the Fermi level ($E_F=14.30$ eV) of beryllium is shown for photon energy in the range of 7-30 eV. There is a qualitative agreement with the measured data of Bartynski *et al.*[5] only for $\hbar\omega<\hbar\omega_p$. The deviation was attributed to the assuming of low value of α as well as to large deviation from free-electron behaviour[6]. Moreover, we have not chosen appropriate symmetry

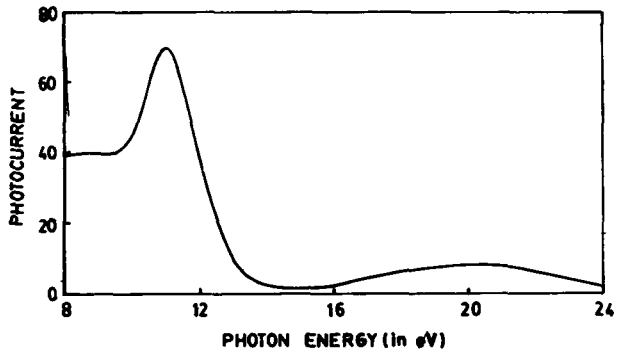

Fig. 1—Plot of photocurrent (arb. units) with photon energy for normal photoemission from the Fermi level of aluminium

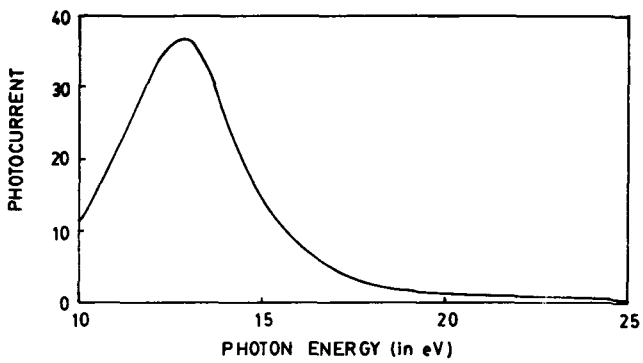

Fig. 2—Plot of photocurrent (arb. units) with photon energy from the Fermi level of beryllium for normal photoemission

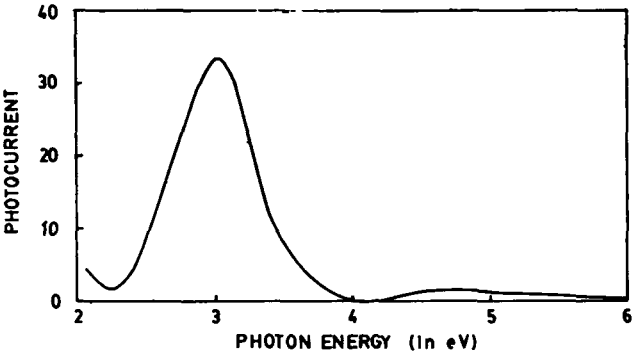

Fig. 3—Plot of photocurrent (arb. units) with photon energy from the Fermi level of potassium for normal photoemission

direction for developing the initial state wavefunction. For example the beryllium energy dispersion data showed[5] free-electron behaviour only along $\bar{\Gamma}\rightarrow\bar{M}$ symmetry line. Recently, Bertel[7] has presented a detailed discussion of the effect of symmetry on metallic surface by making use of group-theoretical technique.

Fig. 3 shows the photocurrent data in the case of metal potassium. It is clear from the graph that maximum occurred at photon energy 3 eV followed by a minimum at around 4.2 eV. A second peak of low magnitude at 4.7 eV was also seen. The photocurrent plot showed similar type of variation qualitatively with the data of aluminium. But this do not seem to be of much importance in photoemission. The reason for this being that the work function of potassium is 4.74 eV and the peak occurs at too low a value of photon energy. The value of dielectric constant $\varepsilon(\omega)$ which leads to this peak may be due to low-energy band structure effects. However, this may play important role during inverse-photoemission. It may be mentioned that the effect of bulk potential is totally neglected in this model which might be the reason for lack of agreement between computed and observed data.

One of the authors (RKT.) acknowledges gratefully the sanction of a research grant by the Department of Atomic Energy, Bombay.

References

1 Das P, Thapa R K & Kar N, *Mod Phys Lett*, B5 1991) 65.
2 Thapa R K, *A theoretical study of photon fields near surfaces with application to photoemission*, PhD Thesis, University of North Bengal, Darjeeling, 1993.
3 *CRC handbook of chemistry and physics*, edited by RC Weast (CRC, Press, Florida), 1987, p E-377.
4 *Handbook of optical constants of solids*, edited by Edward D Pallik (Academic Press, New York), 1991, pp 371 and 429.
5 Bartynski R A, Jensen E, Gustaffson T & Plummer E W, *Phys Rev*, B32 (1985) 1921.
6 Thapa R K & Kar N, *Phys Rev*, B51 (1995) 17980.
7 Bertel E, *Phys Rev*, B50 (1994) 4925.

Surface Review and Letters, Vol. 6, No. 1 (1999) 145–149

RELATIVISTIC TREATMENT OF PHOTOEMISSION INCORPORATING THE SPATIALLY DEPENDENT PHOTON FIELD

R. K. THAPA* and SHIVRAJ GURUNG
Department of Physics, Pachhunga University College, North-Eastern Hill University, Aizawl 796 001 Mizoram, India

ZAITHANZAUVA PACHUAU
Department of Physics, Government Aizawl College, Aizawl 796 001 Mizoram, India

D. T. KHATING
Department of Physics, North-Eastern Hill University, Shillong 793 022 Meghalaya, India

Received 18 September 1998

We discuss a simple theory of photoemission incorporating the relativistically defined initial state wave function for the electronic states. The photocurrent data are calculated in the case of tungsten and silicon.

There has been a lot of interest in photoemission studies of bulk and surfaces of solids, both experimentally and theoretically. Most of the electronic structure of metals has been revealed by the angle-resolved photoemission technique and, as a consequence, this has now become a standard tool for photoemission measurements. It has been seen that most of the authors have not taken into consideration the effect of relativity while applying the Kronig–Penney (KP) model to band-structural studies in photoemission. For example, Thapa and Kar[1–3] have applied it to study the photoemission from metals like W, Si, Al, Pd, etc. But in their studies the relativistic effect on the motion of the electron in the potential well was not taken into consideration while deriving the initial state wave function ψ_i of the electron. Detailed energy band calculations using the relativistic Kronig–Penney (RKP) model have been developed by Davison and Steslicka[5] (DS) by solving the Dirac equation for bulk spinors for which the surface state calculations were also given. In this report, we shall discuss a simple relativistic approach to photoemission study by using the wave function as deduced by DS for the electronic states but by incorporating a locally variant spatial photon field vector. This was then applied to the case of heavy atomic solids like tungsten and silicon.

The photocurrent density formula[6] can be written as

$$\frac{dj(E)}{d\Omega} = \frac{2\pi}{\hbar}|\langle\psi_f|H'|\psi_i\rangle|^2\delta(E-E_f)\delta(E_f-\hbar\omega-E_i) \times f_0(E-\hbar\omega)[1-f_0(E)]\,. \quad (1)$$

The crystal potential model as used by DS[5] for deriving ψ_i is shown in Fig. 1. We have included a surface of width d. The crystal potential is given by $Lt_{\substack{V_3\to\infty \\ b\to 0}} V_3 b = \alpha_0$, with b as the width of the potential

*Author for correspondence.
PACS number: 79.60

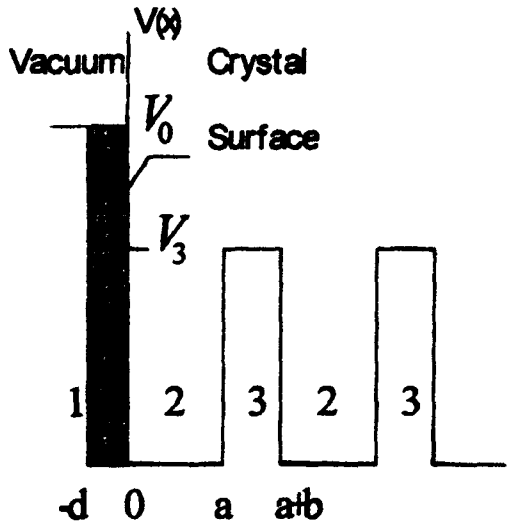

Fig. 1. Model potential as used by DS with the inclusion of a surface of width d.

barrier and $a+b$ the period of the potential, and α_0 is a positive quantity. The crystal surface potential is $V_1 > \varepsilon_0$, where ε_0 is the kinetic energy related to the energy (E) of the electron given by the relation $E = \varepsilon_0 + m_0c^2$, m_0 being the rest mass of the electron. In the k region of constant potential V_k the two-component form of the one-dimensional time-dependent Dirac equation can be written as

$$i\hbar c\frac{d\phi_k^{(1)}}{dx} = (\varepsilon_0 - V_k)\phi_k^{(1)}, \tag{2}$$

$$i\hbar c\frac{d\phi_k^{(2)}}{dx} = \{(\varepsilon_0 - V_k) + 2m_0c^2\}\phi_k^{(1)}. \tag{3}$$

Decoupling Eqs. (2) and (3) leads to

$$i\hbar c\frac{d\phi_k^{(j)}}{dx} = \rho_k^2\phi_k^{(j)}, \quad j = 1,2, \tag{4}$$

where the wave vector

$$\rho_k^2 = \frac{(\varepsilon_0 - V_k)[(\varepsilon_0 - V_k) + 2m_0c^2]}{\hbar^2c^2}. \tag{5}$$

The plane wave solution of Eq. (4) for bulk ($x > 0$) and vacuum ($x < 0$) regions as deduced by DS can be written as

$$\psi_i(x) = \begin{cases} \phi_2(x) = a_2^{(2)}\left\{\begin{pmatrix} -\gamma_2 \\ 1 \end{pmatrix} e^{i\rho_2 x} + \lambda\begin{pmatrix} \gamma_2 \\ 1 \end{pmatrix} e^{-i\rho_2 x}\right\}, & x > 0, \\ \phi_1(x) = \begin{pmatrix} \gamma_1 \\ 1 \end{pmatrix}\beta_1^{(2)}e^{l_1 x}, & x < 0, \end{cases} \tag{6}$$

where $l_1 = -i\rho_1 > 0$ and is real. The constants in Eq. (6) are defined as

$$a_k^{(1)} = -\gamma_k a_k^{(2)},$$

$$\beta_k^{(1)} = \gamma_k\beta_k^{(2)}, \quad \gamma_k = \frac{\varepsilon_0 - V_k}{\hbar c\rho_k},$$

$$\lambda = \frac{\beta_2^{(2)}}{a_2^{(2)}} = \frac{1 - e^{i(\rho_2 - \mu)a}}{e^{-i(\rho_2 + \mu)a} - 1}.$$

μ is the complex wave number and is given by $\mu = \frac{n\pi}{a} + i\zeta$, where n is the band number and ζ is real and > 0.

The final state wave function ψ_f, which is correctly normalized in energy, will be the scattering state of the step potential $V_1 = -V_0\theta(x)$, where $\theta(x)$ is a unit function. The perturbation Hamiltonian H' in Eq. (1) is given by

$$H' = \frac{e}{2mc}(\mathbf{p}\cdot\mathbf{A} + \mathbf{p}\cdot\mathbf{A}), \tag{7}$$

where $\mathbf{p}$ is a one-electron momentum operator and $\mathbf{A}$ is the vector potential. $\mathbf{A}$ is assumed to be a constant in the bulk and vacuum regions, but in the surface region it is a function of x being the solution of Maxwell's equation for dielectric function $\epsilon(x)$. The formula for the vector potential in one dimension following Bagchi and Kar[7] is

$$A_\omega(x) = \begin{cases} A_1 & \text{(bulk)}, \\ \dfrac{A_1\epsilon(\omega)d}{[\epsilon(\omega) - 1]x + \epsilon(\omega)d} & \text{(surface)}, \\ A_1\epsilon(\omega) & \text{(vacuum)}, \end{cases} \tag{8}$$

where A_1 is a constant depending on dielectric function $\epsilon(\omega)$, photon energy $\hbar\omega$ and angle of incidence θ_i. Such models have been used with success in photoemission calculation with simple forms of the initial state wave function.[1-3]

The matrix element in Eq. (1) can now be expanded as

$$
\begin{aligned}
I &= \langle \Psi_f | H' | \Psi_i \rangle \\
&= \int_{-\infty}^{-d} \Psi_f^* A_\omega \frac{d\Psi_i}{dx} dx + \int_{-d}^{0} \Psi_f^* A_\omega \frac{d\Psi_i}{dx} dx \\
&\quad + \int_{-d}^{0} \Psi_f^* \frac{dA_\omega}{dx} \Psi_i dx + \int_{0}^{\infty} \Psi_f^* A_\omega \frac{d\Psi_i}{dx} dx \\
&= I_1 + I_2 + I_3 + I_4 .
\end{aligned}
$$

The integrals I_1, I_2, I_3 and I_4 cannot be solved analytically, and therefore FORTRAN programs will be developed to evaluate each of these integrals for computing photocurrent as a function a photon energy.

We have used the experimentally determined[8] values of dielectric constants $\epsilon(\omega)$ for metal W and semiconductor Si. Since it is strictly a model type of calculation, we have used the same values of the following constants (in a.u.):

Fermi energy $E_F = 0.3768$,

Strength of potential $V_0 = 0.5864$,

Work function $\Phi = 0.1746$,

Width of the potential $a = 6a_0$

(a_0 is the Bohr radius),

Velocity of light $c = 137$,

Surface width $d = 10$.

The relativistic parameters used in the calculations are given by

$$
\begin{aligned}
&\rho_1 = i0.4178, \quad \rho_2 = 0.613, \\
&l_1 = 0.4178, \quad \gamma_1 = -i0.001525, \\
&\gamma_2 = 0.002240441, \\
&\eta = 6 \times 10^{-4}.
\end{aligned}
$$

The values of RKP parameters like β_1, β_2, α_1, α_2 and λ were calculated for each value of band number n. These values were then substituted into the matrix element I for the evaluation of photocurrent. We have calculated photocurrent against incident photon energy ($\hbar\omega$) as a function of the band number (n). Photocurrent was calculated for W and Si for $n = 2, 4, 6, 8, 10$. These is no specific reason

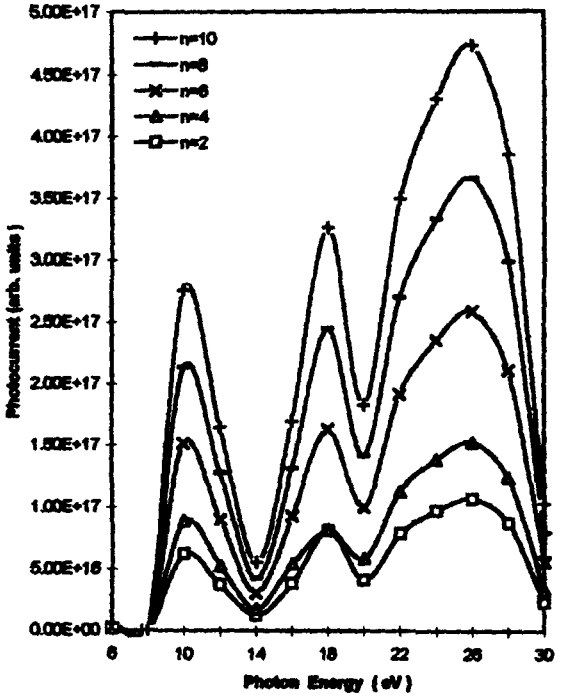

Fig. 2. Plot of photocurrent against energy for various of band number n for metal tungsten.

for the choice of even values of n as the photocurrent data for odd values showed similar[9] trends. In Fig. 2, the plot of photocurrent in the case of W is shown. We find that for all the band numbers the peaks in photocurrent data occurred at photon energies $\hbar\omega = 10, 18, 26$ eV, respectively. The photocurrent peak was minimum at $\hbar\omega = 14$ eV and maximum at $\hbar\omega = 26$ eV.

We have also calculated photocurrent in the case of semiconductor silicon, which is strictly an example of a heavy diatomic solid. The photocurrent data for silicon is shown in Fig. 3. For all the band numbers we find that maxima in photocurrent at photon energy $\hbar\omega = 11$ eV and 20 eV respectively, but the ratio between the peaks at 20 eV and 11 eV is ~ 2.32. But for $\hbar\omega > 20$ eV, the graph drastically went down to a minimum and decayed.

We have already done the photoemission calculations in the case of W and Si using the nonrelativistic Kronig–Penney (NR-KP) model. It has been observed that in NR-KP treatment, the photocurrent showed maxima at values of $\hbar\omega < \hbar\omega_p$ and a minimum occurred at $\hbar\omega \sim \hbar\omega_p$ for both W and Si.

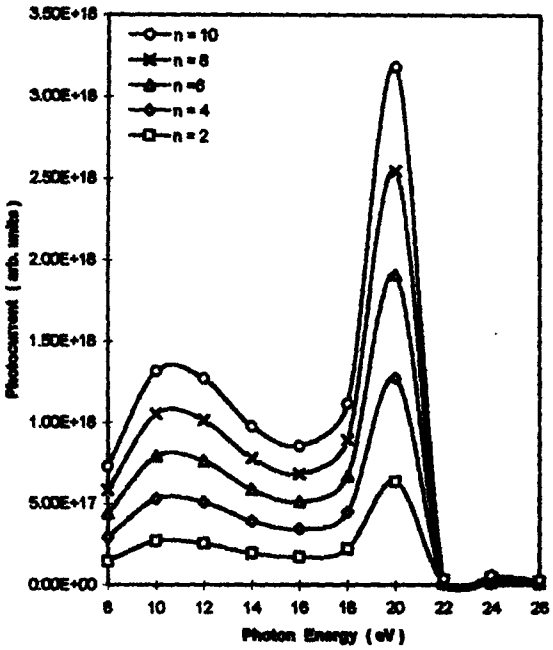

Fig. 3. Plot of photocurrent against photon energy for various values of band number n for semiconductor silicon.

For example, in the case[3] of W, maxima occurred at $\hbar\omega = 21$ eV and a minimum at 26 eV (for W, $\hbar\omega_p = 24.7$ eV). However, in the case[3] of Si, the photocurrent data showed a lot of structures[2,3] instead of only a maximum at $\hbar\omega < \hbar\omega_p$. It also did not show minima at $\hbar\omega_p$ (for Si, $\hbar\omega_p = 16$ eV). The reason for this has been attributed to the behavior of the dielectric response function $\epsilon(\omega)$. However, the behavior of photocurrent data in RKP treatment is completely different from that obtained by using the NR-KP model. For example, in the case of W, we find that for values of photon energies greater than 20 eV, the plot showed a peak in photocurrent data at $\hbar\omega = 26$ eV, a value very close to $\hbar\omega_p$. This is in fact in contradiction with data obtained earlier by other methods[2,3,7,10] wherein normally a minimum was seen at $\hbar\omega = \hbar\omega_p$. Also for values of $\hbar\omega < \hbar\omega_p$, we find two peaks in photocurrent at $\hbar\omega = 10$ and 18 eV with a minimum at $\hbar\omega = 14$ eV. Similarly, in the case of Si as shown in Fig. 3, we see that for a lower photon range the behavior of photoeccurent data showed features similar to that obtained in surface photoeffect. For example, a minimum was observed at $\hbar\omega = 10$ eV, followed by a minimum at $\hbar\omega = 16$ eV, the plasmon energy of Si. There is increase in photocurrent for $\hbar\omega > \hbar\omega_p$ and a maximum is observed at 20 eV photon energy for all the band numbers. The graphs showed minima again at $\hbar\omega = 22$ eV and decayed down towards a minimum for all band numbers for further increase of photon energies.

The interesting feature which is seen in both the case of W and of Si is that for the increase in band numbers the peak in photocurrent also goes on increasing. The only difference is that, in the case of W, the highest peaks in photocurrent is observed at $\hbar\omega = \hbar\omega_p$, whereas for Si it is obtained at photon energy 20 eV, which is greater than its plasmon energy. This can be attributed to the fact that the band width ΔE_b goes on decreasing for the increase in the band number. In other words, the relativistic correction[5] reduces ΔE_b, which causes the electrons to gain sufficient momentum due to rapid spatial variation of the incident radiation to be photoexcited. This in fact causes the enhancement of photocurrent with the increase in n in both the cases of W and of Si. In both the NR-KP and the RKP treatment of photoemission, we find that only in the low frequency regime is photoemission basically a phenomenon occurring due to the spatial variation of the photon field vector. The evidence for this is the occurrence of peaks for $\hbar\omega < \hbar\omega_p$, which has already been established also experimentally by Levinson and others.[10] But the occurrence of peaks in photoemission by using the RKP model may be described as the manifestation of band structure effects in photoemission, which had not been seen in the NR-KP cases.

The main drawback of including the initial state wave function ψ_i as derived by DS[5] in this type of calculations is that it does not take into account the surface width. It has been well defined for both the vacuum and bulk regions. We also conclude from this study that the incorporation of the spatially variant vector potential is not sufficient. For example, the measured ultraviolet photoemission spectra (UPS) data have shown that effects due to spin–orbit coupling cannot be omitted[11] in photoemission spectra. Further Schrödinger's equation solved without the inclusion of spin–orbit interaction will become more and more inadequate[4] in photoemission spectral measurements. There is therefore a need for a relativistic theory of photoemission for accurate presentation of the UPS data. We are still doing

detailed calculations in which the relativistic band-structural effects in photoemission will be studied.

Acknowledgments

R. K. T. acknowledges a research grant and S. G. a junior research fellowship from the Department of Science and Technology, New Delhi. R. K. T. is also grateful to Dr. S. G. Davison of the University of Waterloo, Ontario, Canada, for sending useful literature for this work. Thanks are also due to Dr. C. Thanthianga, Principal of the Pachhunga University College, Aizawl, for being helpful and cooperative.

References

1. R. K. Thapa, *Phys. Stat. Sol.* **B179**, 391 (1993).
2. R. K. Thapa and N. Kar, *Surf. Sci.* **338**, 138 (1995).
3. R. K. Thapa, P. Das and N. Kar, *Mod. Phys. Lett.* **B8**, 361 (1994).
4. G. Borstel, *Appl. Phys.* **A38**, 193 (1985).
5. S. G. Davison and M. Steslicka, *J. Phys. (Solid State Phys.)* **C2**, 1802 (1969); S. G. Davison and J. D. Levine, *Solid State Phys.* **25**, 1 (1970).
6. D. R. Penn, *Phys. Rev. Lett.* **28**, 1041 (1972).
7. A. Bagchi and N. Kar, *Phys. Rev.* **B18**, 5248 (1978).
8. J. Weaver, in *Handbook of Chemistry and Physics of Solids* (CRC, Boca Raton, Ohio, 1987), E-377; D. F. Edward, in *Handbook of Optical Constants of Solids*, ed. E. P. Palik (Orlando Academic, 1985), p. 555.
9. R. K. Thapa and Z. Pachuau (unpublished data).
10. S.-L. Weng, T. Gustafsson and E. W. Plummer, *Phys. Rev. Lett.* **39**, 822 (1977); H. J. Levinson, E. W. Plummer and P. J. Feibelman, *Phys. Rev. Lett.* **43**, 953 (1979).
11. H. Przybylski, A. Baalman, G. Borstel and M. Neumann, *Phys. Rev.* **B27**, 6669 (1983).

Indian J. Phys. **73A** (2), 237–243 (1999)

NOTE

IJP A
— an international journal

Photocurrent calculations in semiconductors using Kronig-Penney model

Zaithanzauva Pachuau[a], Shivraj Gurung, R K Thapa, D T Khating[b] and N Kar[c]

Department of Physics, Pachhunga University College, North-Eastern Hill University, Aizawl-796 001, Mizoram, India

Received 16 December 1997, accepted 21 October 1998

Abstract : Photoemission calculations have been done using the Kronig-Penney model from band state (Fermi level) of semiconductors silicon and gallium arsenide. For the evaluation of photocurrent the initial state wavefunction used is the one deduced by Thapa and Kar [*Indian J Pure Appl Phys* **26** 620 (1988)] [1]

Keywords : Photoemission, semiconductors, Kronig-Penney model

PACS No. : 79 60 Bm

The existence of surface states on semiconductor surfaces was experimentally verified by using the angle integrated photoemission [2]. Moreover their existence is obvious through the pinning of the Fermi level at the surface. However, the semiconductor surfaces are more complex than metal surfaces for the reason that semiconductor surfaces reconstruct [3]. The presence of these reconstructions and atomic displacements on semiconductor surfaces makes the studies of electronic structure a very interesting topic. Of the various tools and techniques, angle resolved photoemission studies has also been widely used in understanding the surface states of semiconductors. Various type of structural models of semiconductors have been proposed [4]. But in this short report, we will be mainly concerned with the photoemission studies by adopting a simple calculational procedure which will be applied to the case of silicon and gallium arsenide.

[a] Department of Physics, Government Aizawl College, Aizawl-796 001, Mizoram, India

[b] Department of Physics, North-Eastern Hill University, Shillong-793 022, India

[c] Department of Physics North Bengal University, Darjeeling-734 430, India

For photoemission calculations the current density may be written with the help of the golden rule expression [5] as

$$\frac{dj(E)}{d\Omega} = \frac{2\pi}{\hbar}\sum \left|\langle \psi_f |\Delta| \psi_i \rangle\right|^2 \delta(E-E_f)\,\delta(E_f - E_i - \hbar\omega)$$

$$\times f_0(E-\hbar\omega)[1-f_0(E)], \qquad (1)$$

where $|\psi_i\rangle\left(|\psi_f\rangle\right)$ refer to the initial (final state), $\Delta = (e/2mc)(A.p + p.A)$, and p being the one-electron momentum operator, A the vector potential of the photon field. Although the one-electron states are treated quite accurately in many photoemission calculations, the variation of the photon fields in the surface region is usually neglected. The model dielectric function which takes into account the bulk, surface and vacuum regions is given [6] by

$$\varepsilon(\omega, z) = \begin{cases} \varepsilon_1 + i\varepsilon_2 = \varepsilon(\omega) & z \le -a \\ 1 + [1-\varepsilon(\omega)]\frac{z}{a}, & -a \le z \le 0 \\ 1, & z \ge 0. \end{cases} \qquad (2)$$

We have used the Drude-Lorentz model for calculating the frequency dependent dielectric constants which is given by

$$\varepsilon(\omega) = \varepsilon_\infty\left[1 - \frac{\omega_p^2}{\omega(\omega + i\gamma_1)}\right] + \frac{(\varepsilon_0 - \varepsilon_\infty)\omega_0^2}{\left(\omega_0^2 - \omega^2 - i\gamma_2\omega\right)}. \qquad (3)$$

In eq (3) above, ε_0 and ε_∞ are the static and high frequency dielectric constants. By using the appropriate values of constants ε_0, ε_∞, γ_1, γ_2 *etc* respectively for silicon and gallium arsenide, the real and imaginary parts of $\varepsilon(\omega)$ were calculated by using eq. (3) which were then applied to eq (2) for computing the fields

Using the electromagnetic field for *p*-polarized radiation, we calculate the photoemission cross section by evaluating the matrix element :

$$\langle \psi_f |\Delta| \psi_i \rangle = \int_{-\infty}^{\infty} \psi_f^*(z)\Delta\psi_i(z)\,dz$$

$$= \int_{-\infty}^{\infty}\left[\psi_f^*(z)A_\omega(z)\frac{d\psi_i}{dz} + \frac{1}{2}\psi_f^*\frac{dA_\omega}{dz}\psi_i(z)\right]dz, \qquad (4)$$

where [6]

$$A_\omega(z) = \begin{cases} A_1, & z \le -a \\ A_1\dfrac{a\varepsilon(\omega)}{[1-\varepsilon(\omega)]z + a}, & -a \le z \le 0 \\ A_1\varepsilon(\omega), & z \ge 0 \end{cases} \qquad (5)$$

A_1 is a constant whose value depends on the angle of the incident radiation (θ_i) and its frequency (ω) and dielectric constants $\varepsilon(\omega)$ In the surface region ($-a \le z \le 0$), the dielectric

function is linearly interpolated between the vacuum and the bulk values. $\psi_f(z)$ in eq. (4) is the free-electron final-state wavefunction given by

$$\psi_f(z) = \left(\frac{1}{2\pi q}\right)^{\frac{1}{2}} \frac{2q}{q+k_f} e^{ik_f z}, \qquad z<0$$

$$= \left(\frac{1}{2\pi q}\right)^{\frac{1}{2}} \left[e^{iqz} + \left(\frac{q-k_f}{q+k_f}\right) e^{-iqz}\right], \quad z>0 \tag{6}$$

where $k_f^2 = 2E_f$, $q^2 = 2(E_f - V_0)$ and $E_f = E_i + \hbar\omega$.

To evaluate the initial state wavefunction $\psi_i(z)$, one solves the one-dimensional Schroedinger's equation

$$\frac{d^2\psi(z)}{dz^2} + k_i^2(z) = -2V(z)\psi(z), \tag{7}$$

where $k_i^2 = 2E_i$ and $V(z)$ is the δ-function potential of the Kronig-Penney (K–P) model.

Let $\phi(z)$ denote the Bloch wavefunction deep inside the metal and $\phi^*(z)$ the time reversal of $\phi(z)$. The eigenfunction in the semi-infinite solid ($z < 0$) was chosen [7] to have the form $\psi_i(z) = \phi(z) - P\phi^*(z)$, where P is the reflection coefficient obtained by matching the wavefunction and its derivative at $z = 0$. One can then show [1] that the initial state wavefunction for $z < 0$ may be written as

$$\psi_i(z) = \left(1 - iPe^{-i\delta}\sin\delta\right)e^{ik_i z} - \left(P - ie^{i\delta}\sin\delta\right)e^{-ik_i z}, \tag{8}$$

where $\cot\delta = \frac{k_i}{g}$, g being the strength of the potential. The initial-state wavefunction outside the metal ($z > 0$) is

$$\psi_i = Te^{-\chi z}, \tag{9}$$

T being the transmission coefficient across the boundary plane and $\chi^2 = 2(V_0 - E_i)$, where V_0 is the surface step potential. From the matching conditions at $z = 0$, one can easily deduce the values of P and T in eqs. (8) and (9) and write the most explicit form of initial state wavefunction $|\psi_i\rangle$. The photoemission cross section was obtained *via*

$$\frac{d\sigma}{d\Omega} = \frac{k^2}{\omega}\sum\left|\langle\psi_f|\Delta|\psi_i\rangle\right|^2. \tag{10}$$

The matrix element $I = \langle\psi_f|\Delta|\psi_i\rangle$ in eq. (10) can be expanded as

$$I = \int_{-\infty}^{\infty}\psi_f^* A_\omega(z)\frac{d\psi_i}{dz}dz + \int_{-a}^{0}\psi_f^* A_\omega\frac{d\psi_i}{dz}dz + \frac{1}{2}\int_{-a}^{0}\psi_f^*\frac{dA_\omega(z)}{dz}\psi_i dz$$

$$+ \int_0^{\infty}\psi_f^* A_\omega(z)\frac{d\psi_i}{dz}dz. \tag{11}$$

In calculating the photocurrent, these integrals were evaluated analytically wherever possible, or numerically by developing a FORTRAN programme. To ensure the convergence, a factor of $e^{-\alpha|z|}$ (α is the scattering factor) was introduced for $z < 0$ which represents the effect of inelastic collisions.

Since it is strictly a model calculation, we have used the same set of data (in atomic units) both for silicon and gallium arsenide. The data used are :

Fermi level (E_F) = 0.463,

Work function (ϕ) = 0.198,

Surface width (a) = 10,

Height of the potential barrier (V_0) = 0.662,

Strength of the potential barrier (g) = 0.60,

Phase factor (δ) = –0.5776,

Scattering factor (α) = 0.35.

We have chosen the initial state energy (E_i) to lie at the Fermi level. The values of the parameters g, δ and α are chosen arbitrarily to fit in such a way that it can reproduce qualitatively the nature of the photon energy dependence of the square of the field. The reason for this being that the matrix element for photoemission cross section is a quadratic function of the photon field.

In Figure 1, we have shown the plot of photocurrent as a function of photon energy ($\hbar\omega$). For the surface width a = 10 a.u., we find that at $\hbar\omega$ = 12 eV, photocurrent peak is

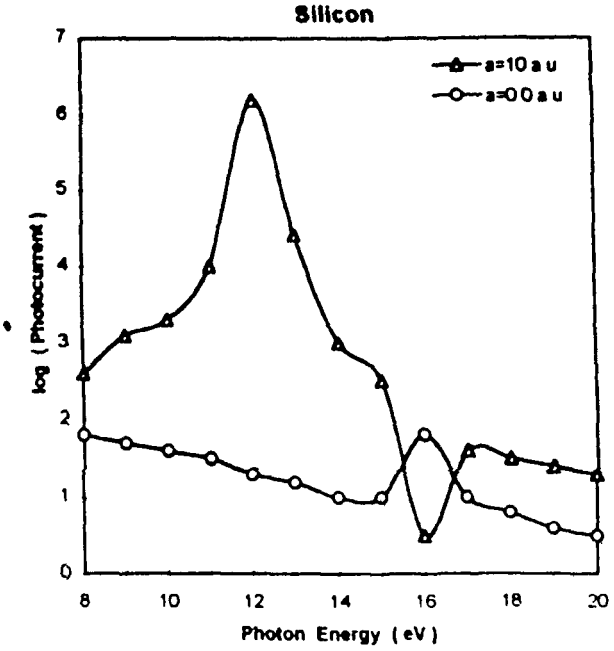

Figure 1. Plots of log (photocurrent) (in arb units) as a function of photon energy for silicon for surface widths a = 10 0 a u and 0 0 using the Drude-Lorentz dielectric model

maximum. It shows a minimum at $\hbar\omega = 16$ eV followed by a small hump at 17 eV. Further increase of $\hbar\omega$ causes the photocurrent to decay towards a minimum value. We have taken the plasmon energy ($\hbar\omega_p$) of silicon to be 16 eV. Interesting feature that is seen here in the case of silicon is that photocurrent data showed behaviour similar at least qualitatively with the earlier results [8] when fields were calculated by using the experimentally measured dielectric constants. For example, the maxima in photocurrent was obtained at $\hbar\omega < \hbar\omega_p$ *i.e.*, at 12 eV photon energy followed by a minima occurring at $\hbar\omega \approx \hbar\omega_p$. For the case of narrow surface width ($a = 0.0$) the behaviour in photocurrent is completely different. We find that a peak of low height in photocurrent occurred but at plasmon energy of silicon. This is quite different behaviour obtained than with the one [8] calculated by using the experimentally determined dielectric constants.

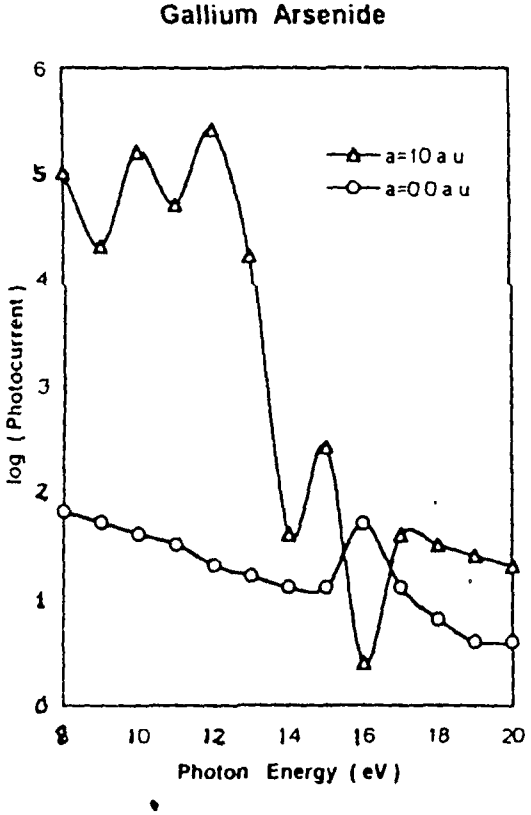

Figure 2. Plots of log (photocurrent) (in arb. units) as a function of photon energy for gallium arsenide for surface widths $a = 10.0$ a.u. and 0.0 using the Drude-Lorentz dielectric model.

In Figure 2, the plot of photocurrent as a function of photon frequency in the case of gallium arsenide is shown for two different surface widths $a = 10.0$ a.u. and $a = 0.0$ respectively, but with the same values of Kronig-Penney parameters as were used in the case of silicon. The photocurrent structures of gallium arsenide data showed three peaks at $\hbar\omega = 10$, 12 and 15 eV respectively but showing a minima at $\hbar\omega = 16$ eV (the assumed plasmon energy of gallium arsenide). Another hump in the photocurrent is seen at 17 eV beyond which the photocurrent decreases gradually. The photocurrent data for

narrow surface width ($a = 0.0$) is found to be similar as in the case of silicon. The reason for this being that for $a = 0.0$, both silicon and gallium arsenide had almost same values of dielectric constants as calculated by using the Drude-Lorentz formula.

Photoemission is considered basically to be a surface effect. It is dependent mainly on the spatial variation of the photon field vector at the surface region. We find therefore that in the case of silicon, the model dielectric response function of Drude-Lorentz seems to work quite fittingly for values of photon energies below and above the plasmon energy. However, strikingly different behaviour is seen in photocurrent in the case of gallium arsenide. For example, we find three peaks in photocurrent for $\hbar\omega < \hbar\omega_p$ a result seen quite different from that of silicon [8] and other metals like aluminium [9], palladium [10], tungsten [8] *etc.* The reason for this may be attributed to the fact that the Drude-Lorentz model for calculating the dielectric constants is not applicable to the case of gallium arsenide. The other reason for the occurrence of such peaks may be that for $\hbar\omega < \hbar\omega_p$ the photon field vector $A_\omega(z)$ as deduced by using the model of Bagchi and Kar [6] is not applicable to the case of compound semiconductor. We cannot rule out the weakness of the K–P model potential as used by Thapa and Kar [1] for deducing the initital state wavefunction ψ_i. The effect of the surface was not taken into consideration while formulating ψ_i for a semi-infinite solid. However, the occurrence of peaks at $\hbar\omega < \hbar\omega_p$ both for silicon and gallium arsenide can be attributed to the spatial variation of vector potential. Lapeyre and Anderson [11] had also experimentally found the existence of surface state in gallium arsenide from the constant initial state spectroscopy. The complicated line shapes in their measurement for the surface states were not fully understood. However, the conclusion found in their measurement was that the photoemission intensity was strongly a polarization dependent.

Though we have not taken into consideration the effect of the type of semiconductor, density *etc*, however, we find that in the case of semiconductors, the spatial dependence of vector potential is an essential ingredient in photoemission calculations. Instead of using the simple type of dielectric formula like that of Drude-Lorentz type, it would be more realistic if one can employ the method as developed by Cappellini [12] *et al* which is specifically defined only for the semiconductors. Further, the inclusion of structure into this type of calculations will enable one to compare the data with experiment in a more appropriate way. For example, a detailed study of photoemission from semiconductor gallium arsenide by using the one-step model of photoemission had been done by Schattke [13]. He had used the Green function-formalism to the valence states in LCAO basis by taking photon field vector as constant in dipole approximation. The photoemission data for the ideal gallium arsenide surface agreed well with the experimental data.

Acknowledgments

RKT acknowledges the sanction of a research grant and SG the award of a fellowship from Department of Science and Technology, New Delhi.

References

[1] R K Thapa and N Kar *Indian J. Pure Appl. Phys.* **26** 620 (1988)

[2] F J Himpsel *Appld. Phys.* **A38** 205 (1985); L F Wagner and W E Spicer *Phys. Rev. Lett.* **28** 1381 (1972)

[3] G P Srivastava *Rep. Prog. Phys.* **60** 561 (1996); E W Plummer and W Eberhardt *Adv. Chem. Phys.* **49** 533 (1982)

[4] K C Pandey and J C Phillips *Phys. Rev. Lett.* **32** 1433 (1974); D Haneman *Phys. Rev.* **121** 1093 (1961)

[5] D R Penn *Phys. Rev. Lett.* **28** 1041 (1972)

[6] A Bagchi and N Kar *Phys. Rev.* **B18** 5248 (1978)

[7] N W Ashcroft and N D Mermin *Solid State Phys.* (Japan : CBS Publishing) p 146 (1976)

[8] R K Thapa and N Kar *Surf. Sci.* **338** 138 (1995)

[9] P Das, R K Thapa and N Kar *Mod. Phys. Lett.* **B35** 65 (1991)

[10] R K Thapa *Phys. Stat. Sol. (b)* **179** 621 (1993)

[11] G J Lapyere and P J Anderson *Phys. Rev. Lett.* **35** 117 (1975)

[12] G Cappellini, R Del Sole, L Reining and F Bechstedt *Phys. Rev.* **B47** 9892 (1993)

[13] W Schattke *Prog. Surf. Sci.* **54** 211 (1997)

ELSEVIER

23 October 2000

Physics Letters A 275 (2000) 459–462

PHYSICS LETTERS A

www.elsevier.nl/locate/pla

Application of Mathieu potential to photoemission from metals

Zaithanzauva Pachuau [a], B. Zoliana [a], D.T. Khating [b], P.K. Patra [c], R.K. Thapa [c,*]

[a] *Department of Physics, Government Zirtiri Residential Science College, Aizawl 796 001, Mizoram, India*
[b] *Department of Physics, North-Eastern Hill University, Shillong 793 022, India*
[c] *Department of Physics, Pachhunga University College, North-Eastern Hill University, Aizawl 796 001, Mizoram, India*

Received 30 June 2000; accepted 30 August 2000

Communicated by J. Flouquet

Abstract

The Mathieu potential is used to define the crystal potential from which the initial state wavefunction for the surface state is derived. The wavefunction is used for photoemission calculations in the case of free electron metals like Al and Be.

PACS: 73.20; 79.60
Keywords: Photoemission; Photocurrent; Wavefunction; Surface; Dielectric function

Over the last few decades interests in the detailed understanding of the physical properties of condensed materials and their surfaces have grown enormously. Further the miniaturization in microelectronics have reached a point where surface properties have become very much dominant. Sufficient progress has been made in the production of two-dimensional structures like multilayers or thin films, which have new and fascinating features. For investigating the electronic properties of clean and adsorbate covered surfaces and thin films, angle-resolved ultraviolet photoemission spectroscopy (ARUPS) has become one of the important tools as it allows measuring the dispersion of the bands for both occupied and unoccupied bands and therefore reveals the structure around the Fermi level with a high level of accuracy [1–4]. In order to interpret the experimental spectra, it is useful to have a quantitative comparison between the theoretical and experimental photoemission data. This demand has led to the developments of various approaches for calculating the photocurrent which ranges from sophisticated but tractable many-body theories [5] to one-electron formulations. Experimental data from ARUPS have been extensively useful in surface physics, and to analyze the data, methods for photoemission calculations have been developed where the wavefunctions for the semi-infinite solid are constructed accurately. However the spatial variations of the electromagnetic fields is generally neglected in such type of calculations. The reason for this being that it is a complex problem and *ab initio* calculations are available only for jellium [6–9]. On the other hand, empirical calcu-

* Corresponding author. Tel: +91-389-328044; Fax: +91-389-323491.
E-mail address: rkt@dte.vsnl.net.in (R.K. Thapa).

0375-9601/00/$ - see front matter
PII: S0375-9601(00)00602-2

lations of the fields near surfaces with the local dielectric functions have been used to interpret the qualitative features in photoemission data from metals and semiconductors. Free electron [10] and Kronig–Penney [11,12] models have been used in such cases for developing the initial state wavefunctions which were then employed to calculate the matrix elements for evaluating the photocurrent.

We report here a simple formalism developed for photoemission calculations in which the free-electron states are derived by using the Mathieu potential [13,14]. The Mathieu potential has been at first used by Statz [15] for surface state calculations. Levine [16] had also used the Mathieu potential for calculating the condition for arbitrary surface terminations. We have used in this formalism the model as described by Davison and Steslicka [13,14] for describing the crystal potential which was then used for deriving the initial state wavefunctions.

The photocurrent density formula [17] from the golden rule approximation can be written as

$$\frac{\mathrm{d}j(E)}{\mathrm{d}\Omega} = \frac{2\pi}{\hbar}\sum|\langle\psi_f|\Delta|\psi_i\rangle|^2\delta(E-E_f) \times\delta(E_f-E_i-\hbar\omega)[1-f_0(E)], \quad (1)$$

where ψ_i (ψ_f) refers to the initial (final) state wavefunction and $\Delta=(e/2m_ec)(\boldsymbol{A}\cdot\boldsymbol{p}+\boldsymbol{p}\cdot\boldsymbol{A})$ where m_e is the mass of the electron, $\boldsymbol{p}$ the one-electron momentum operator and $\boldsymbol{A}$ is the vector potential of the incident photon field. To compute the photon field, we have used the simple model of Bagchi and Kar [17] which has been used earlier also [10–12]. With simple modification the photon field used in our calculation can be written as

$$\tilde{A}_\omega(x)=\begin{cases}A_1, & x<-d\\ \dfrac{A_1\varepsilon(\omega)d}{[1-\varepsilon(\omega)]x+d} & -d\leqslant x\leqslant 0\\ A_1\varepsilon(\omega), & x>0\end{cases} \quad (2)$$

where A_1 is a constant depending on the dielectric function $\varepsilon(\omega)$, photon energy $\hbar\omega$ and the angle of incidence θ_i. To determine $\psi_i(x)$ in Eq. (1) we have included a surface of width d in the crystal potential as shown in Fig. 1. We have considered a nearly

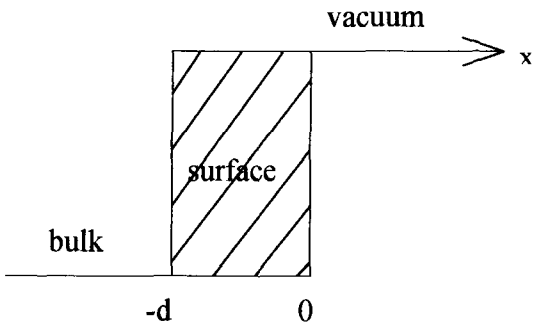

Fig. 1 Model potential used for calculating the initial state wavefunction ψ_i and the photon field.

empty lattice with a finite step potential [13,14]. The initial state wavefunction is given by (in au)

$$\psi_i(x,q)=\begin{cases}\left(\dfrac{1}{4\pi k_i}\right)^{1/2}\phi(x_0,q)\mathrm{e}^{-\eta(x_0-x)}, & (\text{for } \eta>0),\ x\leqslant 0\\ (2\zeta)^{1/2}\mathrm{e}^{-\zeta(x-x_0)}, & (\text{for } \zeta>0),\ x>0\end{cases} \quad (3)$$

where x_0 is the crystal surface location. For a nearly empty lattice with a height of the step potential as ζ, we have since $q\sim 0$, a hybridization parameter $\lambda\cong\tan m'(x_0-\zeta^{-1})$. Also $\phi(x_0,q)\cong\lambda\cos m'x-\sin m'x$ such that $m'=ma/\pi$ where m is the band index and a is the period of the potential. We have chosen the following data both for the case of Al and Be: $x_0=a/2$, $\zeta=12/a$ and $m=1$. The matrix element in Eq. (1) for calculating the photocurrent now reduces to the following:

$$I=\int_{-\infty}^{-d}\psi_f^*\tilde{A}_\omega(x)\frac{\mathrm{d}\psi_i}{\mathrm{d}x}\mathrm{d}x + \int_{-d}^{0}\psi_f^*(x)\tilde{A}_\omega(x)\frac{\mathrm{d}\psi_i}{\mathrm{d}x}\mathrm{d}x + \frac{1}{2}\int_{-d}^{0}\psi_f^*\frac{\mathrm{d}\tilde{A}_\omega(x)}{\mathrm{d}x}\psi_i\,\mathrm{d}x + \int_{0}^{\infty}\psi_f^*\tilde{A}_\omega(x)\frac{\mathrm{d}\psi_i}{\mathrm{d}x}\mathrm{d}x. \quad (4)$$

The photocurrent was calculated as a function of photon energy ($\hbar\omega$) by evaluating the integrals in Eq. (4). The formalism was then applied to the case

of metals Al and Be as they are free electron type of metals. For these metals we have used the experimentally determined dielectric function [18,19] for calculating the photon fields through a subroutine of the main FORTRAN programme.

The plot of the photocurrent as a function of $(\hbar\omega)$ for normal photoemission is shown in Fig. 2. We have shown here the photoemission for a constant initial state for which the energy was located at the Fermi level. As it is a model calculation, we have chosen the location of the Fermi level for both Al and Be to be at 0.43 Hartrees. The photocurrent profile for Al showed a strong photoemission at photon energy $\hbar\omega = 10$ eV. This was followed by a suppressed photoemission and therefore the photocurrent was minimum at $\hbar\omega = 15$ eV (the plasmon energy of Al is $\hbar\omega_p = 15.3$ eV). There is another hump in photocurrent data at $\hbar\omega = 18$ eV. We find that there is a qualitative agreement between the experimental data [20] and the previously calculated results [10]. The experimental data of Levinson et al. [20] showed a maxima in photocurrent at $\hbar\omega = 13$ eV with the occurrence of a minima at the plasmon energy. However in the case of Be the behaviour of the photocurrent is similar to that of Al.

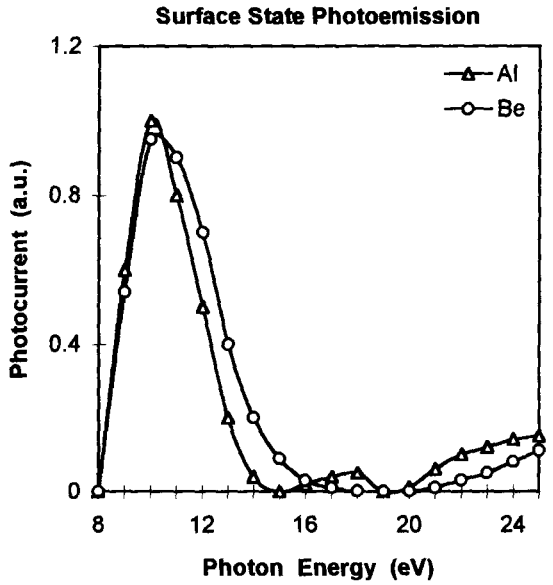

Fig. 2. Plot of photocurrent (normalized to unity) against the photon energy (eV) for Al and Be.

For example it showed a maximum at $\hbar\omega = 10$ eV followed by a minimum but not occurring at $\hbar\omega = \hbar\omega_p$ (the plasmon energy of Be is 19.5 eV) like in the previously calculated results [21]. It showed a minimum in the photocurrent within the photon energy range of 18 eV to 20 eV. There was an enhancement in the photocurrent value for $\hbar\omega > \hbar\omega_p$. We see from the variation of the photocurrent data that even in the case of Be, it showed a qualitative behaviour as seen earlier in the theoretical [21] and experimental data [22].

The features seen in the behaviour of the photocurrent in Al and Be can be attributed to the fact that in the free electron metals the change in bulk potential is too weak to impart sufficient momentum for photoexcitation. The surface photo-effect is due to the rapid variation of photon fields in the surface region. This is evident from the matrix element in Eq. (1) where $\mathrm{d}\tilde{A}_\omega/\mathrm{d}x$ is directly dependent on photocurrent as the photon energy passes through the threshold for photoexcitation. Moreover we have considered a low photon energy photoemission, hence the incident radiation is too weak to photoexcite electrons from the bulk bands. The origin of the peak in the photocurrent data in the case of Be for $\hbar\omega < \hbar\omega_p$ has been explained by Karlsson et al. [23] from the band picture. He attributed this to the existence of the surface state at $\bar{\Gamma}$ with energy 2.8 eV in the bulk energy band gap $\Gamma_3^+ - \Gamma_4^-$.

Though the model presented in this report is very simple, however, the inclusion of the initial state wavefunction (derived by using the Mathieu potential) into the matrix element appears to reproduce the qualitative features as observed earlier in photocurrent data of Al and Be. There are however shortcomings in the formalism developed. For example, we have used the same ψ_i both for the surface and the bulk regions of the solids. Further it is the spatial variation of the photon fields which is monitoring the change in the photocurrent. However it is a simple type of calculations which enables one to see the effect of inclusion of the Mathieu potential also in the photoemission calculations. It would be still appropriate and realistic if one can extend such type of calculations to other metals like d-band or transition type by appropriately incorporating the sine and cosine elliptic functions to the initial state wavefunc-

tions [13,14]. One should also take into consideration the band structure to widen the scope of such studies to electronic structure calculations.

Acknowledgements

Z.P acknowledges gratefully a research grant from the University Grants Commission, Guwahati, India. Thanks are also due to Dr. C. Thanthianga, Principal, Pachhunga University College, Aizawl (India) for extending the necessary facilities. R.K.T. acknowledges the literature received from Mrs. P. Davison, University of Waterloo, Canada.

References

[1] B Feurbacher, B Fitton, R F Willis, Photoemission and Electronic Properties of Surfaces, Wiley, New York, 1978
[2] J E Inglesfield, Rep Prog Phys 45 (1982) 223
[3] J B Pendry, Surf Sci 57 (1976) 679
[4] A Ishii, T Aissaka, Surf Sci 242 (1991) 250
[5] J Braun, Rep Prog Phys 59 (1996) 1267
[6] P J Feibelman, Phys Rev Lett 34 (1975) 1092
[7] P J Feibelman, Phys Rev 12 (1975) 1319
[8] H J Levinson, E W Plummer, J Vac Sci Technol 17 (1980) 216
[9] A Kiejna, Prog Surf Sci 61 (1999) 85
[10] P Das, R K Thapa, N Kar, Mod Phys Lett B 5 (1991) 65
[11] R K Thapa, Phys Stat Sol B 179 (1993) 391
[12] R K Thapa, N Kar, Surf Sci 338 (1995) 138
[13] S G Davison, M Steslicka, Basic Theory of Surface State, Clarendon, Oxford, 1992
[14] S G Davison, J D Levine, Solid State Phys 25 (1970) 2
[15] H Statz, Z Naturforsch 5A (1950) 534
[16] J D Levine, Phys Rev 171 (1968) 701
[17] A Bagchi, N Kar, Phys Rev B 18 (1978) 5240
[18] J Weaver, Handbook of Chemistry and Physics, CRC Press, Boca Raton, Ohio, 1987, for optical data of Al
[19] Handbook of Optical Constants of Solids, E D Pallik (Ed.), Academic, 1991, p 429, for optical data of Be
[20] H J Levinson, E W Plummer, P J Feibelman, Phys Rev Lett 43 (1979) 952
[21] R K Thapa, N Kar, Phys Rev B 51 (1995) 17980
[22] R A Bartynski, E Jensen, T Gustaffson, E W Plummer, Phys Rev B 32 (1985) 1921
[23] U O Karlsson, S A Flodstrom, R Engelhardt, W Gadeka, E E Koch, Solid State Comm 49 (1984) 711